Lift at Zero Reynolds Number

Lionel Bureau, Gwennou Coupier, Thomas Salez

▶ **To cite this version:**

Lionel Bureau, Gwennou Coupier, Thomas Salez. Lift at Zero Reynolds Number. 2022. hal-03719127v1

HAL Id: hal-03719127

https://hal.science/hal-03719127v1

Preprint submitted on 10 Jul 2022 (v1), last revised 9 Nov 2023 (v4)

HAL is a multi-disciplinary open access archive for the deposit and dissemination of scientific research documents, whether they are published or not. The documents may come from teaching and research institutions in France or abroad, or from public or private research centers.

L'archive ouverte pluridisciplinaire **HAL**, est destinée au dépôt et à la diffusion de documents scientifiques de niveau recherche, publiés ou non, émanant des établissements d'enseignement et de recherche français ou étrangers, des laboratoires publics ou privés.

Lift at Zero Reynolds Number

Lionel Bureau,[1,*] Gwennou Coupier,[1,†] and Thomas Salez[2,‡]

[1] *Université Grenoble Alpes, CNRS, LIPhy, F-38000 Grenoble, France*
[2] *Univ. Bordeaux, CNRS, LOMA, UMR 5798, 33400 Talence, France*

(Dated: July 10, 2022)

Lift forces are widespread in hydrodynamics. These are typically observed for big and fast objects, and are often associated with a combination of fluid inertia (*i.e.* large Reynolds numbers) and some specific symmetry-breaking mechanism. In contrast, low-Reynolds-number flows are usually overdamped and do not exhibit such peculiar and interesting features. However, the inclusion of boundary effects qualitatively changes this picture. Indeed, in the context of soft and biological matter, recent studies have revealed the emergence of novel lift forces generated by boundary softness, flow gradients and/or surface charges. The aim of the present review is to gather and analyse this corpus of literature, in order to identify and unify the questioning within the associated communities, and pave the way towards future research around lift effects at low Reynolds numbers.

CONTENTS

Introduction 1

Soft-lubrication lift 2
- Context 2
- The key mechanism 3
- Theoretical developments 5
- Experimental pieces of evidence 9

Elastohydrodynamic lift in external flow 11
- From soft lubrication to bulk elastohydrodynamics 11
- Dynamics of deformable particles under shear flow 11
- Far-field interaction with a rigid wall 12
  - Contributions to lift velocity 13
  - Lift velocity and lift force, the vesicle case 15
  - Other particles 18
- Lift in unbounded Poiseuille flow: "soft-lubrication without walls"? 19
- Migration in a channel 20
- Shape-lift coupling and instability in channels 21
- Curved streamlines 22
- Oscillating flows 22
- Particle-particle interactions 23
  - Pair interaction 23
  - Diffusion in suspensions 26
  - Creation of cell free layers in blood flow 27

Electrokinetic lift 28
- Context 28
- Experimental observations 28
- Origin 29
- Modelling 30
- Comparison with experiments 32
- Concluding remarks 32

Conclusion and perspectives 33

Acknowledgements 34

References 34

INTRODUCTION

We are all familiar with dynamically-induced lift forces in hydrodynamics. These are typically observed for big and fast objects, *e.g.* in aeronautics or ball sports, and result from fluid inertia (*i.e.* large Reynolds numbers) and a symmetry-breaking mechanism, such as wing shape or ball rotation. We define here a lift force as a force acting perpendicularly to the initial motion of the object, which is generally due to its initial acceleration or to its advection by external flows.

While more discrete in everyday life, lift effects do also exist in low-Reynolds-number flows, and often result from a key role played by the flow boundaries. Indeed, the confined hydrodynamic interaction between two objects (*e.g.* a particle, a wall, etc.) or the bulk fluid-structure interaction may break the flow symmetry. This was already understood by Reynolds [1] through his famous tilted slider. In the latter example, a lift force exists due to a fore-aft geometrical asymmetry (see Fig. 1) between two immersed rigid objects in sliding relative motion. However, for a rigid sphere moving along a rigid wall, the time reversal-symmetry of the steady Stokes equations coupled to the fore-aft symmetry of the contact warrants the absence of any emergent normal force in the problem. To overcome this impossibility, in the absence of any inertial effects, other symmetry-breaking mechanisms are thus required, as schematized in Fig. 2.

A prominent example is that of the lift induced by elastic deformations, for which we wish to bridge the gap between two aspects of this phenomenon, that were historically studied by separate research communities. On the one hand, for small gaps between two objects (one of them being often much larger, *e.g.* a wall), *i.e.* in the so-called lubrication regime, the flow between the two objects mediates the hydrodynamic interaction and deforms the elastic surface(s), which in turn modifies the flow profile between the objects and thus the intensity of the net normal force. This strongly-coupled elastohydrodynamic regime is relevant to a wide variety of soft and wet contacts, ranging from roller bearings in industry to biological/physiological systems like mammalian joints or circulating cells in contact with soft endothelial walls within

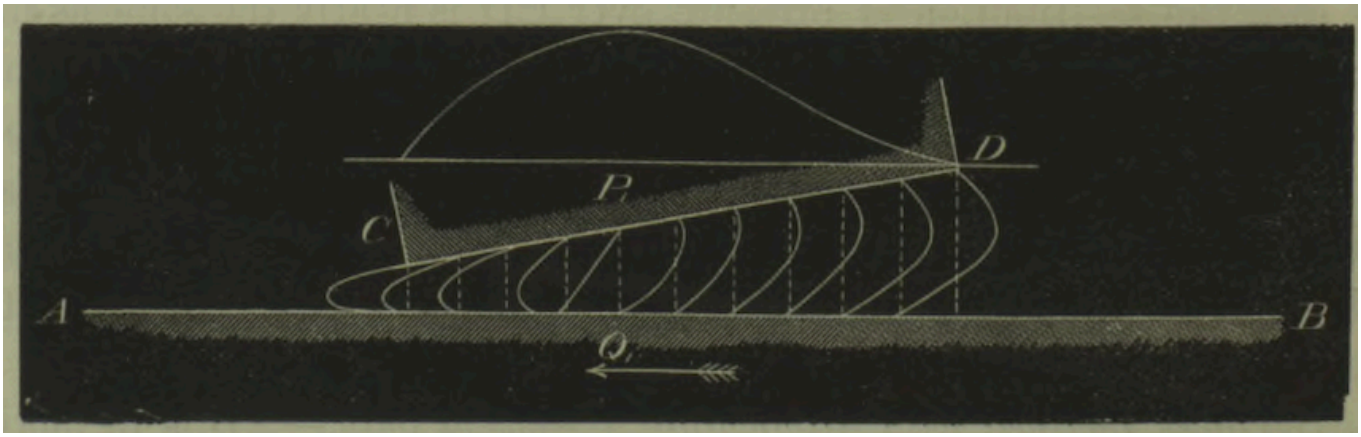

Figure 1. *Reynolds' slider. Despite the time-reversal symmetry of the steady Stokes equations, the fore-aft asymmetry of a tilted immersed slider that moves tangentially to a neighbouring wall generates a difference in the hydrodynamic pressure magnitudes at the front and at the back of the slider. As a consequence, the latter experiences a normal force. This seminal system conceived by Reynolds highlights the leitmotiv of this review: at low Reynolds numbers, a symmetry breaking in transverse motion may generate normal forces. Figure taken from [1].*

blood vessels.

On the other hand, when the objects are too far from each other, the deformation arising from their hydrodynamic interaction vanishes and the resulting force disappears. Yet, in fluidic environments with externally-applied flows, shear forces may maintain flowing bodies in an asymmetric-shape configuration that may still give rise to repelling forces. As the shape is maintained by the shear forces and not by the body-body interaction, these forces will not decrease as quickly with the distance. This configuration is well known, in particular, by the blood-flow community. Indeed, the shear-induced lift of red blood cells is reckoned as the main origin of the creation of a depleted layer near the vessel walls, giving rise to non-linear rheological properties for blood, as well as to complex phase-separation laws at the level of vessel bifurcations. The exact characterization of this lift force, in a context of high cell concentration, is still unresolved in spite of the numerous numerical methods that are *a priori* able to simulate this complex fluid-structure interaction problem. We stress that this shear-induced lift phenomenon requires the considered object to be deformed, which, in the vanishing-Reynolds-number context that we focus on, implies rather soft objects such as biological materials, drops and artificial capsules. We however exclude the particular case of filaments, which have generally a very complex shape dynamics even in the absence of walls, thus rendering difficult our quest for universal mechanisms.

Among other mechanisms giving rise to the symmetry breaking at the heart of lift forces at zero Reynolds number, electrokinetic effects are dominant in the literature. They involve ionic currents taking place when fluid-immersed rigid objects carrying surface charges are in relative motion. Such a phenomenon is typically of interest in microparticle-sorting applications, and an illustration of cases where non-inertial lift forces emerge between objects that are not necessarily deformable.

Those are important mechanisms since they demonstrate that inertial-like effects can be triggered at microscopic and biological scales through a smart role of boundaries. The three mechanisms discussed so far will be the topic of the three chapters of the present review, respectively. Other mechanisms, unexplored yet or marginally explored, will be also briefly mentioned in the perspectives of the concluding section.

SOFT-LUBRICATION LIFT

Context

Soft and wet contacts are widespread in nature and technology. Their rich history in science and engineering involves issues and scales as diverse as the lubrication of roller bearings [4] after the industrial revolution, or the catastrophic geological landslides [5]. The properties of these contacts implicate the coupling between the local hydrodynamic pressure induced by fluid flow and the deformation of the confining solids. Often as well, for stiff surfaces associated with industrial devices, non-Newtonian lubricant effects (*e.g.* piezo-viscous and thermoviscous behaviours) are expected to play an important role [6] and require multiscale numerical modeling [7]. These interesting features for industrial lubricant flows may be considered as more minor corrections in the context of soft materials and small velocities at stake here, despite some potential interest for sorting strategies [8], and are thus not addressed in details in the following.

Recently, such an elastohydrodynamic (EHD) coupling gained attention in the context of confined, soft and biological matter, where very compliant solids and tiny length scales are common [9]. In fact, this coupling could conceivably play a crucial role in the motion of various physiological and biological entities. Examples are numerous and include *e.g.* the incredible frictional properties of mammalian joints [10]

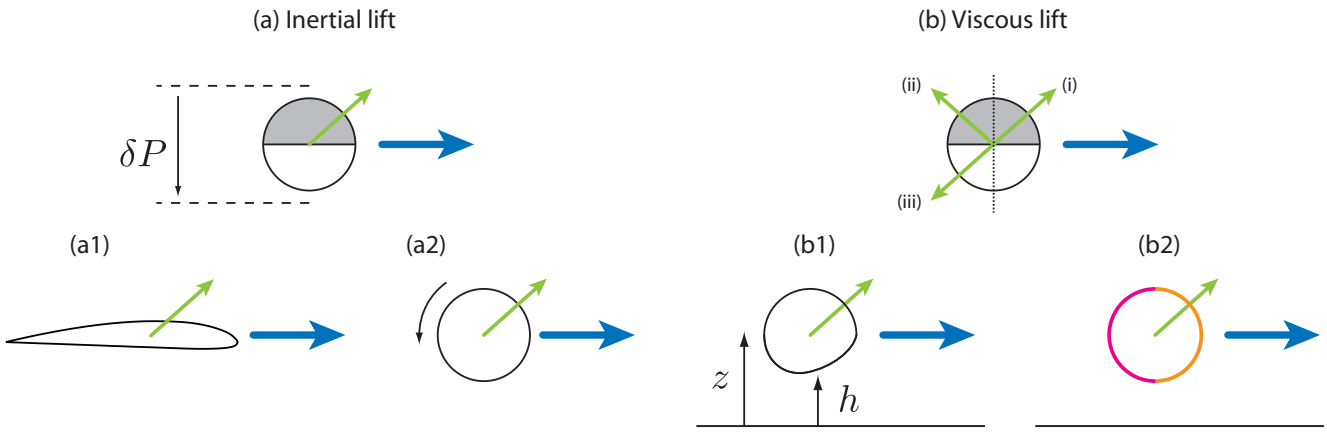

Figure 2. *Required symmetry breakings for inertial and viscous lift forces to arise, transversally to the main motion (blue arrows), leading to tilted trajectories (green arrows). (a) Inertial lift: a bottom-up asymmetry may suffice to create a pressure difference across the particle, leading to the apparition of the lift force. Examples of such a symmetry breaking include (a1) asymmetry in shape as for an airplane wing or (a2) rotation-induced asymmetry, as for a rotating ball sport experiencing a Magnus effect in free space [2], or a sphere in a channel according to the SegrÃl-Silberberg effect [3]. Note that wings often exhibit a fore-aft asymmetry as well, for drag reduction requirements. (b) Viscous lift: even in the presence of bottom-up asymmetry, a fore-aft symmetry prevents the apparition of a lift force. If it was not the case, assuming the particle has a velocity given by (i), a left-right reversal of the boundary conditions (e.g. external flow, gravity field,...) would lead, by fore-aft symmetry of the particle, to the symmetric motion (ii). However, the time reversibility of the steady Stokes equations imposes also that the motion would be according to (iii), thus leading to the impossibility of the existence of a lift force. This marks the strong difference with situations where fluid inertia is not negligible. The additional fore-aft asymmetry may be due to e.g. (b1) the particle geometry or (b2) the boundary conditions at the surface of the particle, that can be linked to charge distribution or slip properties, among others. In most situations, the presence of a wall warrants the bottom-up asymmetry, but we shall also explore cases where lift occurs in the absence of nearby walls but with a vertical flow gradient.*

through the fine interplay between soft cartilage and viscous synovial fluid, or the crucial influence of vessel boundaries on the motion of deformable red blood cells [11]. The normal motion towards a soft wall has been investigated in particular [12–15], with a special attention given to the collision [16] and rebound [17, 18] properties.

Furthermore, through surface-forces apparatus (SFA) [13, 19–23] and atomic-force microscopy (AFM) [24–29], the near-contact EHD (termed soft-lubrication in the following) coupling offers an alternative strategy for micro and nanorheology of fragile soft materials, with the key advantage of avoiding any solid-solid adhesive contact that could alter their properties (see Fig. 3).

The key mechanism

Despite the irrelevance of inertia, a soft-lubrication lift force emerges for elastic bodies moving past each other within a viscous fluid. Essentially, any (initially) fore-aft-symmetric object moving within such a fluid and along a nearby soft wall is repelled from the latter by a dynamically-generated emergent normal force. This force intimately arises from a symmetry breaking in the contact shape (see Fig. 4), and thus the associated flow fields, due to the EHD coupling described above. Qualitatively, the elastic deformation induced by the hydrodynamic pressure generates a self-sustained asymmetric contact similar to the one in Reynolds' rigid slider (see Fig. 1), and thus a normal force. This effect is well known at macroscopic scales, for relatively rigid materials such as car tires undergoing aquaplaning, or industrial roller bearings getting deformed in operating motors and machines.

Moving on to the context of mesoscale physics and soft matter, the earliest theoretical descriptions of such a soft-lubrication lift effect are the ones by Dowson and Jin [31], Lequeux, Grosshans and Hocquart [32], as well as Sekimoto and Leibler [33], to the best of our knowledge. The underlying motivation behind these similar approaches is the calculation of forces between soft curved surfaces undergoing shear, which are important for the interpretation of SFA measurements, the physics of cartilage, and the rheology of a variety of complex fluids such as suspensions of colloidal particles protected by grafted or adsorbed polymer chains, suspensions of gel microparticles, or polymer emulsions and alloys on certain time scales.

The general idea can be illustrated from *e.g.* [33], through the calculation of the soft-lubrication interaction between a cylindrical elastic object of radius R moving at transverse velocity V past and nearby a flat wall (as in Fig. 4), within a viscous fluid of dynamic viscosity μ, both solids being covered by polymer brushes. The latter are modeled as identical thin linear-elastic compressible layers.

A thin linear-elastic compressible layer is equivalent to Winkler's foundation, *i.e.* a mattress of independent springs with a

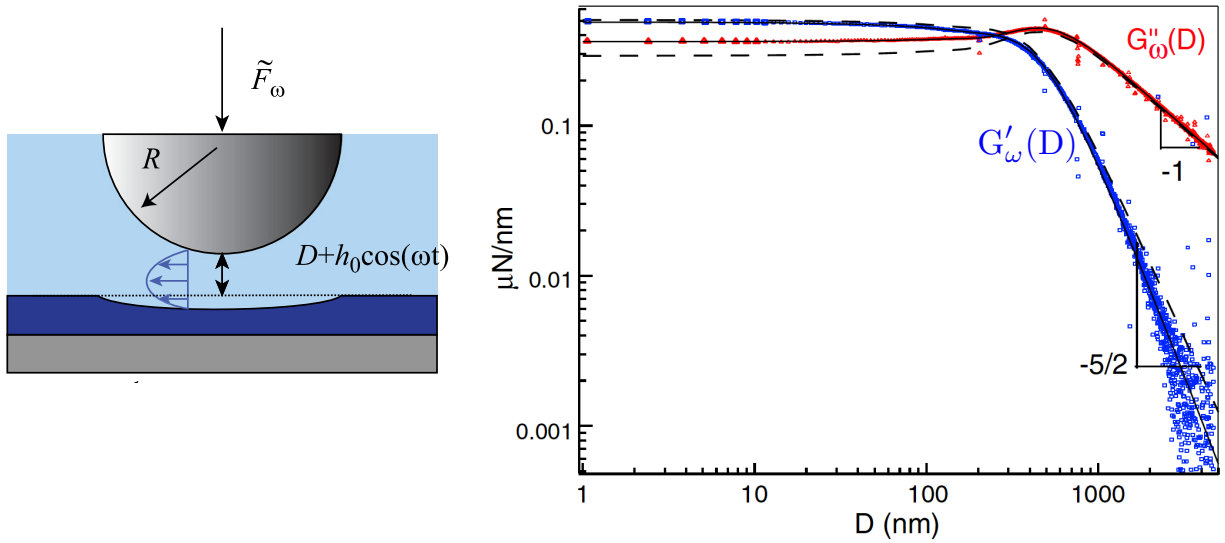

Figure 3. *(left) In a surface-forces apparatus (SFA), a flow between an oscillating sphere and an elastic film is created. (right) Real (blue) and imaginary (red) parts of the force-distance impedance response $G_\omega(D)$ obtained for an elastomer (crosslinked PDMS) and compared to soft-lubrication theory (dashed lines). Figure adapted from [19].*

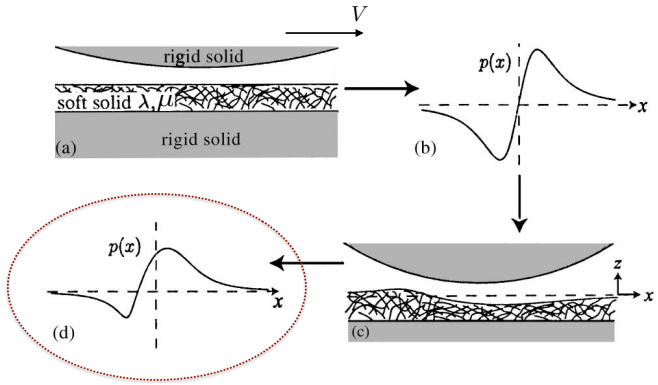

Figure 4. *Principle of the soft-lubrication lift force. For a non-deformed wall (a), the classical lubrication pressure $p(x)$ induced in the viscous fluid by the tangential motion of a sphere at velocity V is antisymmetric in the transverse direction x (b), resulting in a null net force (integral of the pressure along x) in the normal direction z. In contrast, a soft surface is deformed by the pressure field (c). The latter then loses its symmetry (d), which results in a finite emergent normal force: the soft-lubrication lift force. Figure adapted from [30].*

local and linear response to the external pressure field $p(x)$ (see Fig. 5), that was proven to be of great modelling power [34]. In such a description, the normal deformation field is given by $\delta(x) = -Lp(x)/(2G)$, where we introduced an effective shear modulus G as well as an effective thickness L of the mattress, and where we assumed for simplicity a full compressibility (*i.e.* vanishing Poisson ratio). Near its minimum h_0, the steady-state fluid gap profile $h(x)$, along the transverse direction x of motion, is well approximated by a parabola (*i.e.* second-order development of a spherical contact near the apex) corrected by the elastic deformation of the elastic layer induced by the hydrodynamic pressure. It thus follows that:

$$h(x) \simeq h_0 + \frac{x^2}{2R} + \frac{L}{2G}p(x)\ . \qquad (1)$$

Scaling analysis. The main idea is then based on a hierarchical scale separation, by considering that the elastic deformation is small compared to the fluid-gap thickness, which is itself small compared to the cylinder radius. By invoking the steady Stokes equations in the lubrication approximation, it follows that the leading-order pressure magnitude scales as $\sim \mu V\ell/h_0^2$, where $\ell = \sqrt{2Rh_0}$ is the characteristic horizontal length scale, given by the Hertz-like *hydrodynamic radius* emerging from the parabolic approximation in Eq. (1). In such a framework, and in addition to the lubrication condition $h_0/R \ll 1$, one finds $\kappa \sim \mu\sqrt{R}VL/(Gh_0^{5/2})$ as a second natural small parameter of the problem. Then, an expansion of the soft-lubrication flow problem is performed at order 1 in κ. The zeroth-order contribution corresponds to the purely rigid case with gap profile $h^{(0)}(x) \simeq h_0 + x^2/(2R)$ and a zeroth-order pressure field $p^{(0)}(x)$ that can be computed analytically, and that is found to be antisymmetric in x (Fig. 4(b)). This is expected in view of the time-reversal symmetry of the steady-Stokes equations and the fore-aft symmetry of the contact shape. As the normal force per unit length F_z exerted on the cylinder is dominated, in the lubrication approximation, by the pressure contribution (*i.e.* the ratio between the viscous shear stress and the pressure is of order $h_0/\ell \ll 1$), the latter antisymmetry of $p^{(0)}(x)$ implies to evaluate the first correction $p^{(1)}(x)$ induced by the elastic deformation. The magnitude of the latter scales as $\sim \kappa(\mu V\ell/h_0^2)$. Therefore, the resulting normal force per unit

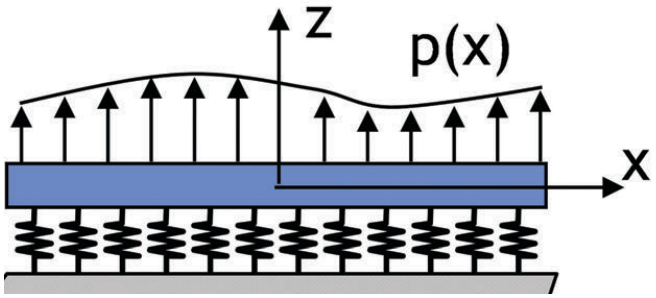

Figure 5. *Schematic involving a Winkler's foundation, i.e. a model and simple type of elastic substrate characterized by an assembly of parallel, independent and identical springs, leading to a local and linear response to the external pressure field $p(x)$. For thin enough, compressible elastic layers, such a toy model even provides a quantitative description of their elastic Green's function. Figure adapted from [34].*

.

length reads, at order 1 in κ:

$$F_z \simeq \int_{-\infty}^{\infty} \mathrm{d}x\, p^{(1)}(x) \sim \frac{\mu^2 V^2 R^{3/2} L}{G h_0^{7/2}} \,. \tag{2}$$

Interestingly, one sees that this soft-lubrication lift force increases with the viscosity of the fluid, driving velocity, compliance, contact area, and confinement. Then, the authors of [33] confront the theoretical predictions with the result of force measurements under shear between surfaces covered with grafted polymer chains. While the observed normal forces in these experiments are often attributed to brush swelling due to external flows, the authors quantitatively argue here that the brush-deformation-induced soft-lubrication lift force is instead the dominant mechanism behind the common observations.

Soft-lubrication theory. Here, as an illustration of the typical method for the readers, we aim at retrieving the scaling result above quantitatively. We place ourselves in the rest frame of the cylinder. We introduce the fluid velocity field $u(x, z)$ along x, and the dimensionless variables: $z = Z h_0$, $h = H h_0$, $x = X\ell$, $u = UV$, $p = P\mu V\ell/h_0^2$, and $F_z = \mathcal{F}_Z \mu V \ell^2/h_0^2$. Hence, the gap profile given by Eq. (1) is non-dimensionalized as:

$$H(X) = 1 + X^2 + \kappa P(X) \,, \tag{3}$$

where:

$$\kappa = \frac{L\mu V R^{1/2}}{\sqrt{2} G h_0^{5/2}} \,. \tag{4}$$

In the lubrication approximation where $h_0 \ll R$, the incompressible steady Stokes equations reduce to [1, 35, 36]:

$$\partial_{ZZ} U = \partial_X P \,. \tag{5}$$

with $\partial_Z P = 0$, In addition, we impose no-slip boundary conditions, through $U(X, Z = -\kappa P) = -1$ and $U(X, Z = H - \kappa P) = 0$. Solving Eq. (5) with these boundary conditions, and invoking the condition of volume conservation yields the Reynolds equation:

$$\partial_X \left(H^3 \partial_X P + 6H \right) = 0 \,. \tag{6}$$

Solving the latter with vanishing pressure in the far field, one can then calculate the dimensionless normal force (per unit length) exerted on the cylinder, through:

$$\mathcal{F}_Z = \int_{-\infty}^{\infty} \mathrm{d}X\; P(X) \,. \tag{7}$$

Since $\kappa \ll 1$, perturbation theory [30] using $P \simeq P^{(0)} + \kappa P^{(1)}$, allows one to integrate Eq. (6) at first order in κ, eventually leading to the dimensionless lift force:

$$\mathcal{F}_Z \simeq \frac{3\pi\kappa}{8} \,, \tag{8}$$

and thus providing Eq. (2) as well as the missing prefactor therein.

Theoretical developments

Let us make a few comments about Eq. (2). This typical asymptotic expression of the soft-lubrication lift force per unit length relies on several assumptions: a 2D problem, a pure linear and local compressible elastic rheology, a vanishing compliance, a near-contact/confinement situation, a parabolic contact shape, etc. It is thus expected to find important modifications of the lift force in more complex or realistic situations. First of all, while the perturbative/asymptotic nature of the approach is expected to hold near contact and at small elastic deformations, through the explicit factor $\sim (\mu V)^2/G$ in the force expression, dimensionality and geometry are expected to modify the dependencies on the various length scales of the problem. Similarly, the exact elastic rheology (compressible vs incompressible, thin vs thick) will modify the constitutive response between the pressure $p(x)$ and the elastic deformation $\delta(x)$. Indeed, while a linear response is expected to hold at small deformations, the simple Hookean proportionality relation $\delta(x)/L \sim p(x)/G$ may be replaced by a nonlocal relation of the type:

$$\delta(x) \sim \frac{1}{G} \int_{-\infty}^{\infty} \mathrm{d}x'\, g(x - x') p(x') \,, \tag{9}$$

where g is the dimensionless elastic Green's function (in a 2D description here), that simply reduces to a Dirac distribution in the Winkler's case discussed above. Qualitatively, δ is still the linear response to the source $p(x)$ with a magnitude set by the compliance $1/G$ (and even a proportionality in Fourier space). Quantitatively, we expect differences depending on the exact Green's function characterizing the response. To go one step further along this line of thought, substrate

Geometry	Material	Lift force
Thin layer	Compressible elastic solid	$\frac{\mu^2 V^2}{2G+\lambda}\frac{H_l R^2}{h_0^3}$
Thin layer with degenerate contact	Compressible elastic solid	$\frac{\mu^2 V^2}{2G+\lambda}\frac{H_l R^{4-(2/n)}}{h_0^{5-(2/n)}}$
Soft slider	Elastic solid	$\frac{\mu^2 V^2}{G}\frac{R^{5/2}}{h_0^{5/2}}$
Thickness $\gtrsim\sqrt{Rh_0}$	Incompressible elastic solid	$\frac{\mu^2 V^2}{G}\frac{R^{5/2}}{h_0^{5/2}}$
Thickness $\ll\sqrt{Rh_0}$	Incompressible elastic solid	$\frac{\mu^2 V^2}{G}\frac{H_l R^{3/2}}{h_0^{5/2}}$
Thin layer	Poroelastic	$\frac{\mu^2 V^2}{2G+\lambda}\frac{H_l R^2}{h_0^3}$
Cylindrical shell $h_s \gg h_0$	Elastic solid	$\frac{\mu^2 V^2}{G}\frac{R^4}{h_s^{5/2}h_0^{3/2}}$
Cylindrical shell $h_s \lesssim h_0$	Elastic solid	$\frac{\mu^2 V^2}{G}\frac{R^{5/2}}{h_s h_0^{3/2}}$
Journal bearing thin layer	Elastic solid	$\frac{\mu\omega^2 R^2}{2G+\lambda}\frac{H_l R^4}{h_0^5}$

Table I. *Different scalings of the soft-lubrication lift force for a sphere in 3D, for various geometries and rheologies of the elastic substrate [37]. Here, μ is the shear viscosity of the lubricant, V the relative tangential speed, ω the angular speed, n the contact-degeneracy parameter, H_l the elastic substrate thickness, R the sphere radius, G the shear modulus of the elastic substrate, h_0 the fluid-gap thickness (noted h in this manuscript) and h_s the shell thickness.*

viscoelasticy and poroelasticity are expected to add one or several new time scale(s) in the problem, rendering the response time-dependent, including memory effects. Similarly, large deformability and/or elastic nonlinearities may induce saturations of the force, beyond the small-deformation scaling in $1/G$ of Eq. (2). Finally, adding non-Newtonian effects, or conservative surface forces, such as van der Waals forces and screened electrostatic interactions, is expected to lead to non-trivial effects and coupling with the EHD picture above. One thus realizes that there was room and need for further theoretical developments around Eq. (2).

Perhaps the most emblematic example of such developments, is the series of work by Skotheim and Mahadevan [30, 37]. Therein, a systematic zoology of various non-conforming and conforming contact geometries and elastic responses was addressed analytically and numerically. This is exemplified in Table I with a collection of lift-force scalings for the particular case of a 3D sphere. This body of work applies the same soft-lubrication framework as the one introduced above, and employs numerical resolutions to go beyond scaling expressions and the small-compliance limit. Interestingly, thanks to the numerical resolution, an optimum in the lift-force-vs-gap-distance behaviour was systematically found. Note that a capillary version of soft lubrication, analogous to the elastic one at stake here, was not addressed therein, but

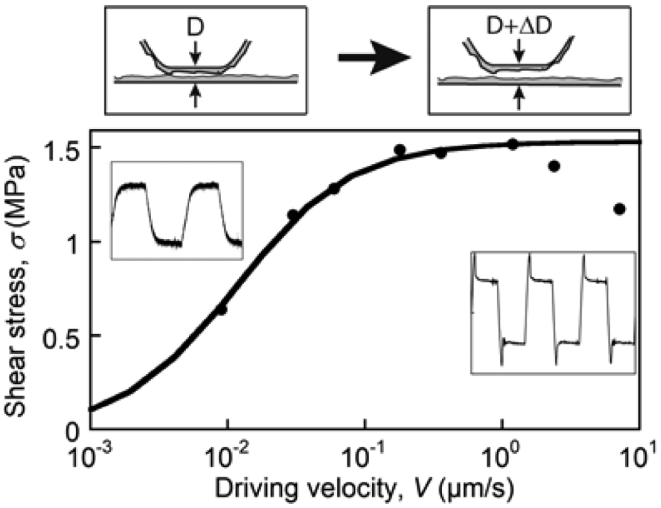

Figure 6. *Shear stress as a function of driving velocity measured with a SFA covered by strongly adhesive polyelectrolyte layers and in presence of a lubricant. Figure taken from [39].*

was studied previously in the context of rising bubbles [38].

Nearly at the same time, and importantly, Beaucourt *et al.* [40] understood the interest of such a lift force in a biophysical context. These authors addressed in particular the case of vesicles, as model biological elastic microparticles, during their motion in water near soft glycocalix layers. Putting numbers on the optimal lift expression, they found forces with magnitudes lying in the physiological range. This work thus highlights the potential importance of such soft-lubricated couplings for the dynamics of red blood cells, and thus biological processes that are essential to life.

To go beyond scaling symbols in the soft-lubrication lift expression for a sphere in 3D is a more intricate task. An elegant solution based on Lorentz's reciprocal theorem was sketched by Stone *et al.* during an oral communication at the 2004 APS-DFD meeting [42]. It was later on systematically explored by Urzay *et al.* [43] for the problem of a sphere translating and rotating near a thin compressible elastic layer. A main finding therein is that the 3D geometry eliminates the occurrence of maximum lift and optimum choice of the material properties. Later on, Urzay generalized the scope to the added role of DLVO intermolecular interactions [44]. There, the competition of the hydrodynamic, intermolecular and deformation effects leads to forces which do not scale linearly with the velocity, and produce a non-additivity of the intermolecular effects. Mainly, the intensity of the repulsive forces is reduced while the intensity of the attractive forces is increased, collectively leading to an effective and reversible EHD adhesion scenario. Besides, a more exotic irreversible EHD adhesion regime was also found. Elastohydrodynamic corrections to the DLVO framework for the critical coagulation concentration of electrolytes were obtained too.

Beyond global quantities, such as the net normal lift force, local details on the contact shape show peculiar features as

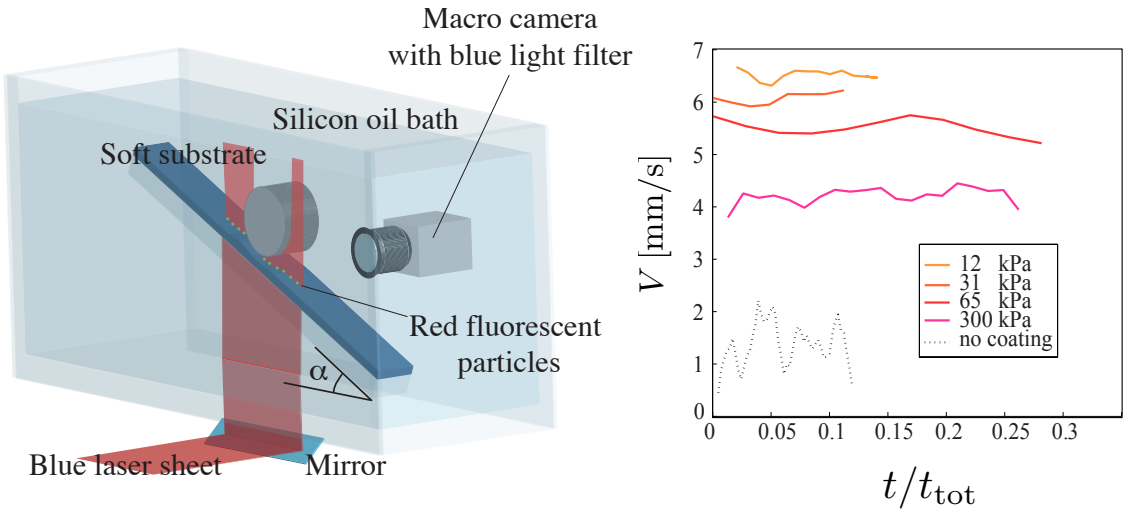

Figure 7. *(left) A rigid cylinder immersed in a viscous bath slides along an inclined plane covered with a thin elastic layer. Fluorescent particles embedded in the latter make it possible to observe its deformation using a laser and a camera. (right) Sliding speed V as a function of normalized time $T = t/t_{tot} = tV_\infty/L$, for several shear moduli of the elastic coating. Here, V_∞ is the time-averaged steady-state sliding speed, L is the total length of the substrate, and t is the time. The dotted line corresponds to the case of a bare glass substrate. Figure adapted from [41].*

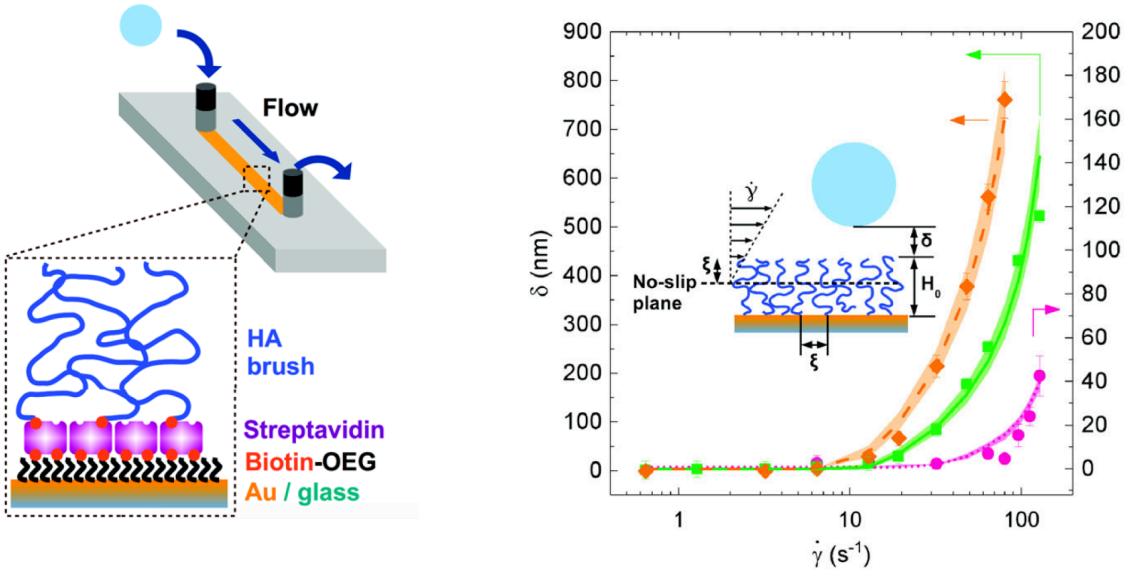

Figure 8. *(left) A glass microbead is advected in an aqueous environment within a microfluidic chamber whose walls are decorated by a biomimetic polymer brush. (right) The distance to the wall is measured versus the imposed shear rate, for three brush elastic moduli (increasing from orange to pink). Theoretical lines including the soft-lubrication lift contribution are fitting the data. Figure adapted from [45].*

well. For instance, in 2D, the self-similar properties of the soft-lubricated contact zone in a high-loading case was investigated by Snoeijer *et al.* [48]. Asymptotic results for a soft sphere in 3D pressed against a hard wall were shown to agree with both experimental and numerical data. Later on, Essink *et al.* [49] managed to obtain analytical scaling laws in the high-loading regime. In this work, the authors described various regimes of soft lubrication for two-dimensional cylinders in lubricated contact with compliant walls. They addressed the limits of small and large entrainment velocities, near thin elastic coatings, both compressible and incompressible. The analysis relies intimately on the introduction of an elastohydrodynamic boundary layer that appears at the edge of the contact region.

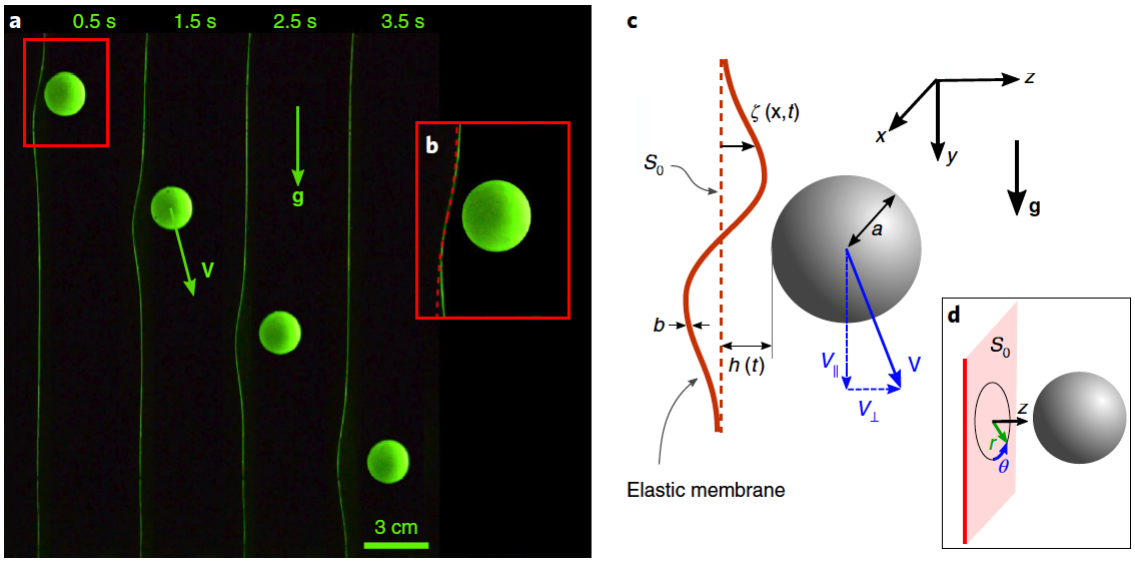

Figure 9. *Gravitational sedimentation of a macroscopic sphere immersed in a viscous fluid, along a vertical membrane under tension, exhibits an important normal drift induced by the soft-lubrication lift. Figure taken from [46].*

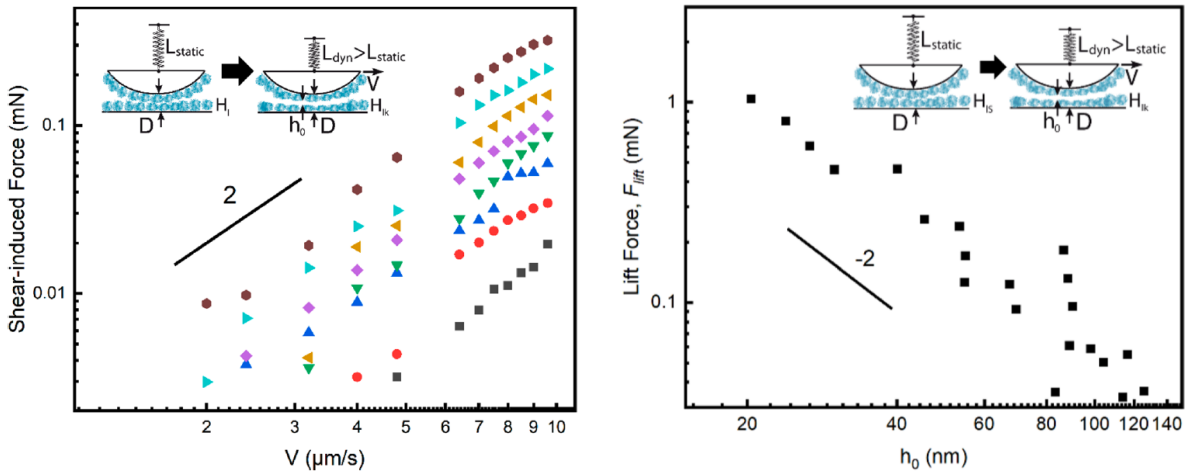

Figure 10. *(left) Shear-induced force as a function of driving velocity measured with a SFA covered by microgel layers and in presence of a lubricant, for various gap thicknesses increasing from brown to grey symbols. (right) Measured lift force as a function of lubricant thickness. Figure adapted from [47].*

So far, the problems studied involved constant fluid gap thickness and transverse velocity. The case of a more general prescribed motion in 2D and 3D near a Winkler's foundation was addressed analytically and numerically by Weekley *et al.* [50]. When the particle moves from rest towards the wall, fluid trapping beneath the particle leads to an overshoot in the normal force on the particle, with trapping at early times and fluid draining at late times. When the particle is pulled from rest away from the wall, a transient adhesive normal force emerges. When a cylinder moves from rest transversely along the wall, an overshoot in the transverse drag appears. However, the case of a free particle immersed in a viscous fluid and near a soft wall, with all degrees of freedom allowed, is relevant to experiments and needed to be addressed. The associated leading-order soft-lubrication interaction matrix was derived by Salez and Mahadevan in 2D [51], and later on by Bertin *et al.* in 3D [52]. Interestingly, when including the particle inertia, a counterintuitive zoology of fluid-inertial-like solutions emerges. These encompass: Magnus-like effects, enhanced sedimentation, adhesive-like EHD forces, roll reversal, oscillations, etc. In addition, the existence of a spontaneous soft-lubrication torque, at next (*i.e.* second) order in κ, was revealed in 2D by Rallabandi *et al.* [53], for compressible and incompressible settings.

We have focused on purely elastic materials in the description above. In such a framework, the softer the material, the larger the effect, until an optimum or saturation eventually occurs. This suggests to employ rather soft materials in practice. However soft gels and elastomers are inevitably prone to poroelastic and viscoelastic effects. While the former have been briefly sketched by Skotheim and Mahadevan in the lift context [30, 37], the latter needed to be incorporated in details. Pandey *et al.* [54] thus analyzed soft-lubricated contacts with viscoelastic walls. In particular, the authors focused on three canonical responses, namely: Kelvin-Voigt, standard linear, and power-law rheologies. They showed how viscoelasticity modifies the contact properties when the time scales of both the substrate and the driving become comparable. Mainly, they found modified asymptotic scaling laws for the lift force, indicating a decrease of the magnitude of the EHD effect due to inner viscous contributions. Later on, Kargar-Estahbanati and Rallabandi [55] employed Lorentz's reciprocal theorem to derive a general integral relation between the soft-lubrication lift force and the linear response function of the soft substrate. They first analyzed the lift force as a function of Poisson's ratio and thickness of the elastic material. Moreover, they found a superposition of steady and oscillating modes whose amplitudes and phases contain information about the elastic and viscous components of the material response, thus opening the way to the fine characterization of the mechanical properties of materials via lift force measurements. Compared to normal mode excitations [13, 19–29], the interest of the lift-force mode for such a purpose is rooted in Eq. (2), where a $\sim V^2$ dependency appears. Therefore, with a sinusoidal excitation, a frequency doubling is expected, thus enabling the use of a region of the spectrum that is disconnected from the excitation one.

As introduced above, Winkler's foundation is the simplest linear and local elastic model (see Fig. 5) [34]. Since it avoids the complication of nonlocal responses associated with elastic materials, it is often used as a simplified model for thought. A natural question emerging from that is how valid such a model is to describe actual physical systems, with a particular focus on the lift problem. In particular, in the limit of strictly incompressible and thin elastic layers, one expects an infinite resistance to deformation, and hence the Winkler's approach breaks down. Chandler and Vella [57] provided an answer to that by formally deriving a lift force that interpolates between the Winkler and incompressible limits for thin elastic layers. They found that the applicability of the Winkler model is not determined by the value of the Poisson ratio alone, but by some compressibility parameter that combines the Poisson ratio with a measure of the layer slenderness, which depends on the problem under consideration. Essentially, for Poisson ratios strictly smaller than 0.5, the crossover to Winkler's model as the thickness is reduced is rooted in the elastic Green's function itself [13, 55].

Finally, the effective compliance of a material, and the lift force as a consequence, can be increased tremendously by using slender geometries, such as membranes and plates. The EHD coupling in such systems was addressed by Daddi-Moussa-Ider and collaborators [58, 59]. In the first article, the authors computed the leading-order frequency-dependent translational and rotational mobilities of an axisymmetric particle immersed in a viscous fluid and moving near an elastic cell boundary allowed to stretch and bend. The authors found that the translation-rotation coupling mobility is primarily determined by bending, whereas shearing mostly affects the rotational mobility. In the second article, the authors derived the lift force exerted on a rigid spherical particle translating parallel to a finite-sized membrane. Specifically, the Lorentz reciprocal theorem was employed, as well as a perturbative expansion for small deformations of the membrane. The authors reported interesting attractive and repulsive regimes depending on the dominant elastic mode at play.

As a concluding remark, we expect no qualitative difference between the two dual situations of a rigid particle near a soft wall and vice versa. This is reminiscent of the admitted equivalence in dry elastic contacts [60, 61].

Experimental pieces of evidence

Despite the above abundant theoretical literature, experimental evidence for such a soft-lubrication lift force in soft matter is recent and scarce.

A preliminary qualitative observation was reported in the context of smart lubricants and adsorbed polyelectrolytes by Bouchet *et al.* [39]. The authors investigated the lubricant properties of a strong polyelectrolyte, in aqueous solutions of different salt concentrations. They first studied how the morphology of the adsorbed layer could be modified by increasing the salt concentration. Then, a complex velocity dependence of the friction was observed, with a maximum value at intermediate velocities and even some hysteresis. A progressive increase in separation between the rubbing surfaces with velocity was also observed (see Fig. 6). These observations were discussed in terms of a possible indication of the presence of a soft-lubrication lift force.

A first quantitative study, by Saintyves *et al.* [41], showed an effective reduction of friction induced by the soft-lubrication lift force. The authors employed a fluid-immersed negatively buoyant macroscopic cylinder moving along a soft inclined wall. They observed a steady-state sliding regime with an effective friction that was significantly reduced relative to the rigid case (see Fig. 7). The observations were rationalized by invoking the soft-lubrication lift. This study was followed up by a work dedicated to the rotational motion of the cylinder [62]. The authors experimentally quantified the steady spinning of the cylinder and theoretically showed that it is due to an aspect-ratio dependent combination of a soft-lubrication torque generated by the flow and the viscous friction on the edges of the finite-length cylinder. The experimental results were consistent with a transition from an edge-effect dominated regime for short cylinders to a gap-dominated soft-lubrication regime when the cylinder is very long. A puzzling

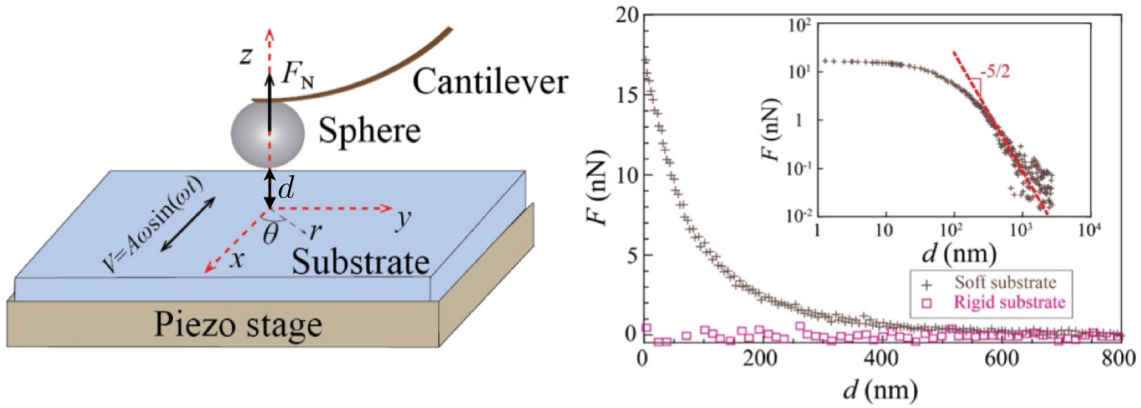

Figure 11. *(left) A soft substrate is fixed atop a rigid piezo stage that is transversally oscillated along time t, at angular frequency ω and with amplitude A. A rigid sphere is glued to an AFM cantilever and immersed in a viscous liquid lubricant near the substrate. The normal force F_N exerted on the sphere at a given distance from the surface is directly measured from the deflection of the cantilever along z. (right) Temporal average F of F_N as a function of the gap distance d to the substrate, for both rigid (silicon wafer) and soft polydimethylsiloxane (PDMS) substrates. The inset shows a log-log representation of the data for the soft substrate where the solid line indicates a* $-5/2$ *power law characteristic of an EHD lift force in the case of a semi-infinite incompressible elastic substrate [37]. Figure adapted from [56].*

feature about these two studies is the fact that the Winkler's foundation describes best the observations, despite the rather incompressible character of the elastomers used. The answer to that puzzle might be given by Chandler and Vella [57] in the lift context. Indeed, for Poisson's ratios strictly smaller than $1/2$, an incompressible layer will eventually behave as a compressible one for small-enough film thicknesses.

Subsequently, an experimental study by Davies *et al.* [45] revealed the significance of the soft-lubrication lift force in biological and microscopic settings. The authors addressed the motion of glass microbeads in a linear shear flow close to a wall bearing a thin soft biomimetic polymer brush. Combining microfluidics and optical tracking, they demonstrated that the steady-state bead-to-surface distance increased with the imposed shear rate (see Fig. 8). The article is concluded by physiological estimates, indicating the potential relevance of the effect for the transport of red blood cells – and thus for life processes.

The same year, a macroscopic study by Rallabandi *et al.* [46] demonstrated the large amplification of the soft-lubrication lift for very compliant boundaries associated with slender geometries (see Fig. 9). The authors combined theory and experiments in order to show that a small particle moving along an elastic membrane through a viscous fluid is repelled from the membrane due to soft-lubrication forces. An analytic expression for the particle trajectory is derived, including a normal migration velocity of the particle that is quadratic in speed and depends on a combination of the tension and bending resistances of the membrane. The quantitative agreement with the theoretical predictions with no fitting parameter indicates once again the presence and relevance of the soft-lubrication lift force. Furthermore, due to the slenderness of the membrane, the effective compliance is large and the effect is strong enough for separation and sorting of particles on the basis of both their size and density. Once again, the relevance for biology – where membranes are widespread – is discussed.

The above recent experimental literature provides confidence in the existence of the soft-lubrication lift force, as well as in its importance at small scales and for biology. However, in these works, the quantitative evidence for the soft-lubrication lift is only indirect since only trajectories and effective friction coefficients are typically measured. A direct measurement was thus needed. The first SFA and AFM direct force measurements of the soft-lubrication lift force at the nanoscale were performed by Vialar *et al.* and by Zhang *et al.* respectively [47, 56]. On the one hand, in the former SFA study, the authors investigated the behavior of mica surfaces coated with microgels under shear and compression. The emergence of velocity-dependent, shear-induced normal forces was observed and quantified (see Fig. 10). Moreover, the data are in agreement with the soft-lubrication lift force but revealed a counterintuitive value of the microgel elastic modulus. On the other hand, Zhang *et al.* employed an AFM colloidal probe near an horizontally-oscillated elastomeric layer and measured the average lift force as a function of the gap size (see Fig. 11), for various driving velocities, viscosities, and stiffnesses. The results are in agreement with a quantitative model developed from the soft-lubrication theory for small compliances [52]. For larger compliances, or equivalently for smaller confinement length scales, an empirical scaling law for the observed saturation of the lift force is proposed and discussed. This high-loading conjecture should be compared in future to recent theoretical developments [49].

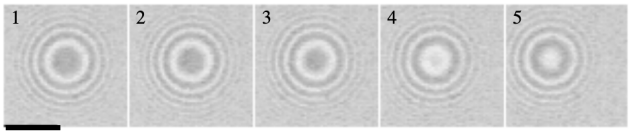

Figure 12. *Shear-induced unbinding of a vesicle: successive RICM images of the contact area of the vesicle with the substrate are shown. The evolution of the interference pattern denotes an increase of the vesicle-to-substrate distance. Figure adapted from [63].*

ELASTOHYDRODYNAMIC LIFT IN EXTERNAL FLOW

From soft lubrication to bulk elastohydrodynamics

At the turn of the millennium, key articles have addressed intermediate – and complex – configurations which are relevant to microfluidics [63–65]: an immersed particle in near-contact elastohydrodynamic interaction with a wall in the presence of external shear forces due to flow.

The lift force upon detachment acting on a heavy, quasi-spherical lipid vesicles lying on a substrate has been determined experimentally by Lorz et al. using RICM technique, that allows to accurately determine the gap profile between a particle and a substrate, if of order some hundreds of nanometers [63] (Fig. 12). They compared it with the expression proposed by Bruinsma [66] in the framework of soft lubrication theory, for a quasi-spherical particle with given surface tension and found that the measured force was 2 orders of magnitude larger than that predicted by this theory. The missing brick was claimed by Seifert in Ref. [65], whose prediction for the lift force matched the experimental one. In a letter published simultaneously in the same journal Cantat and Misbah also provided an expression for the lift force [64]. Both groups considered a vesicle pinned to a rigid substrate by an adhesive potential, and determined, using similar approaches, the lift force acting on the vesicle as it is pinned to the wall at a given distance from it (given by the location of the minimal potential of energy), while being still able to deform and open an asymmetric gap between its surface and the wall, following soft lubrication mechanism. Cantat and Misbah considered a 2D vesicles whose asymmetry is essentially described by its front and back curvatures (allowing for feedback between gap shape and flow stress through the curvature energy of the membrane), and found a $h^{-1/2}$ dependency for the lift force. Seifert considered a 3D vesicle but assumed a linearly increasing gap, and used the adhesion energy as a control parameter, rather than the curvature energy. He found a h^{-1} dependency for the lift force. Both forces depend quadratically on the shear rate, as in other soft lubrication configurations (Table I). However, the exponents that characterize the dependency with gap thickness h are different. Interestingly, Cantat and Misbah also ran numerical simulations of the lift force as a function of shear rate and highlighted a transition between the quadratic regime, when the vesicle is pinned, to a linear regime, when the vesicle is detached. This points to the fact that while the opening of an asymmetric gap is, in the soft lubrication regime, the result of local equilibrium between flow stress and particle elasticity, the shape of the vesicle that is far from the wall is governed by the sole interaction with the bulk flow. For vesicles, it turns out to be independent from the shear rate because of the membrane incompressibility. This regime of shear-induced lift will be discussed in the present section. More recently, a similar case of coupling between adhesion forces and shear-induced lift has been studied for drops on a deformable polymer brush, leading to complex phase diagrams [67].

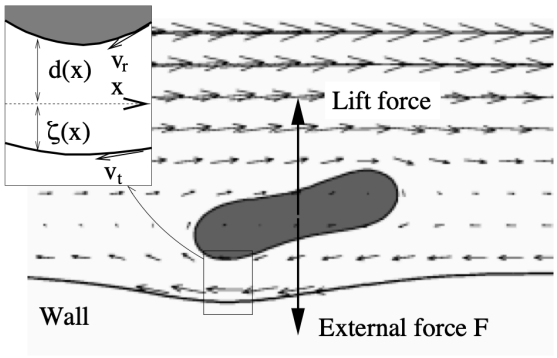

Figure 13. *A deformable particle in a shear flow is elongated and tilted, resulting in a lift away from the wall. In the meantime, deformation of the neighboring elastic wall also induces lift, as in Fig. 4. Figure adapted from [40].*

Another interesting combination between shear-induced lift and soft lubrication is particularly visible in the previously discussed work of Beaucourt et al. [40], where the lift exerted on a sheared particle near a soft wall is calculated in a 2D framework. In addition to substrate elasticity, the authors add the possibility of cell deformation due to the shear flow ; they show that the maximal lift force — which we recall to be apparently a 2D feature — is always reached at similar wall rigidities, but that it increases with cell deformability (see Fig. 13). This article opens a long series of works devoted to the impact of cell deformability under shear flow on the lift force, without considering the effect of wall deformability. Yet, deformation of the particle by its interaction with the wall is still possible in this configuration, and we shall discuss the crossover between the pure shear-induced lift regime and a mixed regime where the soft-lubrication correction must be considered.

Dynamics of deformable particles under shear flow

As particles get further from the wall the hydrodynamic interaction weakens, so does the resulting deformation and subsequent lift force. Yet, if another mechanism maintains the shape asymmetry, lift forces may not decrease as quickly. A prominent example is that of particle asymmetry induced by velocity gradients. The elongational component of the flow,

which is aligned at 45° relatively to the flow direction for a simple shear flow tends to elongate a deformable particle in its direction. Depending on the mechanical properties of the particle, this may result in a fore-aft asymmetry leading to the apparition of a lift force.

Before going further, a quick overview on the dynamics of soft particle under shear flow is needed here, with the aim to focus on the main information needed to understand the dependency of the amplitude of the lift force with the mechanical properties of the considered particle. A non-spherical rigid particle cannot maintain a steady shape under shear flow, due the rotational component. Yet, its transient configuration will exhibit fore-aft asymmetry leading to the apparition of a lift force, whose sign depends on the angle of the particle. Particle with liquid cores can maintain a fixed shape under shear flow while accommodating the rotational stresses by a rotation of their inner fluid. The way they do so depends on the detail of their mechanical properties. Different types of particles are met in the literature.

In this review, the term vesicle will be used to designate a drop of liquid encapsulated by an incompressible elastic layer. The sole elastic deformation energy of this layer is thus associated to bending. In particular, initially spherical vesicles are non-deformable, by virtue of incompressibility of the membrane and of the encapsulated fluid. Vesicles have long been considered as model systems to mimic the main behaviour of more complex cells such a red blood cells. By neglecting the elastic shear contribution of the underlying cytoskeleton, researchers have gained simplicity, that was needed for theoretical modeling purposes and to reduce cost and complexity of numerical simulations. In parallel, models for extensible shells — which are often named capsules — have been developed. Finally, The last ten years have seen the development of more accurate models to describe membranes of cells, that includes the possibility for shear at constant surface in the membrane plane.

The literature on the dynamics under shear flow of liquid drops [68], vesicles [69–89], capsules [90–101], or (models of) red blood cells [102–119] is extended and is still being enriched by studies of increasing refinement in the modeling and in the experimental approach. Adding more complexity to the rheological properties of the membrane leads in general to more complexity in the diagrams of dynamical states. The parameters of the system are usually combined in a set of dimensionless numbers such as reduced volume ν (characterizing initial deflation of the object), viscosity ratio λ between the inner and the outer fluid, and capillary number(s) Ca, that compare hydrodynamic shear with either surface tension or bending rigidity or shear elasticity of the membrane.

An oversimplified picture is that for low λ and high C_a, particles adopt a drop-like behaviour, called tank-treading (TT), where the particle keeps a constant angle θ (see Fig. 14 for notation) relatively to flow direction. For high λ or low C_a, particles behave more like solids and tumble under flow, with a periodic evolution of θ. In between, a rich zoology of motions has been described, from small oscillations around a given angle to off-plane orbital motion. The oscillations of the main axis of the particle is often accompanied by shape oscillations of more or less important amplitude. For ellipsoidal rigid particles, orbits have been exactly described by Jeffery [120] ; this description is also a good proxy for tumbling motion of not too deformable particles like red blood cells [116] or capsules [98] under moderate shear flow.

Far-field interaction with a rigid wall

If a particle is far enough from the wall, the elastohydrodynamic problem decouples as one can first determine the shape from the interaction between the flow and the particle, neglecting the influence of the wall, then consider the resulting drift velocity that emerges by making the flow perturbation due to the flowing body compatible with the boundary conditions on the wall. This corresponds to the 0^{th} order in the soft lubrication approach, which is sufficient here as the required asymmetry is maintained by another mechanism than the direct interaction with the wall.

A fundamental example of this approach is the one of a tank-treading ellipsoidal vesicle in a simple shear flow near a wall, whose dynamics can be calculated independently from the presence of the wall. By setting that the lift velocity of the particle is such that this velocity added to the velocity perturbation due to the particle must vanish on the wall, Olla showed that in the absence of other forces (*e.g.* buoyancy), the lift velocity U_{L} scales as [121, 122]

$$U_{\mathrm{L}} = AR^3|\dot{\gamma}|/z^2 \ . \tag{10}$$

In this expression, $z \simeq h + R$ is the particle-to-wall distance, R a characteristic size of the particle, $\dot{\gamma}$ the shear rate and A a dimensionless prefactor that depends on the cell geometry and mechanical properties. Another theoretical modeling, not assuming ellipsoidal shape a priori, has later on led to the same result [123].

Indeed, this scaling is generic and can be proven by different means. Here, we will first introduce the boundary integral formalism to solve the Stokes flow due to the force distribution on the particle surface ; it will also allow to discuss the different contributions to the lift force, be it far or close to the wall, as developed in particular by Nix et al. in [124]. We generalize their work in a first step to a larger class of particle than that considered by the authors (capsules with no viscosity contrast between the inner and outer fluid), also using the reference work on boundary integral method by Pozrikidis [125] and that of Zhao et al. [126] on the migration of lipid vesicles.

To facilitate the notations and summations, we introduce the position vector $\mathbf{x} = (x_1, x_2, x_3)$, where x_1 corresponds to the flow direction, and x_3 to the direction perpendicular to the wall (located at $x_3 = 0$), i.e. to z in Fig. 2.

Following [125], the flow field at any point $\mathbf{x}_0$ outside the

particle reads

$$u_j(\mathbf{x}_0) = u_j^{\infty}(\mathbf{x}_0) - \frac{1}{8\pi\mu}\int_S \sigma_{ik}(\mathbf{x})n_k(\mathbf{x})G_{ij}(\mathbf{x},\mathbf{x}_0)dS + \frac{1}{8\pi}\int_S u_i(\mathbf{x})T_{ijk}(\mathbf{x},\mathbf{x}_0)n_k(\mathbf{x})dS \quad (11)$$

Here, $\mathbf{u}^{\infty}$ is the imposed flow, σ is the fluid stress tensor such that $\mathbf{f}^{ext} = \sigma \cdot \mathbf{n}$ is the force distribution acting on the surface. We recall that μ is the viscosity of the fluid. $\mathbf{G}$ is the Green's function that is adapted to the boundary condition of the problem and $\mathbf{T}$ is the associated stress tensor. The second and third term of the right-hand side of the equation are called the single and double layer potentials, respectively. In order to account for the presence of body forces, σ can be replaced in the above expression by the modified stress tensor such that $\sigma_{ij}^{MOD} = \sigma_{ij} + \rho\mathbf{g}\cdot\mathbf{x}\delta_{ij}$ [125]. Here, $\mathbf{g}$ is the acceleration field, like gravity, and ρ is the associated quantity, like fluid density. Keeping this in mind, we will drop the MOD superscript from now on.

A more convenient expression can be obtained when one knows the specific mechanical properties of the particle boundary. A widely considered configuration is that of a 2D interface delimiting the interior of the particle, filled with a fluid of viscosity $\mu' \equiv \lambda\mu$ from the surrounding fluid. In that case, Eq. 11 becomes [125]

$$u_j(\mathbf{x}_0) = u_j^{\infty}(\mathbf{x}_0) - \frac{1}{8\pi\mu}\int_S \Delta f_i(\mathbf{x})G_{ij}(\mathbf{x},\mathbf{x}_0)dS + \frac{1-\lambda}{8\pi}\int_S u_i(\mathbf{x})T_{ijk}(\mathbf{x},\mathbf{x}_0)n_k(\mathbf{x})dS. \quad (12)$$

Here, $\Delta\mathbf{f} = \mathbf{f}^{ext} - \mathbf{f}^{int} = (\sigma^{ext} - \sigma^{int}) \cdot \mathbf{n}$ is the discontinuity in the interfacial surface force. It can be written as $\Delta\mathbf{f} = (\rho^{ext} - \rho^{in})\mathbf{g}\cdot\mathbf{x}\,\mathbf{n} + \Delta\xi$, where $\Delta\xi$ is the discontinuity in the surface force that depends only on the interface mechanical properties. For a given model of particle (e.g. a drop, a vesicle, a capsule), and in the absence of significant inertia of the membrane, it can be calculated according to the chosen constitutive law for the surface, as it must equal the opposite of the membrane load. Regarding numerical simulations, Eq. 12 can be implemented to compute the particle dynamics according to a two-step process where first the displacement of the particle membrane is calculated according to Eq. 12, after what the force ξ can be calculated in this new configuration, and so on. This so-called boundary integral method has given rise to several developments regarding numerical schemes be used, following the seminal work of Pozrikidis [127]. In particular, it has successfully been used to describe the motion of drops [128], vesicles [123, 126, 129–131] or capsules [96, 124, 132] in the vicinity of walls. To do this, Green's function that are adapted to the considered boundary conditions must be used, which we describe below. Note that Eq. 12 does not provide a direct expression for the velocity as it appears on both sides of the equation, when $\lambda \neq 1$. This requires to implement adapted numerical schemes to ensure convergence.

For an unbounded domain, the Green's function is called the Stokeslet and describes the flow field created by a point force. We will denote it as $\mathbf{G}^{\infty}$ and it reads

$$G_{ij}^{\infty}(\mathbf{x},\mathbf{x}_0) = \frac{\delta_{ij}}{r} + \frac{r_i r_j}{r^3}, \quad \text{where } \mathbf{r} = \mathbf{x} - \mathbf{x}_0. \quad (13)$$

The associated stress tensor is

$$T_{ijk}^{\infty}(\mathbf{x},\mathbf{x}_0) = -6\frac{r_i r_j r_k}{r^5}. \quad (14)$$

The Green's functions we need here is that satisfying the no slip condition on the wall. A calculation of this semi-infinite Green's function has been proposed by Blake in [133], using Fourier transform. It can be thought as the Green's function associated with other point singularities located at the reflection point $\mathbf{x}^{IM} = (x_1, x_2, -x_3)$ of the initial force. Interestingly, in [133], this interpretation in terms of singularities is obtained a posteriori, after the direct calculation is lead. We are not aware of any direct construction of the semi-infinite Green function based on adequate considerations on the singularities to be chosen to satisfy, at the end, the correct boundary conditions on the wall.

The semi-infinite Green's function reads $\mathbf{G} = \mathbf{G}^{\infty} + \mathbf{G}^{w}$, where the wall Green's function $\mathbf{G}^{w}$ is given by

$$G_{ij}^{w}(\mathbf{x},\mathbf{x}_0) = -G_{ij}^{\infty}(\mathbf{x}^{IM},\mathbf{x}_0) - 2x_3 G_{ij}^{SD}(\mathbf{x}^{IM},\mathbf{x}_0) + 2x_3^2 G_{ij}^{D}(\mathbf{x}^{IM},\mathbf{x}_0), \quad (15)$$

where

$$G_{ij}^{SD}(\mathbf{x},\mathbf{x}_0) = (1-2\delta_{j3})\Big(\frac{\delta_{ij}r_3 - \delta_{i3}r_j + \delta_{j3}r_i}{r^3} - \frac{3r_i r_j r_3}{r^5}\Big) \quad (16)$$

is a Green's function associated with a Stokeslet doublet and

$$G_{ij}^{D}(\mathbf{x},\mathbf{x}_0) = (1-2\delta_{j3})\Big(\frac{\delta_{ij}}{r^3} - \frac{3r_i r_j}{r^5}\Big) \quad (17)$$

is a Green's function associated with a source doublet. By Green's function associated with a doublet, we mean the Green's function allowing for the calculation of the far-field velocity associated with a pair of singularities of opposite sign or direction located at a finite distance.

Similar expressions exist for the stress tensor $T_{ijk} = T_{ijk}^{\infty} + T_{ijk}^{w}$, which can be found in [125], p. 85.

Contributions to lift velocity

The decomposition of the velocity field into a contribution arising directly from the presence of the particle (through the unbounded Green's function and the associated stress tensor) and one from the presence of a wall makes it tempting to discuss their relative contribution to the lift velocity. However, as seen in the last term of Eq. 12, the coupling between u and T makes this distinction tricky in the general case.

For particle with no viscosity contrast, still, this discus-

sion can be carried out, as in [124]. The lift velocity U_L can be thought as the averaged velocity over the particle volume, which can be transformed into a surface integral for incompressible particles: noting that $\vec{\boldsymbol{\nabla}} \cdot (x_3 \mathbf{u}) = u_3$, one finds that

$$U_L = \frac{1}{V}\int_V u_3 dV = \frac{1}{V}\int_S x_3 \mathbf{u}\cdot\mathbf{n}\, dS, \tag{18}$$

where $\mathbf{n}$ is the unit vector normal to the surface.

In the specific situation where $\lambda = 1$, We decompose this lift velocity into two contributions: a self term U^s that arises from the flow created by the particle, without taking into account the presence of a wall, and the wall term U^w, such that $U_L = U^s + U^w$. They are defined as

$$U^s = \frac{1}{V}\int_S x_3 \mathbf{u^s}\cdot\mathbf{n}\, dS, \quad \text{with} \tag{19}$$

$$u_j^s(\mathbf{x_0}) = -\frac{1}{8\pi\mu}\int_S \Delta f_i(\mathbf{x}) G_{ij}^{\infty}(\mathbf{x},\mathbf{x}_0)\, dS \tag{20}$$

and

$$U^w = \frac{1}{V}\int_S x_3 \mathbf{u^w}\cdot\mathbf{n}\, dS, \quad \text{with} \tag{21}$$

$$u_j^w(\mathbf{x_0}) = -\frac{1}{8\pi\mu}\int_S \Delta f_i(\mathbf{x}) G_{ij}^{w}(\mathbf{x},\mathbf{x}_0)\, dS. \tag{22}$$

In an infinite simple shear flow, the whole configuration has a point symmetry with respect to the centre of the particle. Considering two opposite points on the membrane, one can see that the $\mathbf{u^s}\cdot\mathbf{n}$ terms are equal while the x_3 term has opposite sign, whence $U^s = 0$, as expected. The self term therefore represents the effect of the asymmetrical deformation of the particle — due to the presence of the wall — on the particle displacement due to its own created flow field.

For a capsule in a quite narrow range of capillary numbers (of order 0.1-1), it has been shown numerically in [124] that this self term is negative (that is, the particle is attracted towards the wall). Importantly, this self term decays as $(z/R)^{-4}$, where R is the particle typical size. In that it follows the scaling for the evolution of a geometrical parameters characterizing how far the particle is far from pointwise symmetry.

We make the remark here that, to our knowledge, the scaling for the asymmetric contribution in the self term have not been derived formally. We may assume that, in the far-field limit, it may always be negligible compared to the wall term.

In order to comment on the behavior of the wall term U^w, we first consider its far-field limit, which is often the only one considered in models, being the dominant contribution as soon as the particle is far enough from the wall. To that aim, we re-consider the generic case of λ taking any value, as in [126, 134].

Far from the wall, the velocity U^w of the particle may be approximated by that of its center, that we set to be located at position $\mathbf{x}_0 = (0, 0, z)$. This far-field velocity $U^{w,ff}$ thus reads

$$\begin{aligned} U^{w,ff} = &-\frac{1}{8\pi\mu}\int_S \Delta f_i(\mathbf{x}) G_{i3}^{w}(\mathbf{x},\mathbf{x}_0)\, dS \\ &+\frac{1-\lambda}{8\pi}\int_S u_i^0(\mathbf{x}) T_{i3k}^{w}(\mathbf{x},\mathbf{x}_0) n_k(\mathbf{x}) dS, \end{aligned} \tag{23}$$

where $\mathbf{u}^0$ is the leading order term in the velocity on the particle surface.

$G_{i3}^w(\mathbf{x},\mathbf{x}_0)$ indeed represents the flow field created by the singularities from the image system, located at $\mathbf{x}^{IM} = -\mathbf{x_0}$. For $|\mathbf{x}-\mathbf{x_0}| \ll h$, one can expand $G^w(\mathbf{x},\mathbf{x}_0)$ and $T^w(\mathbf{x},\mathbf{x}_0)$ around $\mathbf{x}_0$, such that:

$$\begin{aligned} U^{w,ff} = &-\frac{1}{8\pi\mu} G_{i3}^{w}(\mathbf{x}_0,\mathbf{x}_0)\int_S \Delta f_i(\mathbf{x})\, dS \\ &-\frac{1}{8\pi\mu}\frac{\partial G_{i3}^{w}}{\partial x_k}(\mathbf{x}_0,\mathbf{x}_0)\int_S \Delta f_i(\mathbf{x})(x-x_0)_k\, dS \\ &+\frac{1-\lambda}{8\pi} T_{i3k}^{w}(\mathbf{x}_0,\mathbf{x}_0)\int_S u_i^0(\mathbf{x}) n_k(\mathbf{x}) dS. \end{aligned} \tag{24}$$

In the absence of external force (like gravity) the first term of the right hand side is zero.

The integral that appears in the second term is the dipolar tensor that characterizes the first moment of the force distribution on the particle surface. Depending on the authors, it is sometimes denoted as D_{ik}. We now turn to the usual decomposition of this tensor (see e.g. [135]):

$$D_{ik} = \frac{1}{3} D_{jj}\delta_{ik} + S_{ik} + T_{ik} \tag{25}$$

.

The first term has no impact on the flow, as can be seen by inserting it in Eq. 24: the resulting term is $\propto \partial G_{k3}^w/\partial x_k$, which is the divergence of the Green's function and is 0 (since this function represents a solution of the incompressible Stokes flow). The traceless symmetric tensor

$$S_{ik} = \int_S \Big[\frac{1}{2}(\Delta f_i (x-x_0)_k + \Delta f_k (x-x_0)_i) - \frac{1}{3}\Delta f_j (x-x_0)_j \delta_{ik}\Big]\, dS \tag{26}$$

is often called the stresslet and its asymmetric counterpart T_{ik} is called the rotlet (or couplet, following Batchelor [136]). The latter is proportional to the torque exerted on the particle and is therefore 0 in the absence of external torque. As the stresslet is symmetric, only the symmetrical part $\frac{1}{2}(\frac{\partial G_{i3}^w}{\partial x_k} + \frac{\partial G_{k3}^w}{\partial x_i})$ of the derivative of the Green's function eventually contributes to the lift velocity. Following [124], we call it K_{i3k}^w.

We now make the remark that $T_{i3k}^w(\mathbf{x}_0,\mathbf{x}_0) = -\delta_{ik} p_j(\mathbf{x}_0,\mathbf{x}_0) + 2K_{i3k}^w(\mathbf{x}_0,\mathbf{x}_0)$, where $\mathbf{p}$ is the pressure vector associated with the Green's function [125]. Since the flux of $\mathbf{u}$ through S is 0, its contribution to the lift is 0. As K_{i3k}^w is symmetric, it will act only on the symmetrical part of last integral of Eq. 24.

Finally, in the absence of external force and torque, the lift

velocity is given by the image system of the complete stresslet Σ_{ik}, acting on the center of the particle. It is given by

$$U^{w,ff} = -\frac{1}{8\pi\mu} K^w_{i3k}(\mathbf{x}_0, \mathbf{x}_0)\Sigma_{ik}, \tag{27}$$

where

$$\Sigma_{ik} = S_{ik} + (\lambda - 1)\mu \int_S (u^0_i(\mathbf{x})n_k(\mathbf{x}) + u^0_k(\mathbf{x})n_i(\mathbf{x}))\, dS. \tag{28}$$

This last expression defines more generally the stresslet, for a larger class of particles than Eq. 26. It should be noted that the second term vanishes not only for particles with no viscosity contrast but also for rigid particles [136].

An expression for K^w_{i3k} can be found in [124]:

$$K^w_{i3k} = \frac{1}{8z^2}(-5\delta_{ik} + 9\delta_{k3}\delta_{j3}). \tag{29}$$

This leads to

$$U^{w,ff} = -\frac{9}{64\pi\mu}\frac{\Sigma_{33}}{z^2}. \tag{30}$$

This results generalizes Eq. 10. By coherence with the leading order approximation we made here, one must keep in mind that the stresslet Σ_{33} is that created by the interaction with the external flow, in the absence of wall. This simpler situation opens the way to theoretical determination of the stresslet ; it is then convenient to check the validity (and the associated domain in the z-axis) through full numerical simulations or experiments. To do, one must keep in mind that while the theoretical approach through the determination of the stresslet will provide the lift velocity at a given position for a particle in its stationary dynamics, simulations or experiments provide full trajectories along which the shape at given position might not be the stationary one. Comparing both approach requires to ensure that the typical time needed for shape change is much smaller than the migration time. A priori, this will be achieved for sufficiently high capillary numbers. In practice, this conditions holds in the situations we will describe below. Also, in simple shear flow, the shape depends only weekly on the position. The situation will be more complex in quadratic flows, which will be shown to trigger more complex couplings between shape and lift direction.

To conclude with our discussion on the different contributions to lift, numerical simulations lead in [124] have highlighted that replacing the far-field stresslet by its value at the considered distance from the wall enhances the lift force. The overall contribution of the wall is shown to be smaller, due to the asymmetric deformation (with respect to the point-wise symmetric shape) that has a negative contribution to the lift velocity, as for the self term. It has been shown that it also varies like $(z/R)^{-4}$.

Lift velocity and lift force, the vesicle case

The case of vesicles is interesting for comparing results from different studies as there are only few parameters involved: for large enough capillary numbers such that the hydrodynamic stress overcomes bending forces, the dynamics of vesicles depends only on their initial deflation and on the viscosity contrast [84]. In the range of parameters where tank-treading motion occurs, the shape and angle of inclination of the vesicle are therefore independent of the shear rate, so is the prefactor A given by Olla in Eq. 10. Similarly, the stresslet should scale with the shear rate. We are not aware of studies on lift of vesicles at small capillary numbers, when wrinkles appear due to hydrodynamic forces or Brownian fluctuations and modify the nature and the transition between dynamical regimes in unbounded shear flow [73, 137, 138].

Two different sets of experiments are available in the literature that describe the lift of vesicles of radius of order 10 microns: the lift velocity of vesicles in the absence of gravity has been studied by Callens et al. [139], while the close wall lift force has been measured by Abkarian et al. [72, 140], by balancing it by the vesicle weight.

Experiments for lift velocity were performed in parabolic flights, allowing for successions of normal gravity phases and low gravity phases. In the first phase, sedimentation of vesicles on the bottom plate of a shear chamber allowed for the creation of a well-defined initial condition, while the lift velocity of the vesicle could be measured in the low gravity phase, without being screened by sedimentation. Thanks to this, distances to the wall of up to 7 times the vesicle radius could be explored. Vesicles with inner fluid having the same viscosity inside and outside were studied in [139] while more viscous inner fluids were considered in [141]. In the range $3 \lesssim z/R \lesssim 7$, the distance to the wall is found to scale with time to the power $1/3$, indicating agreement with the far-field scaling. They also found a prefactor that is independent from the shear rate, that was varied by a factor 10. Eventually, sticking to the notations of Eq. 10, the prefactor $A(\nu, \lambda)$ has been determined for reduced volumes $\nu \gtrsim 0.95$ and $\lambda = 1$ [139], 4 and 6.5 [141]. The reduced volume $\nu \leq 1$ characterizes the deflation of the vesicle, therefore its ability to get deformed, and reads $\nu = \mathcal{V}/(\mathcal{A}/(4\pi))^{3/2}$, where $\mathcal{V}$ and $\mathcal{A}$ are the vesicle volume and surface area, respectively. They are both constant due to the inner fluid and membrane incompressibility.

In the experiments by Abkarian et al. [72, 140], vesicles with no viscosity contrast but with density contrast, and $\nu \gtrsim 0.92$, are sheared close to the wall, with shear rates varying by a factor 5 such that different equilibrium positions can be scanned. It is found that at equilibrium the gap h between the vesicle and the wall scales linearly with the shear rate, indicating the following relationship between the lift force F_L:

$$F_L = B(\nu)\mu R^3\dot{\gamma}/h \tag{31}$$

Using both the results of Callens et al. [139] and Abkarian et al. [72, 140] to make comparisons with existing simula-

tions and theories requires first to establish a link between lift velocity and lift force.

In presence of a body force (which is often, in practical cases, gravity), the lift motion is modified and can even vanish if this body force acts opposite to the lift force. Regarding boundary integral framework, the presence of the body force induces an additional term U^g in the migration velocity $U^g = \frac{1}{V}\int_S x_3 \mathbf{u}^g \cdot \mathbf{n}\, dS$, where

$$u_j^g(\mathbf{x_0}) = -\frac{1}{8\pi\mu}\int_S (\rho^{ext} - \rho^{in})\mathbf{g}\cdot\mathbf{x}\, n_i G_{ij}(\mathbf{x}, \mathbf{x}_0)\, dS \quad (32)$$

is the flow field created by the particle due to the presence of a density difference across its membrane. For a sphere of radius R in a unbounded flow, with a gravity field in the direction $-x_3$, solving Eq. 32 would lead to the well-known Stokes law $6\pi\mu R U^g = -P$, where $P = \frac{4}{3}\pi R^3(\rho^{in} - \rho^{ext})$ is the weight of the particle minus the Archimedes force. In presence of a wall at $x_3 = 0$, the expression of G_{ij}^w shows that the first order correction to the velocity would scale like $1/z$. For a sphere settling towards a wall, the full correction for the modified drag force as a function of distance to the wall has been solved by Brenner [142].

$$6\pi\mu R U^g \Lambda(\cosh^{-1}[z/R]) = -P, \qquad \text{with}$$
$$\Lambda(\xi) = \frac{4}{3}\sinh(\xi)\sum_{n=1}^{\infty}\frac{n(n+1)}{(2n-1)(2n+3)} \quad (33)$$
$$\Big[\frac{2\sinh((2n+1)\xi) + (2n+1)\sinh(2\xi)}{4\sinh^2((n+1/2)\xi) - (2n+1)^2\sinh^2(\xi)} - 1\Big]$$

The first order of this correction is given by

$$\Lambda(\cosh^{-1}[z/R]) \simeq 1 + \frac{9}{8}\frac{R}{z}, \quad (34)$$

indicating, in agreement with the intuition, that the presence of the wall increases the drag on the particle.

For deformable particles, this expression of the drag force can be considered as a proxy but one should keep in mind that, even in the absence of external flow, density mismatch between a particle an the surrounding fluid is sufficient to deform it [143, 144].

In the presence of a body force that acts against lift, an equilibrium position in the z direction is found by the particle, corresponding to $U^g + U_L = 0$. Defining the lift force F_L as the force that balances the weight P, one eventually finds, that

$$F_L \simeq 6\pi\mu R U_L \Lambda(\cosh^{-1}[z/R]), \quad (35)$$

where the lift velocity is given by the appropriate expression, and the correction on drag is assumed to be that for a sphere. This expression will serve us as a basis for discussion.

Simulations using boundary integral method have been proposed in several studies [123, 126, 129]. In the absence of gravity, the far-field scaling has been confirmed quantitatively in [129], yet for a narrow range of characteristic parameters of the vesicle. The authors also found that the far-field approximation is valid almost until the particle touches the wall. By contrast, the agreement with the far field approximation is shown to be valid only when $z/R > 4$ in more recent simulations carried out in [126], for $1 \leq \lambda \leq 6$. As seen in Ref. [124] for capsules, the lift velocity close to the wall is smaller than the far-field contribution, confirming on another type of particle the negative contribution of asymmetric (relatively to point-wise symmetry) deformation. By subtracting an extrapolation of the far-field contribution to the total lift velocity (data from Fig. 2 in [126]), we found that this contribution scales also like $(z/R)^{-4}$, as for the capsules in Ref. [124].

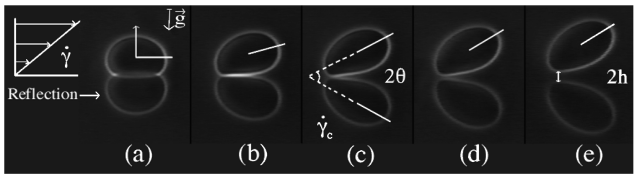

Figure 14. *Sequence of shapes taken by a vesicle as it unbinds and lift away from the wall under simple shear flow. Figure taken from [140].*

All simulations, as well as far-field theoretical calculations lead in [123] that confirmed the far-field scaling of Eq. 30, consider mostly vesicles with reduced volumes higher than 0.95. This corresponds, e.g., to a prolate ellipsoid of long axis 1 and short axis 0.63.

We now address the question of the comparison of these results with the experiments, while also addressing the question of the link between lift force and lift velocity. To that aim, we focus on vesicles with no viscosity contrast and a reduced volume of 0.97, which is documented in experiments [72, 139], simulations by Zhao et al. [126], the model by Olla [122] that assumes ellipsoidal shape and the model by Farutin et al. [123] that makes no assumption on the shape. For all above mentioned studies, but that of Abkarian et al. [72], the lift velocity as a function of distance z between the vesicle centroid and the wall is given, in the absence of gravity. For the sake of comparison with the results of Abkarian et al. [72], we make the assumption that $z = h + R$ (see Fig. 2) and calculate the lift force through Eq. 33. In order to support discussion, the lift force arising from the simulations of Zhao et al. is also calculated using the 1st order approximation of the drag coefficient (Eq. 34) as well as 0th order, i.e. the drag of a sphere in an unbounded flow. The results are presented in Fig. 15.

Regarding far-field behaviour, simulations by Zhao et al. [126], modeling by Farutin et al. [123] and experiments by Callens et al. [139] show very good agreement. By contrast, the lift velocity predicted by Olla [122] is about 30% larger. Comparison between Fig. 7 in Ref. [139] and Fig. 1 in Ref. [123] shows that a vesicle whose shape is not prescribed a priori has a (long axis) / (short axis) ratio that is smaller than that given by the prolate ellipsoid assumption, made by Olla. This may qualitatively explain why, for a given reduced

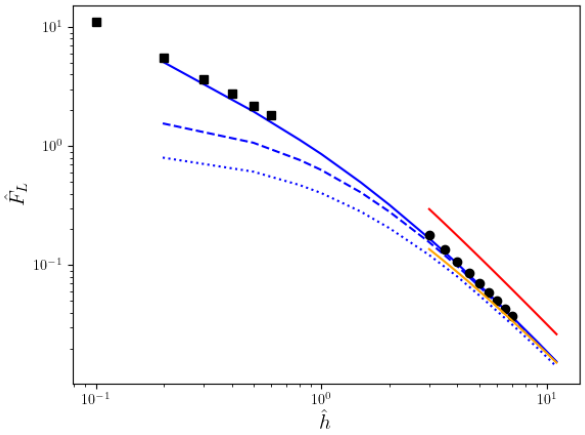

Figure 15. *Dimensionless lift force* $\hat{F}_L = F_L/(\mu\dot{\gamma}R^2)$ *on a vesicle characterized by* $\nu = 0.97$ *and* $\lambda = 1$ *sheared above a wall, as a function of reduced gap size* $\hat{h} = h/R$ *between the vesicle and the wall. R is the radius of a sphere having the same volume as the vesicle. Lines and dots extend on a range where the law has been established in the different studies.* ■*:* $\hat{F}_L = 1.1/\hat{h}$ *according to the close-wall experiments in Ref. [72], Fig. 8. Other data are obtained through* $\hat{F}_L = D\hat{U}_L$ *where* $\hat{U}_L$ *is the dimensionless lift velocity* $U_L/(\dot{\gamma}R)$ *and D the dimensionless drag coefficient, which is taken either as* $D_0 = 6\pi$ *(unbounded domain),* $D_1 = 6\pi(1+9/[8(\hat{h}+1)]$ *(first order approximation of Brenner's drag), or* $D_\infty = 6\pi\Lambda(\cosh^{-1}[\hat{h}+1])$ *(Brenner's drag).* •*:* $D = D_\infty$ *and* $\hat{U}_L = A(0.97)/(\hat{h}+1)^2$ *with* $A(0.97) = 0.11$ *according to the far-field experiments in Ref. [139], Fig. 7 ; Red line: the same with* $A(0.97)$ *given by Olla's model [122] (ellipsoid of aspect ratio 0.705) ; Orange line: the same with* $A(0.97)$ *given by the theoretical model of Farutin et al. (Eq. 5 in [123], for* $\Gamma = 0.021$, Γ *being defined in the referred paper). Note that in Ref. [139], the volume and reduced volumes of the vesicle are known only indirectly through the measurement of its short axis in the vorticity direction and of the projection of its long axis parallel to the z direction. These data are converted into volume and reduced volume through the direct calculation of Farutin et al. [123], which have shown excellent agreement with these experiments [141]. Blue lines:* $\hat{F}_L = D\hat{U}_L$*, where the lift velocity is obtained from direct simulation in [126], Fig. 2 and* $D = D_0$ *(dotted line),* D_1 *(dashed line), or* D_∞ *(full line).*

volume, the lift predicted by Olla is larger than that measured in other studies.

Remarkably, the far field measurements of the lift force by Abkarian et al. [72] are perfectly described by the gravity-free simulations of Zhao et al., who scanned the same range of particle-to-wall distance, providing the drag contribution is that of Brenner for a sphere of equal volume. This agreement is far from being reached if one considers only the 0th (as used in [129]) and 1st order of the drag force.

The conclusion of this aggregation of data is that the $1/\hat{h}$ scaling for the drag force, proposed by Abkarian et al., is therefore recovered, in the close-wall range, by multiplying the multipolar drag coefficient of Brenner with a lift velocity that is composed of a repulsive stresslet contribution that scales as $(\hat{h}+1)^{-2}$ and of an attractive contribution that would be the consequence, by analogy with the analysis of Ref. [124] for capsules, of the asymmetric deformation (with respect to the point-wise symmetry taking place far from the wall). This contribution scales like $(\hat{h}+1)^{-4}$. A geometrical interpretation of this negative contribution is proposed here, based on the observed shape sequences upon unbinding, which are illustrated in Fig. 14 but also seen in numerical simulations for vesicles or capsules [124, 129]. Far from the wall, the vesicle adopts an orientation that roughly follows that of the elongational component of the flow, i.e. 45° relatively to the flow direction. So does its bottom membrane, on average (Fig. 14 (e)). Closer to the wall, the shape of the bottom end of the particle, which is close to the wall, is controlled by the local interaction with the wall, which creates, as in the soft-lubrication framework depicted in Fig. 4, a quasi-horizontal gap with a small opening angle (Fig. 14 (c,d)). Compared to the high opening angle induced by the bulk flow, this reduces the fore-aft asymmetry of the particle, hence a negative correction to the lift velocity. In future works, it would be interesting to examine this hypothesis by comparing the amplitude and scaling of this negative contribution to the lift force of a similar particle moving along the wall without external shear flow (i.e., in the typical soft-lubrication configuration).

Zhao et al. have also run simulations including gravity and found good agreement with the experimental data of Abkarian et al. In the same paper, they compare their simulations of the lift force with the that calculated from the lift velocity times a first order expression for the drag (as in Eq. 34). Unfortunately, we are not able to comment on this approach by lack of definition of some parameters and of detail of calculation by the authors. Other direct simulations of vesicles under gravity have been performed in Ref. [131], but they consider a 2D system. On a quite narrow range of distances, the authors found that the force scales like $1/z^2$ even for z/R close to 1.

We now discuss the evolution of the lift amplitude with the mechanical properties of the vesicle, that are documented in [123, 126, 131, 141]. For a vesicle with no viscosity contrast, the more deflated the vesicle, the faster it migrates, which is due to its increased fore-aft asymmetry. For a given reduced volume, increasing the viscosity contrast leads to a decrease of the inclination angle, therefore of the lift force. For high enough viscosity contrast, increasing asphericity can lead to transition towards tumbling motion, which is preceded by a decrease of the inclination angle, therefore of the lift velocity. To our knowledge, this decrease has not been observed experimentally, but similar phenomena has been shown in Poiseuille flow [130], as will be discussed later on.

In their 2D simulations, Meßlinger et al. have considered the case of tumbling vesicles and shown a non-zero lift force on average, by contrast with the case of a purely rigid object [131]. The reason stems from the elongational component of the flow that makes the vesicle be more elongated when its long axis is along this component than when it is orthogonal to it. Over one rotation period the mean shape is therefore not fore-aft symmetric. Still the mean lift velocity remains much smaller than in the tank-treading regime. A more formal

discussion on this aspect can be found in Ref. [145].

Other particles

We review now the available works from the literature that essentially confirmed Eq. 30, and go discussing what are the limits of this far-field approximation.

Red blood cells Though they are rather complex objects, we start with red blood cells, whose incompressible membrane justifies to make a parallel with the behaviour of vesicles, though the presence of the underlying elastic cytoskeleton induces more complex dependency with the capillary number.

In physiological conditions, red blood cells flow in vessels where the maximal shear rate ranges from 20 to 1500 s^{-1}. In these conditions, cells will essentially exhibit a tumbling-like motion that couples with strong deformations [111, 116].

As seen in Ref. [131] for tumbling vesicles, isolated red blood cells may still migrate. This has been confirmed experimentally in simple shear - like flow (in a large pipe in reality) in the 70' by Goldsmith, who highlighted a 4 μm transverse drift for cells having travelled 1 cm in the flow direction [11]. More than 40 years later, a study in microgravity conditions, similar to that carried out for vesicles in Ref. [139], has quantified the lift of red blood cells in a narrow range of shear rates $10 \leq \dot{\gamma} \leq 50$ s^{-1} [146]. The far-field scaling has been confirmed, with a prefactor $AR^3 = 0.36$ μm^3 (following the notations of Eq. 10) in physiological conditions (i.e. an external fluid of viscosity 1.4 mPa.s close to that of plasma). This factor is increased by a factor 15 if the viscosity is multiplied by 9, indicating the impact of flow stress on the deformation of the cells, that are more elongated and can even make a transition towards a tank-treading like motion [108, 116]. Considering that red blood cells have a mean volume of 90 μm^3 [147], whence $R = 2.8\,\mu$m, this leads to a prefactor A between 0.016 (tumbling-like regime) and 0.15: this latter value is comparable to that found for a vesicle in tank-treading regime.

The value for the lift velocity found in physiological conditions has been calculated to be compatible with the pioneering result of Goldsmith [11]. It should be noted that, at a distance e.g. 4 μm from the wall the lift velocity is about 2 μm/s at a shear rate of 100 s^{-1}, which is comparable to sedimentation velocity [148]. This illustrates the difficulty in measuring experimentally far-field lift velocities.

While numerical simulations of red blood cells under flow are now numerous, we have found no records for this geometrically simple configuration of simple shear flow near a wall, as far as realistic 3D simulations of cells are concerned. We shall come back to this point later on while discussing collective effects.

Capsules. Regarding the impact of mechanical properties, it is shown in Ref. [134] that an increase in viscosity contrast leads to a decrease in lift velocity, as for vesicles. They show that this is the direct result of the increase of the second term in the stresslet expression (Eq. 28), although the first term S_{33} decreases.

In their numerical study, Nix et al. have shown that an increase in the capillary number leads to an increase of the stresslet therefore to an increase of the far-field lift velocity (see Fig. 16) [124]. This result is not that intuitive and it is difficult to extrapolate further than the range explored in their study: as the shear rate is increased, capsules adopt a smaller angle compared to the flow direction but also elongate (contrary to vesicles) [149, 150]. In parallel, as the negative contribution of the term related to particle asymmetry depends more strongly on the capillary number, the range of validity of the far-field approximation depends on this capillary number: as can be seen in Fig. 16, while the far-field approximation is valid even for particles in contact with the wall at low capillary number, this approximation is valid only when $h/R \gtrsim 3$ for a capillary number one order of magnitude larger.

The same range of transition distance between the far-field regime and a more complex set of contributions has been highlighted the same year in Ref. [134], where capsules with different viscosity contrasts are also considered. Again, the lift velocity close to the wall is smaller than the far-field contribution. Phenomenological correction to account for this effect is proposed by the authors.

It should be kept in mind that the vicinity of the wall does not necessarily lead to a decrease of the lift velocity, compared to the far-field contribution: it also depends on the specific interplay between particle dynamics and the presence of the wall. In Ref. [151], a 2D capsule that would tumble in an unbounded flow is maintained close to a wall by a gravity force of varying intensity. The proximity with the wall induces a change in the dynamics that switches from tumbling to tank treading as the force is increased. As a result, the lift velocity increases, such that, in the rather narrow range of parameters explored by the authors, a quasi constant equilibrium height is observed while the force is multiplied by a factor 4.

Finally, for capsules, we have not found any experimental study regarding their lift under simple shear flow.

Drops. Lift on drops of viscosity contrast 0.083 has been experimentally measured by Smart and Leighton in 1991 [152]. Since then, we have found no record of another attempt to measure directly this lift in a simple shear flow ; other works include drop-drop interactions, that will be discussed further. They found that the far-wall velocity follows Eq. 30, and more precisely that

$$U_L = \alpha C_a \dot{\gamma} \frac{R^3}{z^2}. \tag{36}$$

The capillary number C_a reads, in the case of drops, $C_a = \mu\dot{\gamma}R/\sigma$, where σ is the surface tension. The dependency of the prefactor with the capillary number indicates that upon an increase of the flow stress (compared to the elastic restoring force), the drop elongates more, thus inducing a larger lift force.

Expression 36 is similar to that theoretically derived both by

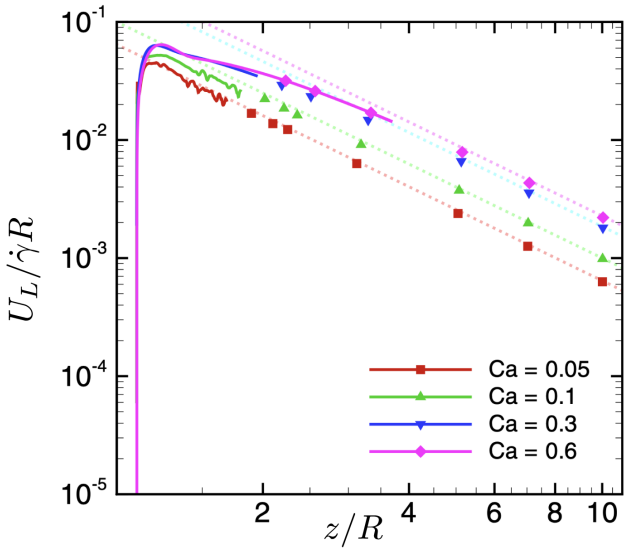

Figure 16. *Lift velocity in simple shear flow for a capsule with a membrane following Neo-Hookean law. Dots and full lines correspond to simulations while the doted line is the far-field approximation (Eq. 30). Figure adapted from [124].*

Chan and Leal [153] and Smart and Leighton [152], under the hypothesis of large distance to the wall and small deformation (hence the linear dependency with C_a). They both proposed an expression for α, which depends on the remaining characteristic parameters λ, the viscosity contrast between the inner and the outer fluids. Both expressions are different but vary by at most 2 % on the whole range of viscosity contrast. $\alpha(\lambda)$ was found to be an increasing function of λ, yet with small variations, from 0.58 when $\lambda \to 0$ to 0.69 when $\lambda \to \infty$. These theoretical results do not match the experimental results, where the lift amplitude is found to be almost 2 times stronger.

Numerical simulations generally find a lift velocity that is slightly smaller than in theoretical works, therefore they agree even less with experiments [128, 134, 154, 155]. These simulations also explored the short-distance behaviour, where a decrease of the lift velocity is observed, compared to the far-wall expression. As for the lipid vesicles of Ref. [126], and as shown in [124] for capsules, we found that the remaining contribution, once the extrapolation of the far field contribution is subtracted, is negative and scales like $(z/R)^{-4}$ (data from Ref. [128], Fig. 5).

With drops, another configuration of interest has been studied by Smart and Leighton, that of a free surface instead of a rigid wall [152]. In this case, the overall expression for the far-surface lift velocity (Eq. 30 is unchanged, but a multiplicative factor 2/3 is introduced. As the stresslet Σ_{33} is that given by the bulk flow, we expect the expression given by the authors to be valid not only for the drops they study. Experimentally, as for the lift due to a rigid wall, their experimental results are above the theoretical prediction.

Lift in unbounded Poiseuille flow: "soft-lubrication without walls"?

Lift in channel flow is the other configuration explored in the literature, as it is relevant for particle handling in microfluidic devices, and to understand biological flows such as blood flow especially.

These flows are characterized by the increased presence of walls but also by linear variations of the shear rate. For large channels (compared to particle size) and in order to gain fundamental understanding of the lift mechanism, it is insightful to consider the case of an unbounded Poiseuille flow that is, a parabolic velocity profile with no walls imposing a condition of zero velocity.

In the soft lubrication framework, the necessary breaking of the bottom-up symmetry in terms of pressure (see Fig. 2 for convention on directions) is obtained by the presence of a wall. The pressure gradient that is created between the particle and the wall is different from that on the other side of the particle, leading to different deformations patterns at the bottom and at the top of particles, eventually leading to the fore-aft asymmetry that induces an overpressure below the particle and makes the apparition of the lift force possible.

This sequence is indeed also possible in the configuration of an unbounded Poiseuille flow where a particle is surrounded by different shear rates on both sides, except when it is located on the central line of the flow. This situation can create an asymmetry in the deformation patterns along the flow direction, making thus possible the apparition of a net lift force. Notably, while in the soft-lubrication framework the creation of a gap resembling that of the Reynolds slider makes it intuitive the sign of the lift force, the deformation arising on both sides of the particle leads to a less clear situation.

Indeed, several scenarii have been predicted. For a drop in a 2D parabolic flow, Chan and Leal have predicted that a drop would migrate outward for a viscosity ratio $0.71 \lesssim \lambda \lesssim 11.35$ but towards the central line for other values of λ [153, 156]. For an axisymmetric Poiseuille flow, the interval for outward migration becomes $0.56 \lesssim \lambda \lesssim 10.2$.

Theoretical and numerical studies on vesicles have shown that vesicles apparently behave differently: in [157], 2D numerical simulations of vesicles with $\lambda = 1$ have evidenced inward migration at almost constant velocity along the trajectory but at the very end, when the particle meets the central line. This results have been confirmed in [158] through a theoretical approach valid in the small deformation approximation. For all λ such that a tank-treading motion takes place, an inward migration is predicted. A tentative physical argumentation in favor of this migration has been given in this paper, which is reported in Fig. 17. Similarly, capsules have been theoretically shown to migrate towards the centerline, in the limit of small deformation (small capillary number) and viscosity contrast smaller than 1 [159].

More systematic theoretical studies performed in [123, 160] for a 3D, axisymmetric flow has however revealed a much more complex situation, for a vesicle of given reduced volume $v = 0.9$. The behaviour strongly depends on the capillary number C_a and on the viscosity ratio λ. For $\lambda = 1$, vesicles migrate towards the center at high capillary number, at a constant velocity but in the vicinity of the center. This situation corresponds to the case most easily studied by theory as a stationary shape can be considered (due to large C_a), as in [123, 158]. At lower C_a, i.e. when the particle has no time to adjust its shape to the surrounding local flow before being advected further, an equilibrium position away from the center is found. For larger viscosity contrasts, outward motion is observed at large C_a whereas metastability was observed at smaller C_a, the vesicle migrating outward or toward a position close to (but not on) the center, depending on its initial position.

A similar study on 2D vesicles with no viscosity contrast has reached similar conclusions [161]: upon a decrease of capillary number a deflated enough vesicle do not converge towards the center but stays at a finite distance from it, adopting an asymmetric shape described as a slipper shape. This situation is also favored by a deflation of the vesicle. A tentative explanation for this phenomenon is proposed by the authors, based on their numerical observation: the transition towards an off-center, asymmetric shape is accompanied by a reduction of the lag, which is anticipated to be a favorable configuration by the authors, despite the increase in internal dissipation inside the particle not being symmetric anymore.

However, arguments based on a minimization of energy or of dissipation are not supported by any fundamental principle in this viscoelastic problem with moving boundaries. Indeed, in Ref. [160], the authors discard both possibilities by showing they are not compatible with their numerical observations — though in the meantime arguments of that kind are being used in Ref. [162]. Improper use of arguments based on dissipation consideration is also discussed in Ref. [163].

A question naturally arises: does this complex behaviour survives in more realistic situations where walls are present ? Walls induce additional lift forces but also additional space dependency of the shape. A secondary question is, how do lift forces due to flow curvature and lift forces due to the presence of wall compare to each other in intensity ? An attempt to answer partly this question can be found in the 2D numerical simulations of Ref. [164] where a vesicle with no viscosity contrast is placed in a semi-bounded parabolic flow, i.e. where only one wall is present (say, at position $z = -z_0$ while the centerline is at $z = 0$). In this case, a vesicle placed at a distance $z > 0$ from the center larger than its typical radius migrates outwards, while it would migrate inwards in the absence of the opposite wall. This indicates, at least in this specific situation, that the lift due to the presence of the wall overcomes that due to the flow curvature, at a distance from the center large than a particle radius.

A more detailed study regarding this question has been carried out by Nix et al. with capsules [132]. They quantified the ratio of the contributions arising from the shear gradient and from the presence of a wall, that grows as the particle approaches the center of a channel. An interesting output of their study is that the drift velocity due to shear gradient hardly depends on the viscosity ratio (in the explored range $1 < \lambda < 5$) while the effect of the wall diminishes with increasing λ – as already discussed here. As a result, the effect of shear gradient is predominant on a larger area within the channel for more viscous particles.

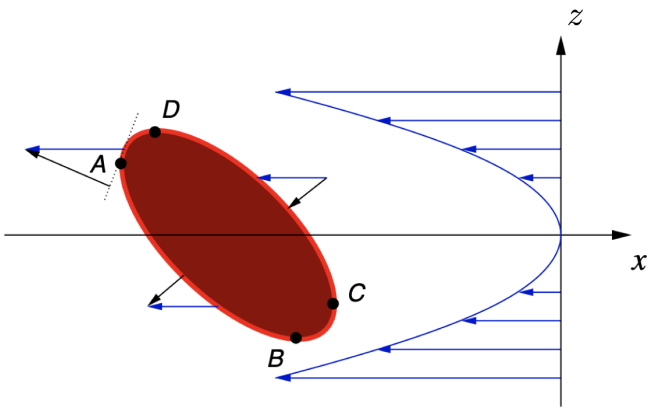

Figure 17. *Creation of an inward lift force in Poiseuille flow for a tank-treading vesicle located at a position $y > 0$ from the central line, according to [158]. The local velocity field can be decomposed into a local shear that dictates the shape of the vesicle and local quadratic correction (blue arrows). The normal contribution of this flow field points downward on segments AB and CD and upward on the two other segments, which are smaller. Hence a negative lift force acting on the particle. This argument is debatable as it does not take into account either the part of the flow that modifies the particle shape but not its position, or the relative intensity of the normal contribution on each segment. In addition, it should also apply per se for liquid drops, and would contradict the finding of Chan and Leal [153]. This illustrates the difficulty in getting an intuitive picture for migration in quadratic flows. Figure taken from [158].*

Migration in a channel

In a channel, using boundary integral method to solve the flow field requires to incorporate more complex Green's function. Even in a 2D case where only two opposite walls are needed, this requires to incorporate multiple image systems [165, 166]. An alternative method consists in considering wall as soft boundaries of known rheological property, such that additional integrals must be considered, with the advantage to handle only the Green's functions for unbounded flow [167]. In all cases, the strong impact of continuous shape evolution due to non-homogeneous shear rates makes it difficult to exhibit a simple scaling for the lift velocity: one cannot simply plunged a particle of given shape into the desired geometry. Yet, several experiments and simulations tend to prove that a scaling $U_L \propto \dot{\gamma}(z)/z^{\alpha}$, with the exponent α close to 1, holds

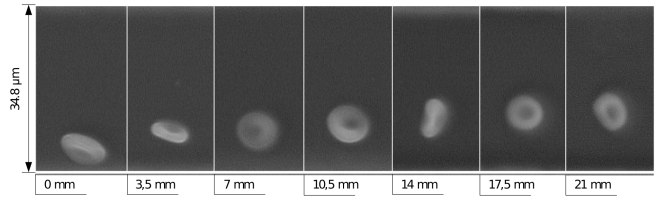

Figure 18. *Lift of a red blood cell in a microchannel: snapshots at different positions along the channel. Figure taken from Ref. [168].*

for several types of particles. In the following, we will denote by r the radius of the channel, and $\hat{r} = r/R$ its dimensionless form, that accounts for the degree of confinement of the particle.

Such a scaling has been first proposed by Coupier et al. for lipid vesicles [130]. By varying experimentally the confinement ($2 \lesssim \hat{r} \lesssim 9$), they showed that, in the range of viscosity contrast $1 \leq \lambda \leq 10$ and of reduced volume $v \geq 0.92$, trajectories from the wall to the center are well described by the law

$$\dot{z} = \xi \frac{R^{\delta+1}\dot{\gamma}(y)}{(z - z_w)^{\delta}}, \tag{37}$$

where δ is close to 1 and ξ a dimensionless parameter that depends on the vesicle properties, similar to A for the drift under simple shear rate (Eq. 10). z_w is the position of the center of mass when the particle is as close as possible to the wall. For the quasispherical vesicles considered in [130], $z_w \sim R$ but in general, it may depend on particle deformability. 2D numerical simulations have provided a similar scaling [130]. Having δ close to 1 can somehow be viewed as an intermediate case between the unbounded parabolic flow (where $\delta = 0$) and the shear flow in presence of a wall (where $\delta = 2$).

The alternative law

$$\dot{z} = \xi \frac{R_0^{\delta+1}\dot{\gamma}(z)}{z^{\delta}}, \tag{38}$$

is formally simpler and has been proposed in subsequent papers [168, 169] to allow for comparison between different situations with no need to take into account the detail of the near-wall interactions.

Simulations of red blood cells yet having a non-physiological viscosity contrast of 1 (and therefore in tank-treading regime) have highlighted an exponent that is essentially in the range 1.2-1.3 for $\hat{r} = 6$ and 8.8 [169].

Similarly to what was found for simple shear flows, the more complex dynamics followed by red blood cells in physiological conditions do not prevent them to follow similar law. Losserand et al. found experimentally through in vitro experiments that on a large range of confinements ($1.5 \lesssim \hat{r} \lesssim 10$), Eq. 38 was followed with an exponent $\delta \simeq 1.3$ (Fig. 18). They also mentioned that a fit of experimental data by a trajectory obtained through Eq. 38 poses practical issue as parameters ξ and δ are strongly correlated: several pairs of values for these parameters indeed lead to reasonable fits. Discussions on the exact value of exponent δ should probably be considered with care.

Regarding the dependency with the particle mechanical properties, the overall picture is that an increase in deformability (through an increase of capillary number or a decrease of the viscosity ratio) leads to an increase in migration velocity towards the center, be it for capsules [169, 170], vesicles [130] or red blood cells [168].

The above mentioned studies focus on the migration from the wall towards the center. As pointed out in [132, 164], this migration is dominated by the wall effect in its vicinity. When the particle approaches the center, shear gradient contribution will become dominant. As discussed previously, the direction of the transverse migration might be reversed. In addition, since the shear rate decreases as the particle approaches the center, the capillary number decreases therefore the particle shape is not any more in a quasi-steady configuration, leading to a more complex coupling between shape and migration. This aspect is discussed in particular in the last pages of Ref. [171].

Shape-lift coupling and instability in channels

While particles approach the centerline, the presence of walls seem not to destroy the complexity seen in unbounded Poiseuille flow. It rather complexifies the picture. In Ref. [167], 2D vesicles with no viscosity contrast are considered, and their behaviour while the confinement and the capillary number are varied is scrutinized. As shown in Fig. 19, increasing the confinement leads to the apparition of another kind of behaviour, which is an oscillation in the lateral position, which can be centered or not, which is called snaking. The possibility to de-stabilize this state towards a stationary shape through a time-varying flow has been explored in Ref. [172].

Remarkably, while a transition from symmetric, centered shape to off-center slipper shape is observed upon a decrease of the capillary number, a transition from symmetric shape towards slipper is also observed upon an increase of the capillary number, as long as a more viscous inner fluid is considered: in Ref. [162], a 2D vesicle with a viscosity contrast of 5 exhibits such a behaviour, which encourages the authors to establish a similitude with experimental observations on red blood cells. The latter indeed exhibit the apparition of slipper shapes upon an increase of flow velocity, in very confined situations [173, 174].

This behaviour for high viscosity contrast particles has been confirmed by 3D numerical simulations of red blood cells [163, 174, 175], but also of vesicles [176] — thus disregarding shear elasticity as an important parameter in this problem. In Ref. [174], the authors explore the full range of parameters relevant for microcirculation, and have furthermore shown that most configurations in the parameter space lead to bistabil-

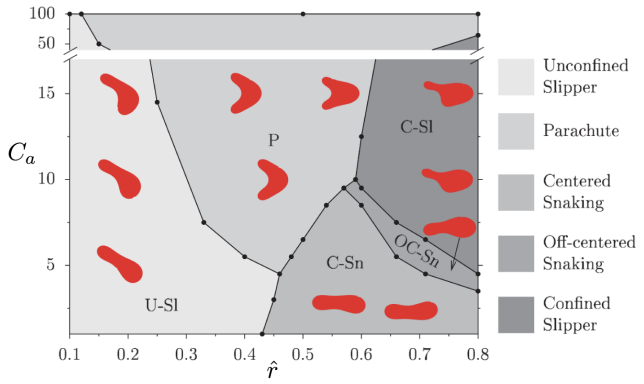

Figure 19. *Diagram for the behaviour of 2D vesicles in a channel, as a function of confinement ratio $\hat{r}$ and capillary number C_a. Figure taken from [167].*

ity between the centered, parachute-like shape and the slipper shape, whose existence depend on the initial condition [174]. Noteworthy, the snaking behaviour observed in 2D simulations, but also in another 3D study [177] does not seem to take place in their study. Similarly, a study of a vesicle placed in a confined simple-shear flow has exhibited similar centered/off-centered transition without snaking dynamics. A very recent study based on experiments and numerical simulations of red blood cells has however highlighted slight oscillation in lateral position of slipper-shaped cells [178]. They could be interpreted as a signature of off-centered snaking. These oscillations are obtained after the flow velocity has been increased progressively, and they tend to disappear after a while, on a time scale that depends on the viscosity contrast. These results suggest that the discussions on the existence of stable states should include the question of the relaxation time needed to exit or enter a given state, which calls for longer simulation times and also makes the comparison with experiments more delicate.

More recently, several experimental developments have taken place for better characterization of shape zoology, including careful design of chips to control initial conditions [179], 3D tomography of flowing cells [180], and machine-learning based methods for high throughput classification [180–182]

While the behaviour of these confined cells may be used as a tool to characterize their individual mechanical properties, it should also be noted that it has direct consequences on the collective behaviour, since the cell shape will directly influence the flow pattern around it, therefore the aggregation-disaggregation dynamics of a train of cells [183–189]

Curved streamlines

Curved channels are frequent in microsystems. While more marginally studied, this configuration has attracted some attention, in particular because this geometry leads to interesting features when inertia comes into play (Dean vortices).

Before considering this complex geometry, Ghigliotti et al. have first considered a model configuration with an unbounded flow consisting in circular streamlines [190]. When placing a 2D vesicles is this flow, they observed that tank-treading vesicle migrate towards the center while tumbling one hardly migrated. They demonstrated that the inward migration velocity is proportional to $NR^2\dot{\gamma}/(r-R)$, where r is the radial position of the vesicle, and N is the normal stress difference, that is related to the cell mechanical properties. Such a result was also predicted by Chan and Leal for a drop [153]. In real systems, be it a curved channel or a Couette device, a wall would be present at some point, therefore inducing outward migration.

Ebrahimi, Balogh and Bagchi have recently demonstrated that indeed a capsule would converge towards an intermediate position between the wall and the centre line, for a channel of circular [191] or rectangular [192] cross section. Being the result of two competing effects lying on the same mechanism, the resulting position is independent from the capillary number. Higher curvature leads to a final position closer to the inner wall.

These studies are, to our knowledge, the sole ones accounting for migration in curved channels at zero Reynolds number. It remains to be determined whether this would greatly affect the flow of particles in channels, where the curved part has necessarily a finite length. In Ref. [192], Fig. 3b, a capsule starting on the central line of the channel is shown to have moved by 5% of the distance to the inner wall after the channel has turned by 180°, for a very sharp turn of curvature radius of 5 times the cell radius. While this will probably lead to negligible effect in most channels of interest, one may still use this effect to induce particle separation by considering channels in spirals. Such a geometry may also be used to validate the above mentioned numerical studies.

Oscillating flows

The case of near centerline migration has shown us that the interplay between migration and shape leads to complex behaviour when a stationary shape cannot be reached. Another way to produce a time lag between shape relaxation and particle migration is to force changes in the applied flow. These changes can be triggered by time varying boundary conditions or by the geometry, a typical situation being structured microchannels.

Following a series of studies on particles dynamics under oscillating unbounded flows [94, 193–197], this more recent field of research has now been explored through several kind of particles and geometries and will probably meet growing interest in the next years, for the rich behaviours that emerge and the potential applications that could be developed.

We first consider a particle placed in a time-periodic harmonic shear flow bounded by a wall. In this problem, a new

dimensionless parameter must be added, which is the ratio $\hat{\omega}$ between the oscillation pulsation and the maximal shear rate. At high enough capillary number such that the particle shape relaxation time is set by the shear rate, the intuitive picture is that, if $\hat{\omega}$ is increased from 0 (corresponding to stationary flow), the particle will face situations where it does not have enough time to re-orient itself after flow reversal, such that it will migrate towards the wall. On average though, the net migration should be positive. In the large $\hat{\omega}$ limit, the picture is that of a fixed shape in a time varying flow, which recovers a fore-aft symmetry when time-averaging is made.

In Ref. [198], 3D simulations of a capsule with no viscosity contrast are considered. In addition to confirming the decrease of the mean migration velocity with $\hat{\omega}$, they also highlighted a non monotonous evolution of this mean velocity, when rescaled by the typical flow velocity, with the capillary number, at given $\hat{\omega}$. This is due to the plateauing of the mean deformation upon an increase in capillary number (in practice, upon an increase in maximal shear rate), because the capsule fails to reach its potential maximal deformation, due to flow reversal. Is is found that the optimal capillary number scales linearly with $\hat{\omega}^{-1}$, in line with the idea that at high capillary number the deformation is not limited by its own deformability but rather by the time $\propto \omega^{-1}$ during which the shear is applied in a given direction.

It is interesting to observe that the notion of time lag between shape deformation and surrounding flow is sufficient to create an effective asymmetry leading to migration even in an unbounded shear flow, providing the particle presents an initial asymmetry, as discussed in Ref. [199] where a wide class of particle is considered.

We are not aware of studies with flow reversal in a Poiseuille flow. Periodic spatial modulation of the channel have instead attracted some attention in the last 10 years, but most focus was on shape changes of centered vesicles or red blood cells [200, 201]. Yet, such a sawtooth channel is argued to be an efficient way to center cells in a microfluidic devices in [202]. However, the picture might turn out to be more complex, according to recent numerical simulations of vesicles in a wavy channel, that have exhibited off-centered equilibrium positions in a configuration where the same vesicles would be centered if the channel was straight [203].

Particle-particle interactions

As two particles cross each other in a flow, they may experience a lift force of similar nature as that induced by the presence of a neighbouring wall. The induced normal displacement has been documented by several experimental and numerical studies. Such fluid-mediated scattering events in a suspension induce a diffusion in all directions. This diffusion has two consequences: mixing in the suspension, and flux along concentration gradients. Contrary to Brownian diffusion, these two phenomena are characterized by coefficients that are *a priori* independent [204], the down-gradient diffusion coefficient being expected to be several times larger than the self-diffusion coefficient [146, 204, 205]. They can, in principle, be deduced from the knowledge of the displacement map of the two particles as a function of their initial relative position [204, 206]. However, this approach poses convergence issues due to the slow decrease of the interaction force with lateral distance between particles [206, 207].

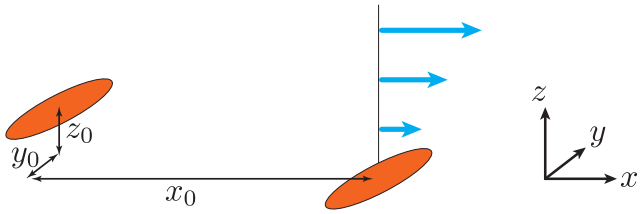

Figure 20. *Fundamental configuration for pair interaction studies*

Pair interaction

By comparison with the lift of a particle close to a wall, the finite extent in all directions of the interacting particles makes this interaction problem even richer. We will first consider two particles in an unbounded shear flow of flow direction x, shear direction z and vorticity direction y, one of them placed at an initial position (x_0, y_0, z_0) from the other, whose center of mass is taken as the origin, with $x_0 < 0$ of large absolute value (see Fig 20). If $z_0 \neq 0$ (for further discussion, we will consider $z_0 > 0$), the two particles will eventually cross each other, which may result in a net displacement $(\Delta y, \Delta z)$ in the two directions perpendicular to flow. This displacement depends a priori on both initial coordinates of the first particle. Along the flow direction, an additional displacement Δx will also be found. Compared to the differential displacement between the particles due to advection, it is however quite small and is seldom commented.

Before turning to deformable particles, it is worth mentioning that the finite duration of the interaction between particles makes it possible to obtain a net separation between solid particles. da Cunha and Hinch proposed a model for the interaction between rough spherical particles, assuming that the approach phase builds up a repulsive force while the separation phase does not [204]. However simple this assumption might seem, the existence of this separation effect was letter on proved experimentally [208].

Pair interaction of identical drops in simple shear flow has been numerically studied in Ref. [206], for different values of viscosity contrast and capillary number. A representative set of their data is shown in Fig. 21. The relative trajectories shown in Fig. 21A show that, for particles not separated in the vorticity direction, a significant shift of order one radius is observed, if the initial position in the shear direction is also of the order one radius. For drops, this shift decreases upon an

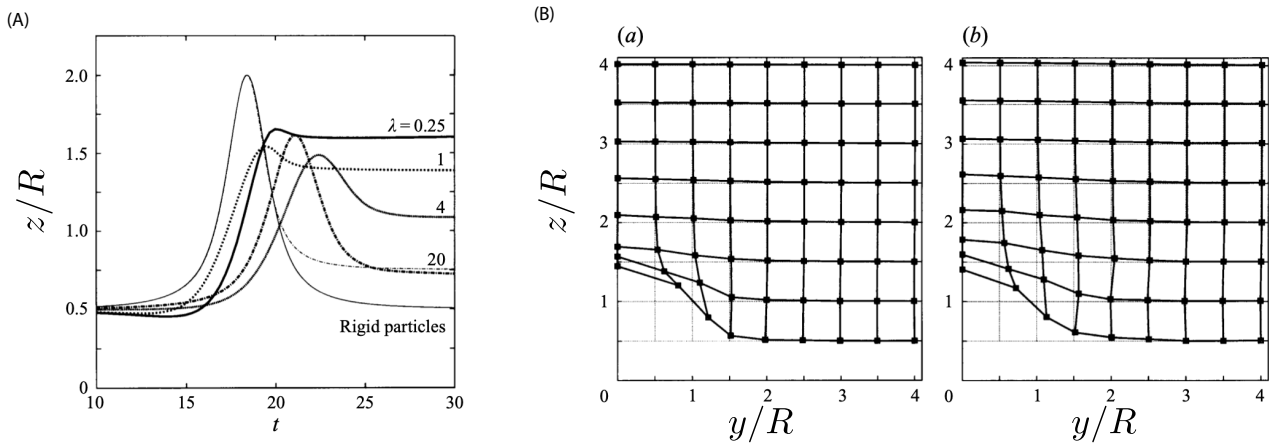

Figure 21. *Pair interaction between two droplets in unbounded shear flow. Adapted from [206]. (A) Evolution of the shift z/R in the shear direction versus time, for a fixed capillary number and various viscosity contrasts indicated on the figure. The fine solid curve corresponds to rigid sphere, and illustrates the absence of net lift, for symmetry reasons similar to that discussed in Fig. 2. The fine dash-dotted curve refers to a configuration not relevant here. The representation in (B) is commonly used in these problems to depict the final position in the z and y directions as a function of initial position. The vertices of the light gray grid indicate the initial positions that were tested, while the vertices of the thick, deformed, one indicate the final positions far from the reference particle. Here, $\lambda = 1$ and in (b) the capillary number is larger than in (a).*

increase of viscosity contrast, which marks a strong difference with the case of a drop above a flat wall, for which the dependency of the lift velocity with λ is weak. The synthesis of the final positions reached depending on the initial positions shows several interesting features that illustrate the complexity of this problem. First, a larger capillary number do not necessarily induce a larger displacement. For small initial z, the contrary even occurs (see Fig. 5 in Ref. [206]). Again, this is in marked contrast with the results for a particle near a wall. This points to a more complex view from the geometrical point of view, since the incoming particle do not only flow above the other one but also hits it initially: in Ref. [206], it is argued that the increased deformability reduces somehow the cross section for near contact interaction at collision.

Though not commented by the authors, a weak attraction in the y direction can be seen for a drop initially located at position $(2R, R)$, in Fig. 21B(b). This phenomenon also appeared later on in other studies.

Fig. 21B also shows that net displacements are much larger in the shear gradient than in the vorticity direction. This implies that diffusion due to collisions in strongly anisotropic, as will be discussed later.

As for lift above a wall, experimental studies on droplet interaction are scarce. In Refs. [209, 210], some trajectories are shown, and confirm the typical trajectories shown in Fig. 21A and the weak net displacement as soon as the initial distance is larger than a few radii, as in Fig. 21B. As can be seen in Fig. 22, the collision between the particles result in the creation in an extended and long-lasting contact between the particles, with the creation of lubrication film. Loewenberg and Hinch have exhibited different scalings for the duration of the approach sequence and have showed that the separation stage is much shorter [206].

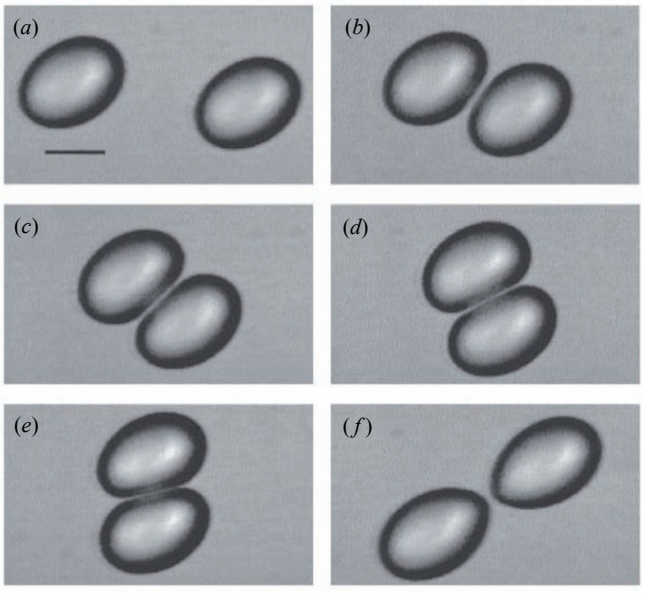

Figure 22. *Succesive snapshots of interacting drops with $\lambda = 1.4$ and $R = 20$ μm. The scale bar is 25 μm. Adapted from [209].*

Capsules are again widely ignored by experimentalists, while several numerical simulations shed light on the detail of their interactions under shear flow. Lac et al. have asked themselves whether the presence of a membrane modifies the drift observed for droplets [211]. Their numerical simulations showed that for capsules with no viscosity contrast placed in the same xz plane, the net displacement is smaller. They also

found a weak effect of the capillary number and of the initial deflation. The same team published a complementary study where they studied the consequence of the capsules not being in the same shear plane (i.e. $y_0 \neq 0$) [212]. By contrast with what is observed on drops, a clear attraction in the vorticity direction is observed for initial separation in the vorticity direction of order the capsule radius and small separation in the shear direction (i.e., small velocity difference). In this situation, the displacement depends strongly on the capillary number, and increases with it. The authors provided no explanation for this phenomenon.

Lac et al. also highlighted the fact that even if the capsule are placed on the same streamline of the unperturbed flow, they may still interact and cross each other. This is due to the flow perturbation associated with the tank-treading motion of the membrane, which have the effect to shift the particle apart: the particle located at $x_0 < 0$ and $z_0 = 0$ will see its z position increasing because of the clockwise tank-treading motion of the membrane of the particle located at the origin.

Another numerical study by Singh and Sarkar confirmed the difference between drops and capsules, the latter showing less cross-stream separation, for viscosity contrast equal to 1. The difference turns out to decrease upon an increase of this viscosity contrast.

Le and Chiam have considered a refined model for capsules that includes bending elasticity (while previous one only included shear elasticity) [213]. They also considered different initial shapes, one of them being the biconcave shape of red blood cells. Finally they considered a viscosity ratio of 4, closer to physiological values for red blood cells. The capsules were kept in the same shear plane.

Instead of particle crossing, they observed for small initial z_0 a motion called spiraling, that consists in oscillations of the particle positions at finite distance from each other. In this paper, the origin of this effect is particularly unclear, as the positions around which oscillations take place correspond to an equilibrium configuration induced by the periodic boundary condition. Moreover, the viscosity ratio apart, the configuration is quite similar to that studied in Ref. [211], where no such motion was described.

Fore small capillary numbers, more deflated capsules exhibit interaction patterns, like a swapping of positions as they collide, or a pairing followed by a rotation of the couple as a whole. This happens in conditions where the capsule would tumble, if isolated in the flow. As these behaviours take place in the middle of the simulation box, they are probably more trustful. This possibility of more complex interactions has been confirmed by other numerical simulations of capsules with no viscosity contrast [214]: for an initial position defined by small enough $|x_0|$, z_0 close to 0 and $y_0 \neq 0$, the initial shift in the z direction due to the flow induced by the reference capsule is not large, essentially because the studied capsule can flow straight. However, the attraction after interaction, as observed in Fig. 21A, is maintained, such that the sign of z is changed, implying a backward motion of the capsule and a new crossing. In the meantime, it is, on average, attracted in the y direction (as already seen in Ref. [212]). Depending on deformability, the interaction might end up there (thus resembling the swapping motion described in Ref. [213]), or go on for one or more additional interaction, leading to what the authors called minuet motion. In agreement with Ref. [213], swapping or multiple swapping (i.e. minuet) is favored by low capillary number.

Pair interaction of vesicles has been studied through experiments, numerical simulations and theory. Using the far field perturbation due to one vesicle (which is proportional to its stresslet and decays as the inverse of the distance squared), Farutin and Misbah proved that, for weakly deformed vesicles with no viscosity contrast, placed in the same shear plane, the net displacement scales as the inverse of the initial position z_0 squared. They also provided an expression for the prefactor, as a function of reduced volume. Their result agrees quantitatively with their own simulations. They did not study the case of initial offset in the y direction. Following the same theoretical framework, Vesicles with high viscosity contrast (but not tumbling) were shown in Ref. [215] to exhibit attraction in both directions as soon as $|y_0| > |z_0|$. The range of validity of this theory makes it however weekly amenable to experimental check.

The case of vesicles with no viscosity contrast not initially placed in the same shear plane was studied through numerical simulations in Ref. [216]. They found that for vesicles with initial position y_0 larger than a threshold which is of order the vesicle radius, attraction in the vorticity direction takes place, while almost no net displacement is observed in the shear direction. The author notes that, while in Ref. [215] the attraction can be interpreted in terms of contribution of the far field perturbation due to the other vesicle, here the small distance between the vesicles makes it necessary to consider additional forces due to the fluid flow in the thin film created between the vesicle, that are deformed by their interaction. This soft-lubrication approach may follow the guidelines of Loewenberg anf Hinch [206]. Numerically, the additional pressure that builds up was particularly discussed in the study of capsules dancing menuet [214].

Experiments between vesicles with $0.28 < \lambda < 3.8$, and reduced volume $\nu \gtrsim 0.75$ placed in the same shear plane were also presented in Ref. [216]. Their main results are shown in Fig. 23. As for most previous studies, a maximal shift of the order one radius is found. Remarkably, and in the limit of the experimental uncertainty the net displacement does not seem to depend much either on the reduced volume or on the viscosity contrast, though both are varied in a large range. The experimental results match well with simulations of vesicles with no viscosity contrast.

In an attempt to rationalize this weak dependency on the mechanical properties of the vesicles, it was proposed to model the interaction between the vesicles as the lift of one vesicle above a wall of finite length $2R$. Assuming the vesicle starting at z_0 moves with velocity $\dot{\gamma}z$ relatively to the vesicle of reference, Eq. 10 leads to $dz/dx = AR^3/z^3$. Integration along the

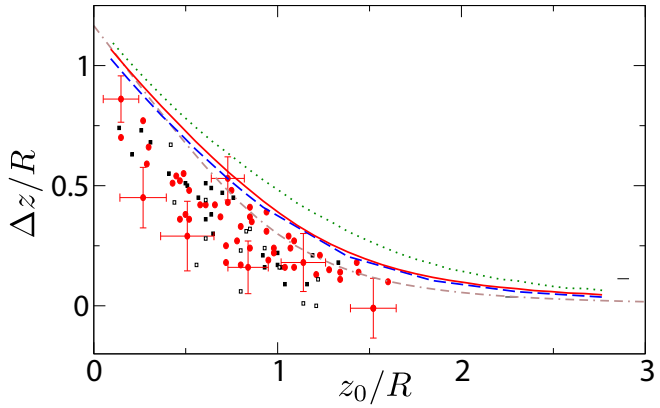

Figure 23. *Net displacement Δz as a function of initial offset z_0 for vesicles places in the same shear plane. Dots correspond to experimental data for vesicles with $0.98 > \nu \gtrsim 0.75$ and $\lambda = 0.28$ (black squares), $\lambda = 1$ (red disks), and $\lambda = 3.8$ (open squares). Dashed line, full line and dotted line: simulations for $\lambda = 1$ and $\nu = 0.95$ with increasing capillary number. Dash-dotted line: simplified model (Eq. 39). Adapted from [216]*

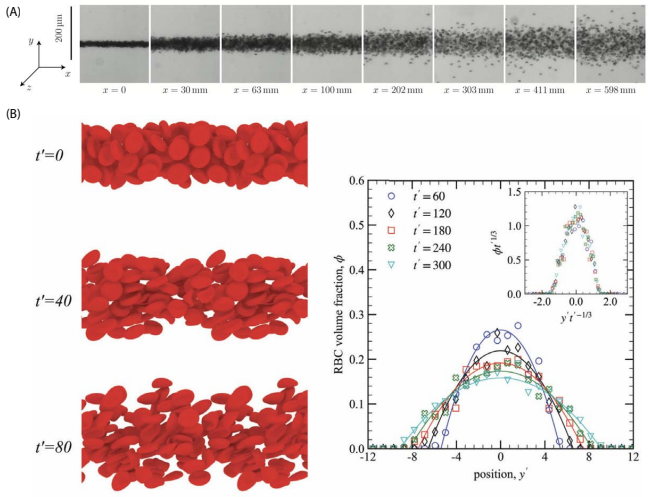

Figure 24. *Shear induced diffusion of interacting particles. (A) A jet of red blood cells injected in a flat channel diffuses in the y direction because of shear in the z direction, thus allowing to determine the f_3 coefficient experimentally. Picture taken from [146]. (B) Simulations of red-blood-cell-like capsules diffusing in a simple shear flow. The cross-stream concentration profile is the truncated parabola expected from the model. Proper rescaling shows a collapse indicating that the width increases as a function of time with exponent 1/3. Picture taken from [225].*

trajectory leads to the net displacement

$$\Delta z = (z_0^4/R^4 + 8A)^{1/4} - z_0/R. \tag{39}$$

A fit of experimental data with this rough model, shown in Fig. 23, showed good agreement with single fitting parameter A close to the typical values found by Olla. The overall amplitude of the interaction curve is set by the maximal displacement $(8A)^{1/4}$. This 1/4 exponent explains why the variations of A with cell mechanical property are smoothed out when net displacement is considered. Note that the long distance limit $z_0/R \gg 1$ of Eq. 39 is $\Delta z \sim 2AR^3/z^3$, which is not in agreement with more accurate theoretical derivations [123]. Yet, this law can serve as a good proxy for estimating the drift due to interaction.

The collision between particles of different properties is of great interest to understand segregation mechanisms within a suspension. A key example is that of blood, where platelets and white cells are often met in the edges of the channels.

In Refs. [217, 218], pairs of capsules with different rigidities are studied ; the key finding is that the stiffer particle is more displaced, although the relative displacement remains quasi constant, in line with the result that for similar capsules the net displacement depends only weakly on the capillary number.

In Ref. [219], interactions between red blood cells and platelets (modeled as smaller and 10 times stiffer particles than red blood cells) are simulated. The displacement of the red blood cell is found to be negligible, while the platelets can be displaced by around 2 of their radii. There is no quantitative study of the interaction process in this paper.

At the level of a suspension, these asymmetric mechanisms lead to segregation effects, as discussed in several recent numerical simulation papers [217, 220–224].

Diffusion in suspensions

In a semi-dilute suspension (such that interactions involving more than 2 particles can be neglected), the effect of multiple pair interactions with random initial relative positions, is to give birth to a diffusive flux.

This flux is one of the ingredients that can be incorporated in continuous models to describe the distribution of concentrations across a flow chamber. It will tend to oppose to the advection due to wall repulsion. As a pair interaction is needed for lateral displacement to occur, the diffusion constant depends linearly on the concentration of diffusing species. Furthermore, the diffusion is anisotropic, due to the inequal displacements in shear and vorticity direction. This results in anisotropic non-linear advection-diffusion equations which can only be analytically solved in some few cases. The type of solutions strongly depends on the boundary conditions of the problem.

For instance, in [226], an initial step function of concentration of asymmetric particles is flowing in a channel where its interface diffuses. The authors found that the widening of the interface is characterized by an exponent 1/2, as for Brownian diffusion. By contrast, it was shown in several studies that a narrow stream of red blood cells [146, 225], or droplets [227] injected in a channel diffuses with an exponent 1/3 (Fig. 24). The difference between the two experiments lies in the boundary conditions: a step function that becomes smoother and smoother can be considered, as long as diffusion hasn't reached its edges, as a function with fixed maximal amplitude.

By contrast, an initially narrow distribution sets a condition of constant integral, and not of constant maximal value. The subdiffusive behaviour is accompanied by the existence of a different family of self-similar distributions, which are truncated parabolas (Fig. 24). This subdiffusion can be understood by the fact that the more the cells diffuse, the less they interact, so the less lateral displacement is produced.

For particles placed in a simple shear flow, the down-gradient diffusive flux for a suspension of local concentration ϕ can be written as

$$\mathbf{J} = -f R^2 |\dot{\gamma}| \phi \nabla \phi. \tag{40}$$

The term $|\dot{\gamma}|\phi$ accounts for the frequency of collisions. The dimensionless prefactor f is related to the detail of the interaction, as described previously for different kind of particles. If the gradient of concentration is in the shear direction, this coefficient is often denoted f_2, and f_3 is the gradient is in the vorticity direction. Although it is possible to describe locally the flow in a channel as a simple shear flow (whose axis depend on the position in the channel) [146], this description in terms of two different coefficients is certainly not sufficient to account for diffusive processes in channels, where shear gradients must also be taken into account. For that reason, most characterization of fluxes were run in simple shear flows, to the exception of the experiments channels of Ref. [146], where simplifying hypothesis had to be made.

While looking at the time-evolution of concentration profiles allows to determine these unknown coefficients f_i, this method becomes more complex if other effects have to be considered, in particular that of the presence of walls. If the time-evolution equation becomes difficult to solve analytically, it is still possible to solve for the resulting stationary distribution, assuming the the diffusive flux and convective flux due to the wall-induced lift can be simply added. If the lift velocity due to the walls is known, this distribution is a function of f_2 only [141, 205, 227, 228].

For droplets, a coefficient f_2 of order 0.2 was experimentally found by Hudson, for drops of viscosity ratio close to 0.2. The dependency with the capillary number was not studied. In the numerical simulations of Malipeddi et al., f_2 is a non monotonous function of the capillary number taking values between 0.2 and 0.45, this maximal value being reached for intermediate capillary number [227]. This behaviour agrees with the calculation of Ref. [206] for the self-diffusivity coefficient, and can be understood as follows: for small capillary numbers, the drops stay spherical and do not diffuse. For large capillary numbers, their deformation is so strong that they elongate in the flow, which results also in a quasi-symmetric situation. This discussion is similar to that held for vesicles near a wall, where such a non monotonous behaviour was observed as a function of reduced volume, that controls their ability to deform.

Coefficient f_2 was experimentally determined for slightly deflated lipid vesicles with no viscosity contrast, and a coefficient 0.06 ± 0.02 was found by two different methods.

For red blood cells, experiments for cells under moderate shear rate — such that they are in a tumbling-like regime — have lead to $f_3 \simeq 0.2$ and $f_2 \simeq 2.7$ [146] [229]. The latter value is strongly different from that found for drops or vesicles ; however, a renormalization of the concentrations by considering the effective volume occupied along time by these tumbling cells lead to find closer results, though the diffusion of red blood cells still appears as stronger. In their numerical simulations, Malipeddi and Sarkar found that f_2 increases from 0.3 to 0.6 as the capillary number increases and allows for transition between a tumbling-like to a tank-treading regime [230]. A small decrease is however observed as the cell transits between the two regimes. These values are much smaller than that found experimentally. A potential explanation could be that the experiments were run in a Poiseuille flow and simplifications in the modeling had to be made to lead to equations that could be solved. Also, the authors mainly studied the non-physiological case $\lambda = 1$, but they showed on selected cases that the diffusion coefficient does not vary much with λ. Considering that strong modifications in a red blood cell dynamics are expected upon a transition to physiological to unity viscosity contrast [108, 116], this point would deserve to be further elucidated.

Regarding self-diffusivity, the difficulty of tracking particles among others makes numerical methods the tool of choice for the determination of diffusion coefficients. Conclusions on the effect of mechanical properties are in line with the previous discussions, see e.g [225].

Finally, we remark that f_3 coefficient has, in general, seldom been measured. In particular, consequences of attraction in the vorticity direction has never been observed, nor introduced in models. As it would reinforce concentration gradients rather than smooth them out, it may lead to interesting problems where initially homogeneous suspensions could become unstable.

Creation of cell free layers in blood flow

The flow of red blood cells in microcirculation is marked by the existence of a cell-free layer (CFL) near the walls [231**?** –234], which has first been observed by Poiseuille almost two centuries ago [235]. This CFL has been acknowledged to be at the origin of the decrease of the apparent viscosity referred to as Fåhræus-Lindquist effect [236] as well as the decrease of the hematocrit in small vessels compared to large ones [237, 238].

In a first approach, one can quantify this depletion layer by zeroing the sum of the advection flux ϕU_L and of the diffusive flux (Eq. 40), for a given mean volume fraction.

Using such a model, one can calculate an analytical relationship between mean concentration and thickness of the CFL, in a simple shear flow where the lift velocity is assumed to be the sum of the lift velocities due to each wall. Doing so, a fit of several data coming from previous simulations or experiments was proposed in Ref. [222]. This result was obtained with a fit parameter A/f_2 of order 0.5 (where A is the constant of Eq.

10 and f_2 that of Eq. 40). This value deserves a comment: in Ref. [222], agreement is found in particular with numerical simulations run by the same group [221], where capsules are considered, whose characteristics are such that they are in a tank-treading regime. For vesicles in tank-treading regimes, the A/f_2 ratio is of order $0.1/0.06 \sim 1.7$ which is indeed of the same order of magnitude as the ratio obtained from the fit. On the other hand, red blood cells in microcirculation are clearly not in such a regime, when isolated. Indeed, for red blood cells, the ratio becomes $0.016/2.7 \sim 0.006$ [146], which is much lower and would lead, when used in the theoretical model, to the absence of CFL.

In summary, using an advection-diffusion model based on the lift of isolated cells and the interaction of isolated pairs leads to correct predictions if one replaces the red blood cells by particles that do not lift and interact by pairs as red blood cells. This questions the relevance of such a modeling whose goal is indeed to establish a micro-meso link between cell mechanical properties and structure of the suspension.

Regarding modeling flux models, this shows that additional ingredients should be considered. In particular, the simple model above neglects several features: the modification of cell-cell interactions in the vicinity of walls, the screening of lift forces by neighboring cells, and the modification of cell dynamics due to the presence of neighboring cells. In this spirit, an attempt to determine the lift force on a cell under an external force directed towards the wall that mimics the effect of neighboring cells can be found in Ref. [151].

Another ingredient may also be considered: in a Poiseuille flow, collisions between globules induce a transverse flow because of the concentration gradient, but also because of the shear rate gradient, which also makes the collision probability asymmetric. One can show that the associated flux reads [222]

$$-(f_2 - 2f_{2s})R^2\Phi^2\frac{\partial|\dot{\gamma}|}{\partial z}, \tag{41}$$

where f_{2s} is the f-coefficient associated with self-diffusion. As f_2 is always greater than $2f_{2s}$ [204], this flux is directed towards the center of the channel. In a channel of radius r, the ratio ζ between the convective flux and this new diffusive flux reads

$$\zeta = \frac{\xi}{R^{1-\delta}(f_2 - 2f_{2s})} \times \frac{r-z}{z^\delta\Phi} \simeq 0.007\frac{r-z}{z^\delta\Phi}, \tag{42}$$

where the last equation was obtained using $R = 2.8\,\mu$m, $\xi = 1.1 \times 10^{-2}$ and $\delta 1.3$ [168], $f_2 = 2.7$ and $f_2/(f_2 - 2f_{2s}) \simeq 9/7$ [146]. For a channel radius of order some tens of microns, a cell even quite close to the wall ($z \simeq R$) and a volume fraction of some 10%, this ratio is $\lesssim 1$, meaning that the effect of asymmetric collision due to shear gradient cannot be omitted and may deserve to be considered as a contributor to the creation of cell free layers.

Finally, modeling the core of the suspension, where the highest concentrations are expected, as a suspension where only pair interactions take place, is probably not relevant. In addition, the modification of the local rheology due to this concentration leads in practice to a plug flow with high shear region near the walls (see, e.g. [239]).

The agreement between the numerical simulations of Ref. [221] — which are not based on red-blood-cell-like objects — and experimental observations on red blood cells, as far as CFL thickness is concerned, leads to question the ability of these to predict other phenomenon impacted by the cell mechanical properties ? More generally, benchmarking of numerical methods on the behaviour of the particles under flow is often partial. Regarding capsules, this can be explained by the lack of experiments quantifying lift, but experimental results on red blood cells under flow do exist [105, 107, 110, 116, 146, 168, 202]. Nevertheless, numerical methods are often validated only through quasi-static standard configurations like micropipette aspiration or optical tweezers stretching — as in Ref. [225] or in Ref. [240] which is used in Ref. [241] to set exhaustive discussion on the dynamics of creation of the CFL in complex networks — or by considering simpler objects like quasi-spherical capsules — as in Ref. [242] — or through the observation of a collective behaviour — as in Refs. [223, 240, 243] — which may hide several offsetting issues. More precisely, it has been shown in Ref. [244] that agreement on quasi-static load is not sufficient. Agreement with experiments under flow would therefore be a plus, keeping in mind that, quoting Ref. [245], " this is in fact not always sufficient as the robustness of the numerical results to physical/numerical parameters may be so large that a good agreement may be reached by chance". Efforts in running comparison with single cell dynamics results has been noticed in the recent literature [219, 224].

ELECTROKINETIC LIFT

Context

In relation to the flow properties of fluid-suspended objects mentioned before, it is of interest to note that, for suspensions of charged particles in an electrolyte, a phenomenon known as the “primary electroviscous effect” has been identified since the 50s (see [246] and references therein), which points to the importance of the coupling between flow and ionic transport near the surface of the particles, resulting in an enhanced viscosity of such suspensions compared to uncharged ones. Along this line, we describe in the following section the electrokinetic effects that give rise to lift forces at play at low Reynolds numbers with rigid objects bearing surface charges.

Experimental observations

In an article published in 1987, Alexander and Prieve described an experimental method designed to determine the

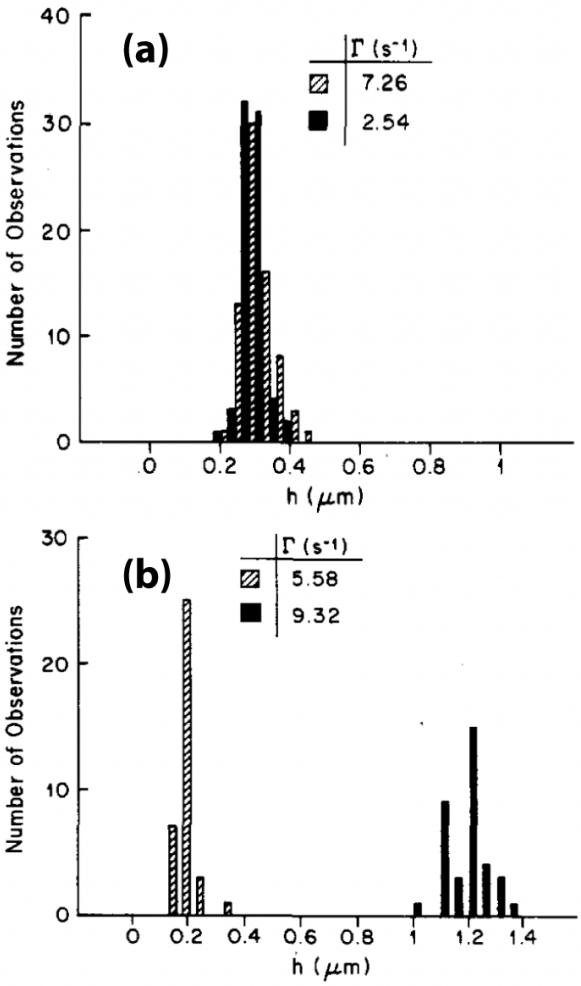

Figure 25. Histograms of bead/wall distances obtained at two different shear rates Γ in water/glycerol mixtures of (a) $\mu = 2.9 \times 10^{-3}$ Pa.s^{-1} and $K = 2$ μS.cm^{-1}, and (b) $\mu = 630 \times 10^{-3}$ Pa.s^{-1} and $K = 0.046$ μS.cm^{-1}. Adapted from [247].

interaction potential between a colloidal particle and a surface [247]. Their approach consisted in measuring the temporal fluctuations of the translation velocity of a bead driven by a shear flow near a flat wall, and to rely on theoretical results established previously by Goldman, Cox and Brenner [248] in order to infer, from their velocity measurements, the distance between the bead and the wall, using the following relationship between bead velocity V, shear rate $\dot{\gamma}$, bead radius R and bead/wall distance h [248]:

$$V(h) \simeq \dot{\gamma} R \frac{0.7431\,(1 + h/R)}{0.6376 - 0.2 \ln (h/R)} \tag{43}$$

Doing so, they assumed that the shear flow did not perturb the equilibrium colloidal forces to be characterized (arising from electrostatic double layer interactions in their experiments). In order to validate experimentally such a hypothesis, they performed a series of measurements in which they varied the strength of the shear flow (the shear rate at the wall, $\dot{\gamma}$), and the viscosity of the suspending fluid (working with various water/glycerol mixtures). While they indeed measured no effect of $\dot{\gamma}$ in low viscosity fluids, they unexpectedly observed that, in liquids with high glycerol contents, the flowing beads travelled at a larger distance from the wall at higher shear rates (Fig. 25).

This first observation was followed by more systematic studies by Bike and Prieve [249] and Wu *et al.* [250], who investigated in more details the role of shear rate and suspending fluid composition on the observed lift of flowing particles. Their findings are summarized in Fig. 26: both groups of authors observed, as initially found by Alexander and Prieve, that the bead/wall distance increases as the shear rate is increased, this effect being much more pronounced in fluids of higher glycerol content.

Origin

The observed phenomenon being amplified in high glycerol content fluids, this rules out hydrodynamic inertial effects to be at the origin of the lift, as those would rather be weakened upon increasing the fluid viscosity, which is the case at increasing concentrations of glycerol. As noted already by Alexander and Prieve [247], high glycerol content fluids also exhibit lower conductivities, which rather hints to an electrokinetic origin, with a lift force associated to the streaming potential arising from the relative motion of two charged surfaces.

Indeed, when a solid bearing surface charges is in motion relative to a polar liquid, the fluid flow associated with this motion induces currents of ions within the near-surface Debye layer that screens the surface charges from the electroneutral bulk liquid. Such a charge transport within the Debye layer is compensated for by the buildup of currents in the bulk of the surrounding fluid (Fig. 27a). An electric field is induced by these streaming currents, which has two consequences: (i) it sets the Maxwell (electrical) stress acting on the body; and (ii) it creates an electro-osmotic flow that perturbs the initial driving flow. In addition, polarization of the ionic concentrations in the liquid surrounding the particle gives rise to a diffusio-osmotic flow perturbing further the driving flow. These osmotic phenomena thus contribute to the net hydrodynamic stress acting on the solid. For a charged sphere purely translating in an unbound polar fluid, all these effects result in an extra drag acting on the sphere, along the direction of motion, but no force acting transverse to the motion of the bead. Any factor breaking the axial symmetry of this situation will induce a force transverse to the motion, *i.e* a lift force: this can be for instance an angular velocity imposed to the bead [251], or the presence of another solid/liquid boundary (electrically charged or not) near the flowing particle (Fig. 27b).

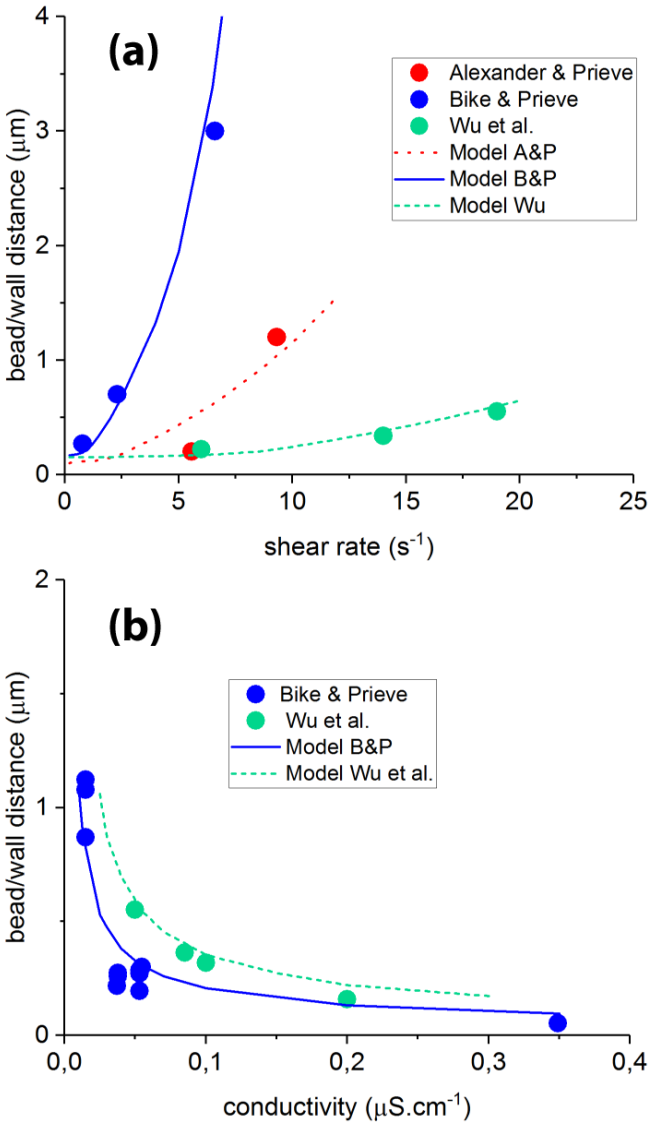

Figure 26. (a) bead/wall gap distance as a function of imposed fluid shear rate, taken from references [247] (red symbols), [249] (blue symbols), and [250] (green symbols). (b) distance as a function of carrying fluid conductivity, taken from [249] (blue symbols), and [250] (green symbols). In (a) and (b), lines correspond to theoretical predictions using a lift force as computed from Eq. 46, as described in the text. Theoretical curves in (a) were obtained with $\psi = -40$ mV and ionic strength $C_\infty = 2\times10^{-4}$ M (model A&P), $\psi = -45$ mV and $C_\infty = 10^{-4}$ M (model B&P), $\psi = -40$ mV and $C_\infty = 1.6\times10^{-4}$ M (model Wu). Curves in (b) were obtained with $\psi = -30$ mV (model B&P) and $\psi = -40$ mV (model Wu), with C_∞ varied in the range $10^{-4} - 2.5\times10^{-3}$ M.

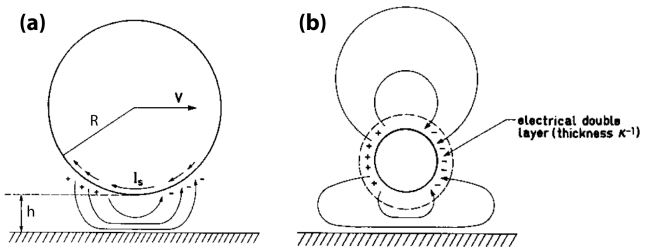

Figure 27. (a) A charged particle of radius R translating in a fluid at velocity V and at a distance h of a flat surface. The bead/fluid relative motion sweeps charges within the Debye layer that screens the bead surface charges, resulting in near-surface currents (I_s). (b) The field associated to the dipole induced by the streaming currents displays a non-axial symmetry due to the proximity of the wall, which results in a force acting transversally to the bead motion. Adapted from [252].

Modelling

Soon after the initial observations described above, several groups of authors have attempted to establish a theoretical description of the phenomenon for a bead of radius R translating at velocity V at a distance h from a flat wall (see Fig. 27). This formally amounts to solving a set of equations consisting of (i) the Nernst-Plank equation describing the convection-diffusion of ionic species, (ii) the Poisson equation relating the electric potential to the density of charges in the fluid, (iii) the Stokes equation accounting for Coulomb forces, balancing pressure, viscous and electrostatic forces, and (iv) the continuity equation (fluid incompressibility). These are associated to boundary conditions imposing no slip, no normal current, and electric potential on each solid surfaces.

Such coupled electro- and hydrodynamic problems are mathematically quite involving. We skip here all the technical aspects related to solving, present qualitatively the assumptions made in the various theoretical studies and provide the analytical expressions obtained for the lift force under these assumptions.

As summarized by Cox [253], the solutions of such a type of problems depend, in addition to the distance between the solids, their shape and relative motion, on the following parameters:

- the Peclet number $Pe = VR/D_1$, with D_1 the diffusion coefficient of (say) cations, comparing convection to diffusion effects,
- D_1/D_2, the ratio of cation to anion diffusivities,
- the Debye length $\kappa^{-1} = \sqrt{\epsilon k_B T/(2z^2e^2c_\infty)}$, *i. e.* the extension of the ion cloud screening surface charges, with ϵ the fluid permittivity, k_BT the thermal energy, z the valency of the ions, e the elementary charge, and c_∞ the bulk (number) ion concentration,
- the Hartmann number $\lambda = 2c_\infty k_B TR/(\mu V)$, with μ the fluid dynamic viscosity, giving the relative importance of electrical body forces on fluid flow,
- the particle, ψ_p, and wall, ψ_w, surface potentials (or their dimensionless forms $\tilde{\psi}_{p,w} = \psi_{p,w}ze/(k_BT)$

A number of attempts have been made in order to determine the normal force that could arise from electro- and hydrodynamic couplings when a bead flows near a flat wall.

Bike and Prieve [254] employed the lubrication approximation combined with the assumption that the Debye layer κ^{-1} is smaller than the gap h, *i.e.* $\kappa^{-1} \ll h \ll R$ (this is the so-called "thin Debye layer limit"), and computed an electrokinetic lift force F_{BP1} reading:

$$F_{BP_1} = \left(\frac{\epsilon}{4\pi}\right)^3 \frac{\pi R V^2}{K^2 h^3} \left[0.384\psi^2 + 0.181\psi\Delta\psi + 0.0242(\Delta\psi)^2\right] \quad (44)$$

where ϵ and K are the fluid permittivity and conductivity, $\psi = (\psi_w + \psi_s)/2$ and $\Delta\psi = \psi_w - \psi_s$. The above expression was obtained by accounting only for the Maxwell stress arising from the streaming potential, and neglecting *a priori* other electro-osmotic perturbations of the driving flow.

The same authors also derived, in a subsequent article [255] in which they relaxed the lubrication approximation, an expression for the lift force that holds for $h \gtrsim R$:

$$F_{BP_2} = \left(\frac{\epsilon}{4\pi}\right)^3 \frac{27\pi R^2 V^2}{16K^2(R+h)^4} (\psi_s + 2\psi_w)\,\psi_s \quad (45)$$

This expression coincides with that obtained by Van de Ven et al. when $\psi_w = 0$ [252].

Equations (44) and (45) both capture qualitatively the fact that the lift force, hence the bead/wall distance, is expected to be larger at larger shear rates (recalling that $V \sim \dot{\gamma} R$) and for lower solution conductivity K. However, when used with physically sound values for ψ, ϵ and K, none of the above expressions allows to quantitatively account for the steady-state bead/wall distances measured experimentally, with computed lift forces several orders of magnitude too low to explain observations [252, 254–256] (see Fig. 26).

The problem was tackled later by Cox [253], who pointed out that, in contrast to what was assumed in previous works, the dominant contribution is not due to the Maxwell stress alone but arises from the electro-osmotic flow generated by the streaming potential, which perturbs the driving flow. Cox derived a general solution scheme, using asymptotically matched expansions in $\delta = 1/(\kappa R)$, which is valid in the thin-Debye-layer limit. This framework was employed by several authors in order to address the specific problem of a charged sphere translating at speed V and rotating at angular velocity Ω in the vicinity of a charged wall [250, 257, 258]. In references [250] and [257], derivations were made for a cylinder/flat geometry, followed by the use of Derjaguin approximation to convert the obtained result to the sphere/flat situation, whereas the work reported in [258] was obtained directly for a sphere. We thus provide below the expression for the electrokinetic lift force derived by Tabatabaei *et al.* [258] [259]:

$$F_{Taba} = \frac{12\pi\epsilon^2(k_BT)^3R^2}{25(ze)^4 c_\infty h^2} \times \left\{ \left[\left(\frac{G_p}{D_1} + \frac{H_p}{D_2}\right) + \left(\frac{G_w}{D_1} + \frac{H_w}{D_2}\right) \right]^2 (V + R\Omega)^2 - \alpha_3 \left[\left(\frac{G_p}{D_1} + \frac{H_p}{D_2}\right) - \left(\frac{G_w}{D_1} + \frac{H_w}{D_2}\right) \right]^2 \left(V^2 - R^2\Omega^2\right) \right\} \quad (46)$$

with $\alpha_3 \simeq -1.66678$, and the quantities G_i and H_i defined as:

$$G_i = \ln \frac{1 + e^{-\tilde{\psi}_i/2}}{2}, \quad H_i = \ln \frac{1 + e^{\tilde{\psi}_i/2}}{2} \quad (47)$$

where $i = (w, p)$ stands for wall and particle. The above expression was shown by the authors to hold valid for low and moderate (of order a few unities) Peclet numbers [258].

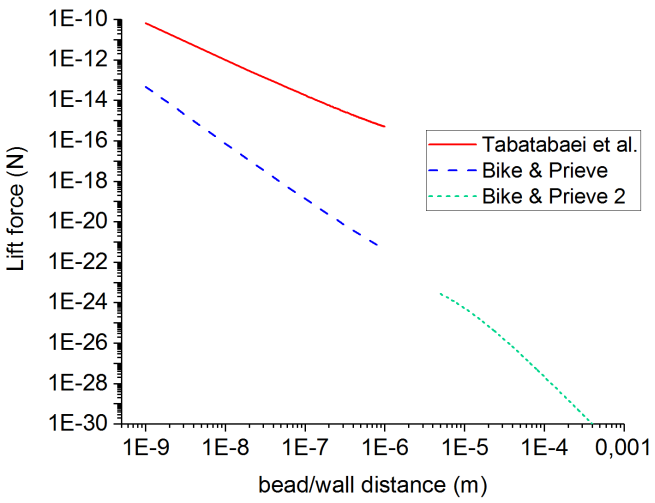

Figure 28. Comparison of lift force predictions computed using Eq. 46 (Tabatabaei et al., red line), Eq. 44 (Bike & Prieve, blue dashed line), and Eq. 45 (Bike & Prieve 2, green short-dashed line), in the case of a pure translation motion ($\Omega = 0$ in Eq. 46). Computation were done using $R = 5\ \mu$m, a salt concentration $C_\infty = 10^{-5}$M (with the number concentration per cubic meter $c_\infty = C_\infty \times 10^3 \times N_A$), $T = 300$ K, $\psi_w = \psi_s = -50$ mV, and $\epsilon = 80\epsilon_0$ taken for aqueous suspending fluid. A shear rate $\dot{\gamma} = 10\ \text{s}^{-1}$ was used to compute $V(h)$ according to Eq. 43. Diffusion coefficients were set to $D_1 = 1.33 \times 10^{-9}\ \text{m}^2.\text{s}^{-1}$ and $D_2 = 2 \times 10^{-9}\ \text{m}^2.\text{s}^{-1}$ (typical for Na^+ and Cl^- in water), and solution conductivity K estimated as $K = e^2 c_\infty (D_1 + D_2)/k_BT$.

For the sake of comparison, we have plotted on Fig. 28 the electrokinetic lift forces predicted by Eqs. 44, 45 and 46, as a function of bead/wall gap distance h. It clearly appears that, in addition to the different h-dependence predicted by the theories, the lift force computed by Tabatabaei *et al.* using Cox's framework is several orders of magnitude larger than that computed by Bike and Prieve.

More recently, Yariv, Schnitzer and Frankel pointed out an

inconsistency in Cox's solution scheme [260]. These authors noted that the Hartmann, λ, and Peclet, Pe, numbers are not independent, but linked via $\lambda Pe \sim 1/\delta^2$, with $\delta = \kappa^{-1}/R$. Therefore, in the $\delta \to 0$ limit used in [253], λ and Pe cannot be both of order 1, contrary to what was assumed by Cox. Yariv *et al.* therefore revisited Cox's scheme in a series of papers treating the two cases $\{Pe \gg 1, \lambda = O(1)\}$ [260, 261] and $\{\lambda \gg 1, Pe = O(1)\}$ [262, 263] separately.

In the $\{Pe \gg 1, \lambda = O(1)\}$ limit, they find a lift force which, as assumed by Bike and Prieve, is governed by the contribution of the Maxwell stress, and derive an expression that reduces to Eq. 44 above [261]. In the opposite limit where $\lambda \gg 1$ and $Pe = O(1)$, Schnitzer and Yariv demonstrate that the leading contribution to electroviscous effects is due to the diffusio-osmotic flow resulting from salt concentration polarization, and derive an expression for the lift force that is identical to the one obtained by Tabatabaei *et al.* [263]. It thus appears that, in spite of the improper assumption made by Cox, a fortuitous cancellation of errors in the solution scheme has led Tabatabaei *et al.* to reach a valid expression for the lift force.

Comparison with experiments

Let us now estimate the order of magnitude of λ and Pe typically encountered in the experiments described in the first section: with beads of radius R of micrometric size, flowing at a velocity V being a fraction of $\dot{\gamma}R$, and an ionic diffusion coefficient in high viscosity solutions of $D \simeq 10^{-12}$ m^2.s^{-1}, one finds a Peclet number in the range $0.5 - 10$ for shear rates in the range $1 - 10$ s^{-1}. Conversely, with salt concentration of about 10^{-4} M in solutions of viscosity $\mu \sim 1$ Pa.s, the Hartmann number falls in the range $100 - 1000$ for the same range of shear rate. Under such conditions, the $\{\lambda \gg 1, Pe = O(1)\}$ limit identified by Yariv *et al.* seems appropriate for a direct comparison of theoretical predictions with experimental observations.

As was done in previous studies [250], we compute the bead/wall distance at steady-state from the following force balance:

$$F_{lift} + F_{Debye} = F_{grav} \tag{48}$$

in which the electrokinetic force F_{lift} and the double-layer force F_{Debye} both repel the bead from the surface and balance the gravity F_{grav} that brings the bead towards the wall. The latter merely reads:

$$F_{grav} = \frac{4\pi}{3} R^3 g \Delta\rho \tag{49}$$

with $g = 9.81$ m.s^{-2} and $\Delta\rho \simeq 200$ kg.m^{-3} for polystyrene beads in glycerol.

The repulsive double-layer force is given by [250]:

$$F_{Debye} = 128\pi R k_B T c_\infty \kappa^{-1} \tanh\left(\frac{ze\psi_w}{4k_BT}\right) \tanh\left(\frac{ze\psi_p}{4k_BT}\right) \exp(-\kappa h). \tag{50}$$

The lift force is computed from Eq. 46, in which we substitute Eq. 43 for $V(h)$ and use the following result from reference [248] in order to compute the angular velocity $\Omega(h)$:

$$\Omega(h) \simeq \dot{\gamma} \frac{0.4218}{0.6376 - 0.2 \ln(h/R)} \tag{51}$$

We then solve Eq. 48 numerically for h, for a given set of parameters $\{R, \dot{\gamma}, T, c_\infty, \epsilon, z, D_1, D_2, \psi_p, \psi_w\}$. Quantitative comparison between predictions and observations is done by taking the values of R and $\dot{\gamma}$ reported in the experimental studies, $T = 300$ K, $\epsilon = 43\epsilon_0$ for the permittivity of glycerol, and $z = 1$ for monovalent salts. Diffusion coefficients of ionic species are estimated from their known values in water divided by the dynamic viscosity of the suspending fluid reported in the experimental studies, which leads to D_1 and $D_2 \sim 10^{-12}$ m^2.s^{-1} (see caption of Fig. 26 for detailed values). Once D_1 and D_2 are set, concentration c_∞ is chosen in order to match the reported value of solution conductivity using $K = e^2 c_\infty (D_1 + D_2)/k_BT$. Finally, for the sake of simplicity we set $\psi_p = \psi_w = \psi$, and use ψ as the only free parameter in the model.

Doing so, we find that the lift force derived by Tabatabaei *et al.* [258] or Schnitzer and Yariv [263] allows us to quantitatively account for the various experimental observations, using sensible values for ψ ranging from -30 mV to -45 mV. Such an agreement is illustrated on Fig.26. It is, to the best of our knowledge, the first comparison of the theoretical predictions of electroviscous lift effects with the whole set of available experimental data obtained by different groups.

Concluding remarks

We have shown in the previous section that electrokinetics can indeed account quantitatively for the lift of a charged sphere flowing near a surface in a polar fluid. The recent theoretical work by Yariv *et al.*, revisiting the pioneer study of Cox, allows identifying the relevant mechanisms underlying the buildup of an electrokinetic lift force. It thus appears that the symmetry breaking of the linear Stokes flow in such problems is associated to the streaming potential that builds up when counterions in the Debye layer are swept by the flow. This potential gives rise to both a non linear Maxwell stress and to osmotic flows controlled by the non linear transport of charges in the vicinity of the flowing object, both contributing to the lift force, with weight depending on the Peclet number, *i.e.* on the relative importance of convection and diffusion of ions.

In the context of particle sorting, the study performed by Hollingsworth and Silebi directly points to the relevance of such flow-induced electrokinetic lift forces [264]. The authors performed capillary hydrodynamic fractionation of submicron-sized particles suspended in low conductivity aqueous media, and showed that a proper theoretical description of their measurements of separation factors required accounting for electrokinetic lift forces between the flowing beads and the walls of the capillary.

It is important to recall however that, in practice, such electrokinetic lift phenomena are of sizeable magnitude only in low conductivity fluids. As a consequence, fluidic applications relying on electrokinetics for *e.g.* particle separation/manipulation in aqueous medium often do not rely solely on flow-induced electrokinetic effects but rather exploit non-inertial lift forces arising in the presence of an externally applied electric field [265].

The above point also implies for example that in biological situations, at ionic strength $\simeq$ 150 mM and $D \simeq 10^{-9}$ m^2.s^{-1}, electrokinetic lift of cell-sized objects is essentially not relevant. As an illustration of this, we have plotted on Fig. 29 a series of force/separation distance curves for a bead carried by a fluid containing 100 mM of monovalent salt, computed for various values of the ion diffusion constant. The steady-state distance between the bead and the wall can be read off the graphs as the point at which the normalized interaction force crosses the horizontal dashed line. It can thus be seen that deviations from the static equilibrium distance, due to electrokinetic lift, are observable only for diffusion coefficients below 10^{-11} m^2.s^{-1}.

While we have, in this section, focused our attention on the generation of lift forces of electrokinetic origin when a bead moves parallel to a wall in a shear flow, it is worth mentioning that recent works have addressed, both experimentally and theoretically [266–268], the issue of electrokinetic effects in squeeze-flow geometries, *i.e.* when a bead moves perpendicularly close to a wall, and their role on the overall repulsion between the surfaces. Finally, it is of interest to note, in the framework of this review, that theoretical efforts have recently been made in order to provide a description of the combined effects of electrokinetics and elastohydrodynamics in the emergence of lift forces [269, 270].

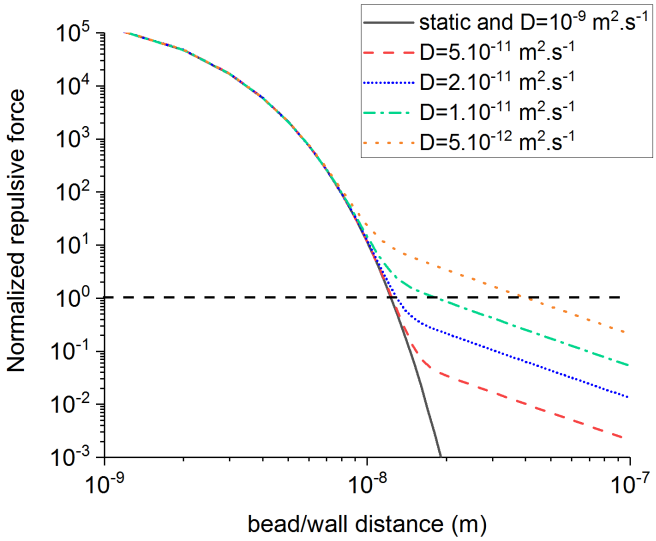

Figure 29. $(F_{Debye} + F_{lift})/F_{grav}$ as a function of h for beads of $R = 5$ μm, $\dot{\gamma} = 10$ s^{-1}, $C_\infty = 0.1$ M (physiological range). Intersection with horizontal line shows the steady-state (or static equilibrium) value of h. No differences between static and $D = 10^{-9}$ m^2.s^{-1} (order of magnitude for sodium in water), so no effect of electrokinetic lift. Effect visible only for $D < 10^{-11}$ m^2.s^{-1}.

CONCLUSION AND PERSPECTIVES

From the above review, we understand that there exists several mechanisms for lift forces at zero Reynolds number. They invariably involve viscous flows as well as soft or charged boundaries – which are all widespread ingredients in the physics of transport and mobility at small scales. These mechanisms are thus highly-relevant to micro- and nanofluidics as well as for biological flows. In some cases, the magnitudes of these lift forces are comparable to surface and biological forces, and might thus have been overlooked in the interpretation of some results and phenomena. Besides, such effects might be controlled and employed towards applications, through *e.g.* rheology, transport, filtering... In the reminder, we list a few elements of perspective.

Regarding interactions in shear flows, our review highlights the necessity to better understand interactions in the crossover zone $z \sim R$ between soft-lubrication effects and shear-induced lift. Interactions between particles exhibit a rich variety of behaviours, including attraction, whose impact at the level of a suspension have not yet been discussed. As noted above, the creation of a cell-free layer in a blood stream (and, by extension, in any other confined flow of deformable particles) has not yet been modeled in a framework that relies on what is known about cell-cell and cell wall interaction. Layering effects have been reported in such suspensions, which are still unexplained [271–276].

Besides, lift forces may play some role in the fascinatingly-low and puzzling effective friction coefficients of mammalian cartilaginous joints, among other possible mechanisms [277]. They might also allow for a smart tuning of the bulk and interfacial rheology of dense suspensions [278], including the shear-thickening effect. Indeed, if a lubricated-to-dry-contact transition [279] is proved to be the microscopic mechanism of such a macroscopic manifestation, then the soft-lubrication lift between soft particles might repel/remove that transition. Besides, wall softness is expect to play a role too [280]. More marginally, landslides are resulting from flows in poroelastic rocks and their mechanism remains a puzzle [5]. Elastohydrodynamic couplings may contribute as well.

Also, as a symmetry-breaking mechanism is a central ingredient for the appearance of lift forces at zero Reynolds numbers, one could design in future new lift strategies inde-

pendently of softness and charges. Slip inhomogeneities [281], surfactant gradients and thus Gibbs elasticity at capillary interfaces, as well as compressibility effects in gaseous layers, are possible examples among numerous others.

Beyond lift forces, other non-trivial EHD couplings have been revealed [44, 50–52], with important consequences including adhesive-like forces and enhanced sedimentation effects, among others. The experimental investigations of these scenarios is an important task for the future. Similarly, looking for an active soft-lubrication lift is an exciting perspective as *e.g.* bacterial colony formation might be affected by it.

EHD couplings are effective ways to reduce or optimise frictional properties [4]. This has been investigated both experimentally and theoretically with rough or patterned substrates [282–284] and might have important implications for robotics [285]. Moreover, prey capture by animals can be associated to lubrication through viscous adhesion [286]. A natural question emerges on if, and how, elasticity of the tongue/prey could play a role and modify the picture of the capture dynamics.

Finally, a route previously followed by hydrodynamics – through nanofluidics and beyond – was to investigate the effects of system downscaling and hence the limits of the classical continuum description at small scales due to *e.g.* surface forces, thermal fluctuations and eventually quantum effects. We expect a similar interest in investigating nanoconfined EHD, with fascinating perspectives for fundamental physics and biophysics.

ACKNOWLEDGEMENTS

The authors thank L. Mahadevan, B. Saintyves, C. H. Venner, J. H. Snoeijer, A. Pandey, M. Essink, B. Rallabandi, H. Stone, V. Bertin, A. Maali, Y. Amarouchene, C. Drummond, K. Sekimoto, M. Cloitre, F. Lequeux, N. Fillot, O. Bäumchen, T. Podgorski, S. Losserand, A. Farutin, C. Misbah, V. Vitkova, A.-V. Salsac and S. Mendez for fruitful discussions. They acknowledge financial support from the European Union through the European Research Council under ERC Consolidator grant n°101039103 *EMetBrown*. Views and opinions expressed are however those of the authors only and do not necessarily reflect those of the European Union or the European Research Council. Neither the European Union nor the granting authority can be held responsible for them. They also acknowledge financial support from the Agence Nationale de la Recherche (ANR-21-ERCC-0010-01 *EMetBrown*, ANR-21-CE06-0029 *SOFTER*, ANR-21-CE06-0039 *FRICOLAS*). Finally, they thank the Soft Matter Collaborative Research Unit, Frontier Research Center for Advanced Material and Life Science, Faculty of Advanced Life Science at Hokkaido University, Sapporo, Japan.

* lionel.bureau@univ-grenoble-alpes.fr
† gwennou.coupier@univ-grenoble-alpes.fr
‡ thomas.salez@cnrs.fr

[1] O. Reynolds, Philos. Trans. R. Soc. Lond. **177**, 157 (1886).
[2] G. Dupeux, A. L. Goff, D. Quéré, and C. Clanet, New J. Phys. **12**, 093004 (2010).
[3] G. Segre and A. Silberberg, Nature **189**, 209 (1961).
[4] J. A. Greenwood, Lubricants **8** (2020).
[5] C. S. Campbell, J. Geol. **97**, 653 (1989).
[6] N. Fillot, H. Berro, and P. Vergne, Tribology Letters **43** (2011).
[7] J. P. Ewen, H. A. Spikes, and D. Dini, Tribology Letters **69** (2021).
[8] S. Yang, S. S. Lee, S. W. Ahn, K. Kang, W. Shim, G. Lee, K. Hyun, and J. M. Kim, Soft Matt. **8**, 5011 (2012).
[9] F. Brochard-Wyart, Comptes rendus Physique **4(2)**, 207 (2003).
[10] V. C. Mow, M. H. Holmes, and W. M. Lai, J. Biomech. **17**, 377 (1984).
[11] H. L. Goldsmith, Fed. Proc. **30**, 1578 (1971).
[12] N. J. Balmforth, C. J. Cawthorn, and R. V. Craster, J. Fluid Mech. **646**, 339 (2010).
[13] S. Leroy and E. Charlaix, J. Fluid Mech. **674**, 389 (2011).
[14] Y. Wang, G. A. Pilkington, C. Dhong, and J. Frechette, Current Opinion in Colloid and Interface Science **27**, 43 (2017).
[15] P. Karan, J. Chakraborty, and S. Chakraborty, Journal of the Indian Institute of Science **98**, 159 (2018).
[16] R. H. Davis, J.-M. Serayssol, and E. Hinch, J. Fluid Mech. **163**, 479 (1986).
[17] P. Gondret, E. Hallouin, M. Lance, and L. Petit, Physics of Fluids **11**, 2803 (1999).
[18] M. R. Tan, Y. Wang, and J. Frechette, Phys. Rev. Fluids **4**, 084305 (2019).
[19] S. Leroy, A. Steinberger, C. Cottin-Bizonne, F. Restagno, L. Léger, and E. Charlaix, Phys. Rev. Lett. **108**, 264501 (2012).
[20] R. Villey, E. Martinot, C. Cottin-Bizonne, M. Phaner-Goutorbe, L. Léger, F. Restagno, and E. Charlaix, Phys. Rev. Lett. **111**, 215701 (2013).
[21] Y. Wang, C. Dhong, and J. Frechette, Phys. Rev. Lett. **115**, 248302 (2015).
[22] Y. Wang, M. R. Tan, and J. Frechette, Soft Matter **13**, 6718 (2017).
[23] Y. Wang and J. Frechette, Soft Matter **14**, 7605 (2018).
[24] D. Y. C. Chan, E. Klaseboer, and R. Manica, Soft Matter **5**, 2858 (2009).
[25] I. U. Vakarelski, R. Manica, X. Tang, S. J. O'Shea, G. W. Stevens, F. Grieser, R. R. Dagastine, and D. Y. C. Chan, Proceedings of the National Academy of Sciences **107**, 11177 (2010).
[26] F. Kaveh, J. Ally, M. Kappl, and H.-J. Butt, Langmuir **30**, 11619âĂŞ11624 (2015).
[27] D. Guan, E. Charlaix, R. Z. Qi, and P. Tong, Physical Review Applied **8**, 044010 (2017).
[28] Y. Wang, B. Zeng, H. T. Alem, Z. Zhang, E. Charlaix, and A. Maali, Langmuir **34**, 1371 (2018).
[29] F. Basoli, S. M. Giannitelli, M. Gori, P. Mozetic, A. Bonfanti, M. Trombetta, and A. Rainer, Frontiers in Physiology **9**, 1449 (2018).
[30] J. M. Skotheim and L. Mahadevan, Phys. Rev. Lett. **92**, 245509 (2004).
[31] D. Dowson and Z. M. Jin, J. Phys. D: Appl. Phys. **25**, A116 (1992).
[32] F. Lequeux, D. Grosshans, and R. Hocquart, Polymers for Advanced Technologies **3**, 33 (1992).
[33] K. Sekimoto and L. Leibler, Europhys. Lett. **23**, 113 (1993).
[34] D. A. Dillard, B. Mukherjee, P. Karnal, R. C. Batra, and F. J., Soft Matter **14**, 3669 (2018).

[35] G. K. Batchelor, An Introduction to Fluid Dynamics (Cambridge University Press, 1967).
[36] A. Oron, S. Davis, and S. Bankoff, Rev. Mod. Phys. **69**, 931 (1997).
[37] J. M. Skotheim and L. Mahadevan, Physics of Fluids **17**, 092101 (2005).
[38] K. Sugiyama and F. Takemura, J. Fluid Mech. **662**, 209âĂŞ231 (2010).
[39] A.-S. Bouchet, C. Cazeneuve, N. Baghdadli, G. S. Luengo, and C. Drummond, Macromolecules **48**, 2244 (2015).
[40] J. Beaucourt, T. Biben, and C. Misbah, Europhysics Letters **67**, 676 (2004).
[41] B. Saintyves, T. Jules, T. Salez, and L. Mahadevan, Proceedings of the National Academy of Sciences **113**, 5847 (2016).
[42] H. Stone, M. Abkarian, and R. T. Bonnecaze, APS-DFD Meeting, Seattle (2004).
[43] J. Urzay, S. G. Llewellyn Smith, and B. J. Glover, Physics of Fluids **19**, 103106 (2007).
[44] J. Urzay, J. Fluid Mech. **653**, 391 (2010).
[45] H. S. Davies, D. Debarre, N. El Amri, C. Verdier, R. P. Richter, and L. Bureau, Phys. Rev. Lett. **120**, 198001 (2018).
[46] B. Rallabandi, N. Oppenheimer, M. Y. B. Zion, and H. A. Stone, Nature Physics **14**, 1211 (2018).
[47] P. Vialar, P. Merzeau, S. Giasson, and C. Drummond, Langmuir **35**, 15605 (2019).
[48] J. H. Snoeijer, J. Eggers, and C. H. Venner, Physics of Fluids **25**, 101705 (2013).
[49] M. H. Essink, A. Pandey, S. Karpitschka, C. H. Venner, and J. H. Snoeijer, J. Fluid Mech. **915** (2021).
[50] S. J. Weekley, S. L. Waters, and O. E. Jensen, Q. Jl Mech. Appl. Math **59**, 277 (2006).
[51] T. Salez and L. Mahadevan, J. Fluid Mech. **779**, 181 (2015).
[52] V. Bertin, Y. Amarouchene, E. Raphael, and S. Thomas, arXiv2104.00900 (2021).
[53] B. Rallabandi, B. Saintyves, T. Jules, T. Salez, C. Schönecker, L. Mahadevan, and H. A. Stone, Phys. Rev. Fluids **2**, 074102 (2017).
[54] A. Pandey, S. Karpitschka, C. H. Venner, and J. H. Snoeijer, J. Fluid Mech. **799**, 433 (2016).
[55] A. Kargar-Estahbanati and B. Rallabandi, Physical Review Fluids **6**, 034003 (2021).
[56] Z. Zhang, V. Bertin, M. Arshad, E. Raphaël, T. Salez, and A. Maali, Phys. Rev. Lett. **124**, 054502 (2020).
[57] T. G. Chandler and D. Vella, Proceedings of the Royal Society A **476**, 20200551 (2020).
[58] A. Daddi-Moussa-Ider, M. Lisicki, and S. Gekle, J. Fluid Mech. **811**, 210 (2017).
[59] A. Daddi-Moussa-Ider, B. Rallabandi, S. Gekle, and H. A. Stone, Phys. Rev. Fluids **3**, 084101 (2018).
[60] K. L. Johnson, Contact mechanics (Cambridge University Press, 1985).
[61] D. Maugis, Contact, adhesion and rupture of elastic solids (Springer, 2000).
[62] B. Saintyves, B. Rallabandi, T. Jules, J. Ault, T. Salez, C. SchÃűnecker, H. A. Stone, and L. Mahadevan, Soft Matter **16**, 4000 (2020).
[63] B. Lorz, R. Simson, J. Nardi, and E. Sackmann, Europhys. Lett. **51**, 468 (2000).
[64] I. Cantat and C. Misbah, Phys. Rev. Lett. **83**, 880 (1999).
[65] U. Seifert, Phys. Rev. Lett. **83**, 876 (1999).
[66] R. Bruinsma (1995), vol. 332, pp. 61–75.
[67] F. Y. Leong and D.-V. Le, Physics of Fluids **33**, 043303 (2021).
[68] J. M. Rallison, Annual Review of Fluid Mechanics **16**, 45 (1984).
[69] K. H. de Haas, C. Blom, D. van den Ende, M. H. G. Duits, and J. Mellema, Phys. Rev. E **56**, 7132 (1997).
[70] F. Rioual, T. Biben, and C. Misbah, Phys. Rev. E **69**, 061914 (2004).
[71] V. Kantsler and V. Steinberg, Phys. Rev. Lett. **95**, 258101 (2005).
[72] M. Abkarian and A. Viallat, Biophysical J. **89**, 1055 (2005).
[73] H. Noguchi and G. Gompper, Phys. Rev. E **72**, 011901 (2005).
[74] H. Noguchi and G. Gompper, J. Phys. Cond. Matter **17**, S3439 (2005).
[75] V. Kantsler and V. Steinberg, Phys. Rev. Lett. **96**, 036001 (2006).
[76] M.-A. Mader, V. Vitkova, M. Abkarian, A. Viallat, and T. Podgorski, Eur. Phys. J. E **19**, 389 (2006).
[77] C. Misbah, Phys. Rev. Lett. **96**, 028104 (2006).
[78] M.-A. Mader, H. Ez-Zahraouy, C. Misbah, and T. Podgorski, Eur. Phys. J. E **22**, 275 (2007).
[79] H. Noguchi and G. Gompper, Phys. Rev. Lett. **98**, 128103 (2007).
[80] V. V. Lebedev, K. S. Turitsyn, and S. S. Vergeles, Phys.Rev. Lett. **99**, 218101 (2007).
[81] G. Danker, T. Biben, T. Podgorski, C. Verdier, and C. Misbah, Phys. Rev. E **76**, 041905 (2007).
[82] V. Kantsler, E. Segre, and V. Steinberg, Europhys. Lett. **82**, 58005 (2008).
[83] J. Deschamps, V. Kantsler, and V. Steinberg, Phys. Rev. Lett. **102**, 118105 (2009).
[84] A. Farutin, T. Biben, and C. Misbah, Phys. Rev. E **81**, 061904 (2010).
[85] T. Biben, A. Farutin, and C. Misbah, Phys. Rev. E **83**, 031921 (2011).
[86] N. Zabusky, E. Segre, J. Deschamps, V. Kantsler, and V. Steinberg, Phys. Fluids **23**, 041905 (2011).
[87] A. Farutin, O. Aouane, and C. Misbah, Phys. Rev. E **85**, 061922 (2012).
[88] A. Farutin and C. Misbah, Phys. Rev. Lett. **109**, 248106 (2012).
[89] A. Laadhari, P. Saramito, and C. Misbah, Phys. Fluids **24**, 031901 (2012).
[90] D. Barthès-Biesel and J. M. Rallison, J. Fluid Mech. **113**, 251ÃŘ267 (1981).
[91] S. Ramanujan and C. Pozrikidis, J. Fluid Mech. **361**, 117ÃŘ143 (1998).
[92] E. Lac and D. Barthès-Biesel, Physics of Fluids **17**, 072105 (2005).
[93] J. M. Skotheim and T. W. Secomb, Phys. Rev. Lett. **98**, 078301 (2007).
[94] S. Kessler, R. Finken, and U. Seifert, Eur. Phys. J. E **29**, 399 (2009).
[95] P. Bagchi and R. M. Kalluri, Phys. Rev. E **80**, 016307 (2009).
[96] J. Walter, A.-V. Salsac, and D. Barthès-Biesel, J. Fluid Mech. **676**, 318ÃŘ347 (2011).
[97] E. Foessel, J. Walter, A.-V. Salsac, and D. Barthès-Biesel, J. Fluid Mech. **672**, 477ÃŘ486 (2011).
[98] C. Dupont, A.-V. Salsac, and D. Barthès-Biesel, J. Fluid Mech. **721**, 180 (2013).
[99] C. Dupont, F. Delahaye, D. Barthès-Biesel, and A.-V. Salsac, J. Fluid Mech. **791**, 738 (2016).
[100] D. Barthès-Biesel, Ann. Rev. Fluid Mech. **48**, 25 (2016).
[101] X. Zhang and M. D. Graham, Phys. Rev. Fluids **5**, 023603 (2020).
[102] D. Morris and A. Williams, Biochim. Biophys. Acta **550**, 288ÃŘ296 (1979).
[103] H. L. Goldsmith and J. Marlow, Proc. R. Soc. B **182**, 351 (1972).

[104] M. Bitbol, Biophys. J. **49**, 1055 (1986).
[105] W. Yao, Z. Wen, Z. Yan, D. Sun, W. Ka, L. Xie, and S. Chien, Journal of Biomechanics **34**, 1501 (2001).
[106] M. Abkarian, M. Faivre, and A. Viallat, Phys. Rev. Lett. **98**, 188302 (2007).
[107] J. Dupire, M. Socol, and A. Viallat, Proc. Nat. Acad. Sci. USA **109**, 20808 (2012).
[108] T. Fischer and R. Korzeniewski, J. Fluid Mech. **736**, 351 (2013).
[109] M. Levant and V. Steinberg, Phys. Rev. E **94**, 062412 (2016).
[110] L. Lanotte, J. Mauer, S. Mendez, D. A. Fedosov, J.-M. Fromental, V. Claveria, F. Nicoud, G. Gompper, and M. Abkarian, Proc. Nat. Acad. Sci. **113**, 13289 (2016).
[111] J. Mauer, S. Mendez, L. Lanotte, F. Nicoud, M. Abkarian, G. Gompper, and D. A. Fedosov, Phys. Rev. Lett. **121**, 118103 (2018).
[112] D. Cordasco and P. Bagchi, Phys. Fluids **25**, 091902 (2013).
[113] D. Cordasco and P. Bagchi, J. Fluid Mech. **759**, 472 (2014).
[114] Z. Peng, A. Mashayekh, and Q. Zhu, J. Fluid Mech. **742**, 96ÃŘ118 (2014).
[115] K. Sinha and M. D. Graham, Phys. Rev. E **92**, 042710 (2015).
[116] C. Minetti, V. Audemar, T. Podgorski, and G. Coupier, J. Fluid Mech. **864**, 408 (2019).
[117] F. Guglietta, M. Behr, L. Biferale, G. Falcucci, and M. Sbragaglia, Soft Matter **16**, 6191 (2020).
[118] Mignon, Thierry and Mendez, Simon, Math. Model. Nat. Phenom. **16**, 23 (2021).
[119] A. F. Gallen, M. Castro, and A. Hernandez-Machado, Soft Matter **17**, 9587 (2021).
[120] G. B. Jeffery, Proc. R. Soc. Lond. A **102**, 161 (1922).
[121] P. Olla, J. Phys. A: Math. Gen. **30**, 317 (1997).
[122] P. Olla, J. Phys. II France **7**, 1533 (1997).
[123] A. Farutin and C. Misbah, Phys. Rev. Lett. **110**, 108104 (2013).
[124] S. Nix, Y. Imai, D. Matsunaga, T. Yamaguchi, and T. Ishikawa, Phys. Rev. E **90**, 043009 (2014).
[125] C. Pozrikidis, Boundary integral and singularity methods for linearized viscous flow (Cambridge University Press, 1992).
[126] H. Zhao, A. P. Spann, and E. S. G. Shaqfeh, Phys. Fluids **23**, 121901 (2011).
[127] C. Pozrikidis, J. Comp. Phys. **169**, 250âĂŞ301 (2001).
[128] W. S. J. Uijttewaal, E.-J. Nijhof, and R. M. Heethaar, Phys. Fluids A **5**, 819 (1993).
[129] S. Sukumaran and U. Seifert, Phys. Rev. E **64**, 011916 (2001).
[130] G. Coupier, B. Kaoui, T. Podgorski, and C. Misbah, Phys. Fluids **20**, 111702 (2008).
[131] S. Meßlinger, B. Schmidt, H. Noguchi, and G. Gompper, Phys. Rev. E **80**, 011901 (2009).
[132] S. Nix, Y. Imai, and T. Ishikawa, Journal of Biomechanics **49**, 2249 (2016).
[133] J. R. Blake, Proc. Camb. Phil. Soc. **70**, 303 (1971).
[134] R. K. Singh, X. Li, and K. Sarkar, J. Fluid Mech. **739**, 421âĂŞ443 (2014).
[135] J. Yeomans, D. Pushkin, and H. Shum, Eur. Phys. J. Spec. Top. **223**, 1771âĂŞ1785 (2014).
[136] G. K. Batchelor, J. Fluid Mech. **41**, 545âĂŞ570 (1970).
[137] J. Deschamps, V. Kantsler, E. Segre, and V. Steinberg, Proc. Nat. Acad. Sci. USA **106**, 11444 (2009).
[138] D. Abreu and U. Seifert, Phys. Rev. Lett. **110**, 238103 (2013).
[139] N. Callens, C. Minetti, G. Coupier, M. Mader, F. Dubois, C. Misbah, and T. Podgorski, Europhys. Lett. **83**, 24002 (2008).
[140] M. Abkarian, C. Lartigue, and A. Viallat, Phys. Rev. Lett. **88**, 068103 (2002).
[141] L. Bureau, G. Coupier, F. Dubois, A. Duperray, A. Farutin, C. Minetti, C. Misbah, T. Podgorski, D. Tsvirkun, and M. Vysokikh, C. R. Mécanique **345**, 78 (2017).
[142] H. Brenner, Chem. Eng. Sci. **16**, 242 (1961).
[143] Z.-H. Huang, M. Abkarian, and A. Viallat, New Journal of Physics **13**, 035026 (2011).
[144] G. Boedec, M. Jaeger, and M. Leonetti, J. Fluid Mech. **690**, 227 (2012).
[145] P. Olla, Phys. A **278**, 87 (2000).
[146] X. Grandchamp, G. Coupier, A. Srivastav, C. Minetti, and T. Podgorski, Phys. Rev. Lett. **110**, 108101 (2013).
[147] O. K. Baskurt, R. A. Farley, and H. J. Meiselman, American Journal of Physiology-Heart and Circulatory Physiology **273**, H2604 (1997).
[148] D. Matsunaga, Y. Imai, C. Wagner, and T. Ishikawa, J. Fluid Mech. **806**, 102âĂŞ128 (2016).
[149] A. Walter, H. Rehage, and H. Leonhard, Colloid Polym. Sci. **278**, 169âĂŞ175 (2000).
[150] E. Lac, D. Barthès-Biesel, N. A. Pelekasis, and J. Tsamopoulos, J . Fluid Mech. **516**, 303âĂŞ334 (2004).
[151] D. S. Hariprasad and T. W. Secomb, Phys. Rev. E **90**, 053014 (2014).
[152] J. R. Smart and D. T. Leighton, Physics of Fluids A: Fluid Dynamics **3**, 21 (1991).
[153] P. C.-H. Chan and L. G. Leal, J. Fluid Mech. **92**, 131âĂŞ170 (1979).
[154] W. S. J. Uijttewaal and E. J. Nijhof, J . Fluid Mech. **302**, 45âĂŞ63 (1995).
[155] M. Kennedy, C. Pozrikidis, and R. Skalak, Comp. Fluids **23**, 251 (1994).
[156] L. G. Leal, Ann. Rev. Fluid Mech. **12**, 435 (1980).
[157] B. Kaoui, G. Ristow, I. Cantat, C. Misbah, and W. Zimmermann, Phys. Rev. E **77**, 021903 (2008).
[158] G. Danker, P. M. Vlahovska, and C. Misbah, Phys. Rev. Lett. **102**, 148102 (2009).
[159] A. Helmy and D. Barthès-Biesel, Journal de Mécanique Théorique et Appliquée **1** (1982).
[160] A. Farutin and C. Misbah, Phys. Rev. E **89**, 042709 (2014).
[161] B. Kaoui, G. Biros, and C. Misbah, Phys. Rev. Lett. **103**, 188101 (2009).
[162] N. Tahiri, T. Biben, H. Ez-Zahraouy, A. Benyoussef, and C. Misbah, Microvasc. Res. **85**, 40 (2013).
[163] A. K. Dasanna, J. Mauer, G. Gompper, and D. A. Fedosov, Frontiers in Physics **9** (2021).
[164] B. Kaoui, G. Coupier, C. Misbah, and T. Podgorski, Houille Blanche **5**, 112 (2009).
[165] M. Thiébaud and C. Misbah, Phys. Rev. E **88**, 062707 (2013).
[166] A. Nait-Ouhra, A. Guckenberger, A. Farutin, H. Ez-Zahraouy, A. Benyoussef, S. Gekle, and C. Misbah, Phys. Rev. Fluids **3**, 123601 (2018).
[167] B. Kaoui, N. Tahiri, T. Biben, H. Ez-Zahraouy, A. Benyoussef, G. Biros, and C. Misbah, Phys. Rev. E **84**, 041906 (2011).
[168] S. Losserand, G. Coupier, and T. Podgorski, Microvasc. Res. **124**, 30 (2019).
[169] Q. M. Qi and E. S. G. Shaqfeh, Phys. Rev. Fluids **2**, 093102 (2017).
[170] S. K. Doddi and P. Bagchi, Int. J. Multiphase Flow **34**, 966 (2008).
[171] H. Li and G. Ma, Phys. Rev. E **82**, 026304 (2010).
[172] Z. Boujja, C. Misbah, H. Ez-Zahraouy, A. Benyoussef, T. John, C. Wagner, and M. M. Müller, Phys. Rev. E **98**, 043111 (2018).
[173] G. Tomaiuolo, M. Simeone, V. Martinelli, B. Rotoli, and S. Guido, Soft Matter **5**, 3736 (2009).
[174] A. Guckenberger, A. Kihm, T. John, C. Wagner, and S. Gekle, Soft Matter **14**, 2032 (2018).

[175] N. Takeishi, H. Yamashita, T. Omori, N. Yokoyama, and M. Sugihara-Seki, Micromachines **12** (2021).
[176] D. Agarwal and G. Biros, Phys. Rev. Fluids **5**, 013603 (2020).
[177] D. A. Fedosov, M. Peltomäki, and G. Gompper, Soft Matter **10**, 4258 (2014).
[178] S. M. Recktenwald, K. Graessel, F. M. Maurer, T. John, S. Gekle, and C. Wagner, Biophys. J. **121**, 23 (2022).
[179] F. Reichel, J. Mauer, A. A. Nawaz, G. Gompper, J. Guck, and D. A. Fedosov, Biophysical Journal **117**, 14 (2019), ISSN 0006-3495.
[180] G. Simionato, K. Hinkelmann, R. Chachanidze, P. Bianchi, E. Fermo, R. van Wijk, M. Leonetti, C. Wagner, L. Kaestner, and S. Quint, PLOS Computational Biology **17**, 1 (2021).
[181] A. Kihm, L. Kaestner, C. Wagner, and S. Quint, PLOS Computational Biology **14**, 1 (2018).
[182] J. Martin-Wortham, S. M. Recktenwald, M. G. M. Lopes, L. Kaestner, C. Wagner, and S. Quint, Applied Physics Letters **118**, 123701 (2021).
[183] J. L. McWhirter, H. Noguchi, and G. Gompper, Proc. Nat. Acad. Sci. USA **106**, 6039 (2009).
[184] G. Ghigliotti, H. Selmi, L. E. Asmi, and C. Misbah, Physics of Fluids **24**, 101901 (2012).
[185] G. Tomaiuolo, L. Lanotte, G. Ghigliotti, C. Misbah, and S. Guido, Physics of Fluids **24**, 051903 (2012).
[186] V. Claverìa, O. Aouane, M. Thiébaud, M. Abkarian, G. Coupier, C. Misbah, T. John, and C. Wagner, Soft Matter **12**, 8235 (2016).
[187] N. Takeishi and Y. Imai, Sci. Rep. **7**, 5381 (2017).
[188] O. Aouane, A. Farutin, M. Thiébaud, A. Benyoussef, C. Wagner, and C. Misbah, Phys. Rev. Fluids **2**, 063102 (2017).
[189] F. c. Yaya, J. Römer, A. Guckenberger, T. John, S. Gekle, T. Podgorski, and C. Wagner, Microcirculation **28**, e12693 (2021).
[190] G. Ghigliotti, A. Rahimian, G. Biros, and C. Misbah, Phys. Rev. Lett. **106**, 028101 (2011).
[191] S. Ebrahimi, P. Balogh, and P. Bagchi, J. Fluid Mech. **907**, A28 (2021).
[192] S. Ebrahimi and P. Bagchi, J . Fluid Mech. **929**, A30 (2021).
[193] T. Nakajima, K. Kon, N. Maeda, K. Tsunekawa, and T. Shiga, Am. J . Physiol. **259**, H1071 (1990).
[194] J. Dupire, M. Abkarian, and A. Viallat, Phys. Rev. Lett. **104**, 168101 (2010).
[195] H. Noguchi, Phys. Rev. E **81**, 061920 (2010).
[196] M. Zhao and P. Bagchi, Phys. Fluids **23**, 11901 (2011).
[197] D. Matsunaga, Y. Imai, T. Yamaguchi, and T. Ishikawa, J . Fluid Mech. **762**, 288âĂŞ301 (2015).
[198] L. Zhu, J. Rabault, and L. Brandt, Physics of Fluids **27**, 071902 (2015).
[199] M. Laumann, P. Bauknecht, S. Gekle, D. Kienle, and W. Zimmermann, Europhys. Lett. **117**, 44001 (2017).
[200] H. Noguchi, G. Gompper, L. Schmid, A. Wixforth, and T. Franke, Europhys. Lett. **89**, 28002 (2010).
[201] S. Braunmüller, L. Schmid, and T. Franke, J. Phys.: Condens. Matter **23**, 184116 (2011).
[202] A. Amirouche, J. Esteves, A. Lavoignat, S. Picot, R. Ferrigno, and M. Faivre, Biomicrofluidics **14**, 024116 (2020).
[203] M. Laumann, W. Schmidt, A. Farutin, D. Kienle, S. Förster, C. Misbah, and W. Zimmermann, Phys. Rev. Lett. **122**, 128002 (2019).
[204] F. Da Cunha and E. Hinch, J. Fluid Mech. **309**, 211 (1996).
[205] S. D. Hudson, Phys. Fluids **15**, 1106 (2003).
[206] M. Loewenberg and E. Hinch, J. Fluid Mech. **338**, 299 (1997).
[207] Y. Wang, R. Mauri, and A. Acrivos, J. Fluid Mech. **357**, 279 (1998).
[208] F. Blanc, F. Peters, and E. Lemaire, Phys. Rev. Lett. **107**, 208302 (2011).
[209] S. Guido and M. Simeone, J. Fluid Mech. **357**, 1 (1998).
[210] C.-Y. Wang, C.-B. Zhang, X.-Y. Huang, X.-D. Liu, and Y.-P. Chen, Chinese Physics B **25**, 108202 (2016).
[211] E. Lac, A. Morel, and D. Barthès-Biesel, J. Fluid. Mech. **573**, 149 (2007).
[212] E. Lac and D. Barthès-Biesel, Phys. fluids **20**, 040801 (2008).
[213] D.-V. Le and K.-H. Chiam, Phys. Rev. E **84**, 056322 (2011).
[214] X.-Q. Hu, X.-C. Lei, A.-V. Salsac, and D. BarthÃĺs-Biesel, Journal of Fluid Mechanics **892**, A19 (2020).
[215] P.-Y. Gires, G. Danker, and C. Misbah, Phys. Rev. E **86**, 011408 (2012).
[216] P.-Y. Gires, A. Srivastav, C. Misbah, T. Podgorski, and G. Coupier, Phys. Fluids **26**, 013304 (2014).
[217] A. Kumar and M. D. Graham, Phys. Rev. E **84**, 066316 (2011).
[218] R. K. Singh and K. Sarkar, Phys. Rev. E **92**, 063029 (2015).
[219] G. Závodszky, B. van Rooij, B. Czaja, V. Azizi, D. de Kanter, and A. G. Hoekstra, Phys. Fluids **31**, 031903 (2019).
[220] A. Kumar and M. D. Graham, Phys. Rev. Lett. **109**, 108102 (2012).
[221] A. Kumar, R. G. Henríquez Rivera, and M. D. Graham, J. Fluid Mech. **738**, 423 (2014), ISSN 1469-7645.
[222] R. G. H. Rivera, X. Zhang, and M. D. Graham, Phys. Rev. fluids **1**, 060501 (2016).
[223] H. Ye, Z. Shen, and Y. Li, J. Fluid Mech. **861**, 55âĂŞ87 (2019).
[224] X. Zhang, C. Caruso, W. A. Lam, and M. D. Graham, Phys. Rev. Fluids **5**, 053101 (2020).
[225] A. R. Malipeddi and K. Sarkar, Soft Matter **17**, 8523 (2021).
[226] R. Rusconi and H. A. Stone, Phys. Rev.Lett. **101**, 254502 (2008).
[227] A. R. Malipeddi and K. Sarkar, J . Fluid Mech. **868**, 5âĂŞ25 (2019).
[228] T. Podgorski, N. Callens, C. Minetti, G. Coupier, F. Dubois, and C. Misbah, Microgravity Sci. Technol. **23**, 263 (2011).
[229] Note1, the values given here were re-calculated from the original article [146] where the authors use for R the maximal radius 3.6 μm ; in this review, $R = 2.9$ μm is based on the cell volume.
[230] Note2, the values given here were re-calculated from the original article [225] where the authors use for R the maximal radius 4 μm ; in this review, $R = 2.9$ μm is based on the cell volume.
[231] D. A. Fedosov, B. Caswell, A. S. Popel, and G. E. Karniadakis, Microcirculation **17**, 615 (2010).
[232] V. Narsimhan, H. Zhao, and E. S. G. Shaqfeh, Phys. Fluids **25**, 061901 (pages 21) (2013).
[233] Microvascular Research **99**, 57 (2015).
[234] J. M. Sherwood, J. Dusting, E. Kaliviotis, and S. Balabani, Biomicrofluidics **6**, 024119 (2012).
[235] J.-M. Poiseuille, Comptes rendus hebdomadaires des séances de l'Académie des sciences **1**, 554 (1835).
[236] R. Fåhræus and T. Lindqvist, Am. J. Physiol. **96**, 562 (1931).
[237] R. Fahraeus, Physiological Reviews **IX**, 241 (1929).
[238] A. S. Popel and P. C. Johnson, Annu. Rev. Fluid Mech. **37**, 43 (2005).
[239] S. Roman, A. Merlo, P. Duru, F. Risso, and S. Lorthois, Biomicrofluidics **10**, 034103 (2016).
[240] P. Balogh and P. Bagchi, J. Comp. Phys. **334**, 280 (2017).
[241] P. Balogh and P. Bagchi, J. Fluid Mech. **864**, 768âĂŞ806 (2019).
[242] S. K. Doddi and P. Bagchi, Phys. Rev. E **79**, 046318 (2009).
[243] D. A. Fedosov, W. Pan, B. Caswell, G. Gompper, and G. E. Karniadakis, Proc. Nat. Acad. Sci. USA **108**, 11772 (2011).

[244] J. Sigüenza, S. Mendez, and F. Nicoud, Biomech. Model. Mechanobiol. **16**, 1645âĂŞ1657 (2017).

[245] F. Nicoud, V. Zmijanovic, and S. Mendez, Comp. Meth. Biomech. Biomed. Eng. **22**, S78 (2019).

[246] E. J. Hinch and J. D. Sherwood, J. Fluid Mech. **132**, 337 (1983).

[247] B. M. Alexander and D. C. Prieve, Langmuir **3**, 788 (1987).

[248] A. J. Goldman, R. G. Cox, and H. Brenner, Chem Eng Sci **22**, 653 (1967).

[249] S. Bike, L. Lazarro, and D. Prieve, Journal Of Colloid And Interface Science **175**, 411 (1995).

[250] X. Wu, P. Warszynski, and T. VandeVen, Journal Of Colloid And Interface Science **180**, 61 (1996).

[251] A. S. Khair and B. Balu, Electrophoresis **40**, 2407 (2019).

[252] T. van de Ven, P. Warszynski, and S. Dukhin, Journal Of Colloid And Interface Science **157**, 328 (1993).

[253] R. Cox, J. Fluid Mech. **338**, 1 (1997).

[254] S. Bike and D. Prieve, Journal Of Colloid And Interface Science **136**, 95 (1990).

[255] S. Bike and D. Prieve, Journal Of Colloid And Interface Science **154**, 87 (1992).

[256] S. Bike and D. Prieve, Journal Of Colloid And Interface Science **175**, 422 (1995).

[257] P. Warszynski, X. Wu, and T. van de Ven, Colloids Surf. A Physicochem. Eng. **140**, 183 (1998).

[258] S. M. Tabatabaei, T. G. M. van de Ven, and A. D. Rey, Journal Of Colloid And Interface Science **301**, 291 (2006).

[259] Note3, the provided expression for F_{Taba} is obtained by "re-dimensionalizing" the dimensionless forms reported in [258] as equations (7.3) and (7.4). Doing so, we noted a series of misprints in the original article by Tabatabaei et al.: (i) dimensionless forces $\tilde{F}$ should read $\tilde{F} = F/(\mu V R)$ (and not $\tilde{F} = F/(\mu V)$ as in eq. 2.2 in [258]), and (ii) the dimensionless lift force of eq. 7.3 should read $\tilde{F_z} = 4\pi\lambda Pe^2(\kappa^{-1}/R)^4(h/R)^{-2} f_z$ (and not $\tilde{F_z} = 4\pi Pe^2(\kappa^{-1}/R)^4(h/R)^{-2} f_z$).

[260] E. Yariv, O. Schnitzer, and I. Frankel, J. Fluid Mech. **685**, 306 (2011).

[261] O. Schnitzer, I. Frankel, and E. Yariv, Mathematical Modelling Of Natural Phenomena **7**, 64 (2012).

[262] O. Schnitzer, I. Frankel, and E. Yariv, J. Fluid Mech. **704**, 109 (2012).

[263] O. Schnitzer and E. Yariv, J. Fluid Mech. **786** (2016).

[264] A. Hollingsworth and C. Silebi, Langmuir **12**, 613 (1996).

[265] X. Lu, J.-P. Hsu, and X. Xuan, Langmuir **31**, 620 (2015).

[266] F. Liu, A. Klaassen, C. Zhao, F. Mugele, and D. van den Ende, J Phys Chem B **122**, 933 (2018).

[267] C. Zhao, W. Zhang, D. van den Ende, and F. Mugele, J Fluid Mech **888** (2020).

[268] M. R. Matus, Z. Zhang, Z. Benrahla, A. Majee, A. Maali, and A. WÃijrger, Electroviscous drag on squeezing motion in sphere-plane geometry (2022), URL `https://arxiv.org/abs/2201.01022`.

[269] J. Chakraborty and S. Chakraborty, Phys Fluids **23** (2011).

[270] K. G. Naik, S. Chakraborty, and J. Chakraborty, Soft Matter **13**, 6422 (2017).

[271] M. Thiébaud, Z. Shen, J. Harting, and C. Misbah, Phys. Rev. Lett. **112**, 238304 (2014).

[272] Z. Shen, G. Coupier, B. Kaoui, B. Polack, J. Harting, C. Misbah, and T. Podgorski, Microvasc. Res. **105**, 40 (2016).

[273] Z. Shen, A. Farutin, M. Thiébaud, and C. Misbah, Phys. Rev. Fluids **2**, 103101 (2017).

[274] Q. Zhou, J. Fidalgo, L. Calvi, M. O. Bernabeu, P. R. Hoskins, M. S. Oliveira, and T. Krüger, Biophysical Journal **118**, 2561 (2020).

[275] H. Feng, H. Huang, and X.-Y. Lu, Phys. Fluids **33**, 013302 (2021).

[276] V. Audemar, T. Podgorski, and G. Coupier, Phys. Fluids **34**, 042013 (2022).

[277] S. Jahn and J. Klein, Physics Today **71**, 48 (2018).

[278] S. P. Meeker, R. T. Bonnecaze, and M. Cloitre, Phys. Rev. Lett. **92**, 198302 (2004).

[279] M. Wyart and M. E. Cates, Phys. Rev. Lett. **112**, 098302 (2014).

[280] M. E. Rosti, M. N. Ardekani, and L. Brandt, Phys. Rev. Fluids **4**, 062301 (2019).

[281] A. Rinehart, U. Lacis, T. Salez, and S. Bagheri, Phys. Rev. Fluids **5**, 082001 (2020).

[282] B. N. J. Persson and M. Scaraggi, J. Phys.: Condens. Matter **21** (2009).

[283] N. Moyle, H. Wu, C. Khripin, F. Bremond, C.-Y. Hui, and A. Jagota, Soft Matter **16**, 1627 (2020).

[284] C.-Y. Hui, H. Wu, A. Jagota, and C. Khripin, Tribology Letters **69** (2021).

[285] Y. Peng, C. M. Serfass, A. Kawazoe, Y. Shao, K. Gutierrez, C. N. Hill, V. J. Santos, Y. Visell, and L. C. Hsiao, Nature Materials (2021).

[286] F. Brau, D. Lanterbecq, L.-N. Zghikh, V. Bels, and P. Damman, Nature Physics **12**, 931 (2016).